NASA-CR-193302

141

Effects of an Aft Facing Step on the Surface of a Laminar Flow Glider Wing

GRANTOR - NASA AMES RESEARCH CENTER
DRYDEN FLIGHT RESEARCH FACILITY

GRANTEE - CAL POLY STATE UNIVERSITY

GRANT NUMBER NCC 2-701

1/1/91 - 6/30/93

Principal Investigator

Dr. Doral R. Sandlin

Student Investigator

Neal Saiki

June 1993

(NASA-CR-193302) EFFECTS OF AN AFT FACING STEP ON THE SURFACE OF A LAMINAR FLOW GLIDER WING Final Report, 1 Jan. 1991 - 30 Jun. 1993 (California Polytechnic State Univ.) 141 p

N93-31855

Unclas

G3/02 0175476

ABSTRACT

Effects of an Aft Facing Step on the Surface of a Laminar Flow Glider Wing.

Neal Saiki

April 1993

A motor glider was used to perform a flight test study on the effects of aft facing steps in a laminar boundary layer. This study focuses on two dimensional aft facing steps oriented spanwise to the flow. The size and location of the aft facing steps were varied in order to determine the critical size that will force premature transition. Transition over a step was found to be primarily a function of Reynolds number based on step height. Both of the step height Reynolds numbers for premature and full transition were determined. A hot film anemometry system was used to detect transition.

ACKNOWLEDGMENTS

This thesis is a product of a NASA Ames/Dryden research grant. Support for all of the flight tests came from the NASA Dryden Flight Research Center. The author would like to thank all of the people at NASA without whose help this study would not be possible.

TABLE OF CONTENTS

List of Tables

Page

List of Figures

Page

Symbols

α	angle of attack
C	wing chord
$Cl_{A/C}$	aircraft lift coefficient
Cl	section lift coefficient
Cl_d	section drag coefficient
C_m	pitching moment coefficient
Cl_{TS}	test section lift coefficient
C p	pressure coefficient
d	distance between waves
δ_1	displacement thickness
δ_2	momentum thickness
δ_3	energy thickness
h	step height
h'	wave height
H_{12}	boundary layer shape factor, δ_1/δ_2
H_{32}	boundary layer shape factor, δ_3/δ_2
H_i	indicated pressure altitude
K	boundary layer shape factor
Λ	boundary layer shape factor
v	kinematic viscosity
OAT	outside air temperature
P_a	ambient air pressure
P_o	standard atmosphere sea level pressure
q	dynamic pressure

ρ	air density
$Re_{h\,cr}$	critical step height reynolds number
$Re_{h\,fl}$	fully turbulent step height reynolds number
Re_h	step height reynolds number
RMS	root mean square
S	projected wing area
s_h	streamwise distance to step
$s_{tr\,nat}$	streamwise distance to natural transition location without step
s_{tr}	streamwise distance to transition in the influence of the step
s_w	streamwise distance to wave
T	outside air temperature
t	wave height
t'	adjusted wave height
T_o	standard atmosphere sea level temperature
U	airflow velocity
u	local airflow velocity
U_∞	freestream velocity
V_c	calibrated airspeed
V_e	equivalent airspeed
V_i	indicated airspeed of aircraft
Vic	indicated airspeed corrected for instrument error
V_t	true velocity of aircraft
W	weight
x/C	distance along chord normalized to chord length
Z	boundary layer shape factor
ΔV_c	scale altitude correction
ΔV_{ic}	instrument correction

ΔV_{pc} position error correction

CHAPTER 1

Introduction

Benefits of Natural Laminar Flow

The achievement and maintenance of natural laminar flow (NLF) is of prime concern in these days of high fuel costs. By maintaining large portions of NLF over an aircraft surface, the skin friction drag is reduced, thus increasing efficiency. Figure 1 illustrates the significant drag reduction benefits achievable on a medium sized business jet (Holmes et al., 1984). Each bar represents the cumulative effect on total aircraft drag as more of the surfaces are made to use NLF. Fuel economy improvements on the order of 25% are possible given the steady cruise conditions typical of commuter aircraft.

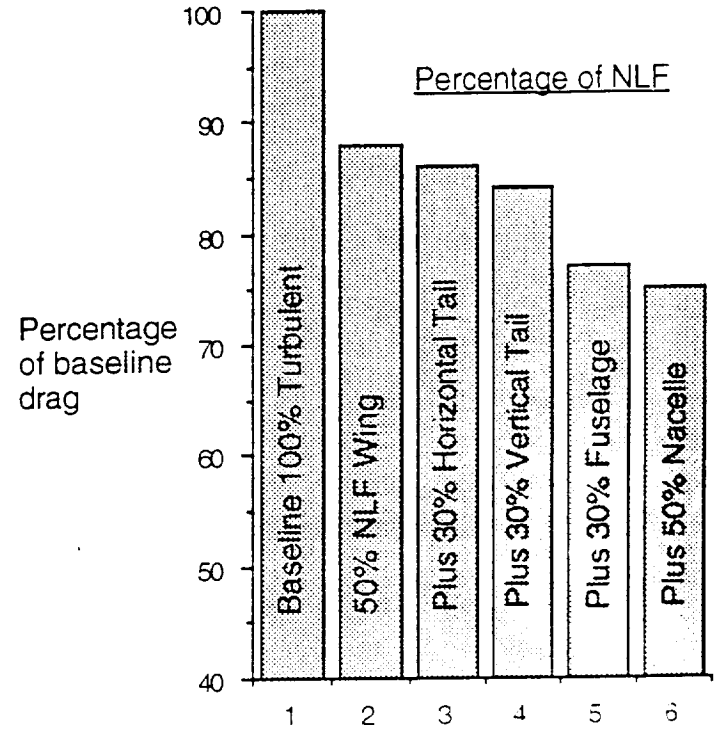

Figure 1. -Predicted drag benefits of laminar flow on a business jet.

The first aircraft to utilize a NLF airfoil was the North American P-51 Mustang. Unfortunately this aircraft did not achieve the extensive laminar flow that was predicted in the wind tunnel. Wing surface excrescences such as rivets, sheet metal

gaps, and waviness caused premature transition and the sensitive handling characteristics of the P-51. In fact, most of the experiments of that era support the conclusion that extensive laminar flow could not be achieved with the crude metal airframe fabrication methods of the time (Anderson, J., 1985).

In more recent years, construction techniques such as molded composite wings and bonded aluminum skins have made extensive laminar flow easier to achieve. Wing surfaces can now be made without joints or waviness, but the tradeoff can be increased production costs. This has brought about the need for further research into the maximum allowable excrescence size that can be tolerated on a wing surface without causing premature transition.

In some cases it is desirable to force transition in order to avoid flow separation. When encountering an adverse pressure gradient (decelerating flow), laminar boundary layers are more prone to separation then turbulent boundary layers. By tripping the flow prior to the adverse pressure gradient, the flow may remain attached. On a NLF wing this means that premature separation and stalling can be avoided with the use of an excrescence to force transition. In this case it is necessary to know the minimum excrescence size that causes transition.

Scope of This Study

One common type of surface excrescence are the aft facing steps that occur at the junction of sheet-metal panels on aircraft wings. This study focuses on two dimensional aft facing steps oriented spanwise to the flow. The size and location of the aft facing steps are varied in order to determine the critical size that will force premature transition.

The test vehicle was a PIK-20E motor glider. This dual mode aircraft is capable of self launched takeoff with the engine out and gliding flight with the engine

stored. The wings have natural laminar flow for up to 57% of the chord which makes a good testbed for NLF experiments.

In order to detect boundary layer transition, hot film anemometers were bonded to the wing surface in order to determine the chordwise location of transition. These sensors work as heated temperature probes which measure the increased cooling caused by turbulent flow. The data from the sensors were collected and stored in an onboard computer.

In addition to the computer recorded data, flight conditions (airspeed, altitude, and temperature) were read from cockpit instruments and manually recorded by the pilot.

Purpose of this Study

One of the reasons for performing this particular study is that there were some conflicting results from previous wind tunnel excrescence studies. Results from a recent NASA F-14 Variable Sweep Transition Flight Experiment has indicated that previous excrescence tolerance criteria may be unnecessarily stringent. In some cases the predicted excrescence size for transition was exceeded by a factor of three without causing premature transition (Anderson, B., 1990). Because of these discrepancies, this study was conducted in order to retest excrescence tolerances using a flight vehicle.

Aft facing steps were chosen for testing due to there simple geometry and tendency to trip the boundary layer. Aft facing steps are often found on wing surfaces and are still a problem even on composite wings. Leading edge flaps, de-icing boots and other devices can leave steps at there juncture to the wing surface. These irregularities can be closely modeled by the aft facing steps tested in this study.

There have been several previous studies of aft facing step transition. The main purpose of this experiment is to reevaluate the existing wind tunnel studies with flight test data. A motor glider was chosen for this study because it has certain advantages over a wind tunnel. Experiments performed on a glider wing are subject to low level atmospheric turbulence, whereas the free stream turbulence inherent in a wind tunnel can cause premature transition resulting in conservative tolerances (Braslow and Muraca, 1978).

The secondary purpose of this study is to examine the influence of pressure gradient on excrescence tolerances. Natural laminar flow is promoted by long runs of favorable pressure gradient (accelerating flow) which limits the growth of two dimensional Tollmien-Schlichting wave disturbances. Previous excrescence studies were conducted in a zero pressure gradient flow field. In contrast, by testing on an aircraft wing, the excrescences can be tested in the actual chordwise pressure gradient which occurs on an airfoil surface.

CHAPTER 2

Transition Criteria

In order to make the purpose of this report clearer it is necessary to first define the transition criteria used in this study. Transition behind a step has been traditionally defined as a function of step height Reynolds number (Re_h) as defined by figure 2 and equation 1.

$$Re_h = \frac{U * h}{\nu} \qquad (1)$$

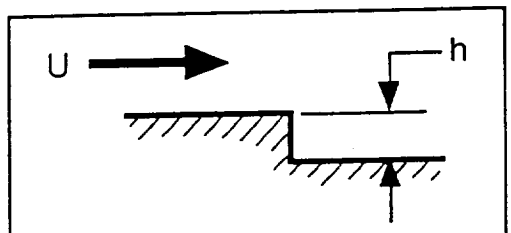

Figure 2. -Step dimensions.

In equation 1, U is the airflow velocity, h is the step height, and ν is the kinematic viscosity. It is optional whether the airflow velocity term in equation 1 should be free stream velocity or local velocity over the step. Traditionally the value of free stream velocity, U_∞, is used for simplicity, but the use of local velocity, u, is adopted in this report. Greater accuracy is obtained by using local velocity. Unless otherwise noted, all Reynolds numbers in this report are based on local velocity.

When a laminar boundary layer encounters an aft facing step there are three categories of transition (Fig. 3) which can occur behind an aft facing step (Lurz, 1980).

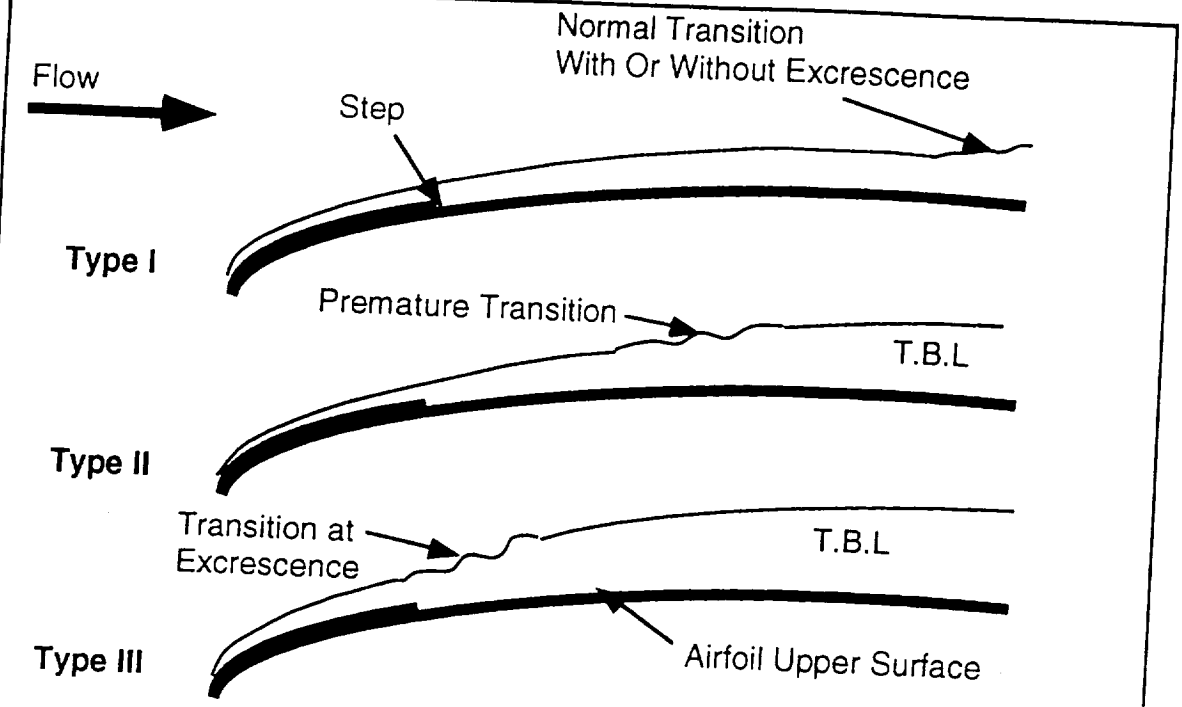

Figure 3. -Three types of transition.

In Type I transition, the step Reynolds number is so small that there is no influence on the natural transition of the plate. The transition location and step Reynolds number for the Type I flow are described in equation 2.

$$s_{tr} = s_{tr\ nat} \text{ and } Re_h < Re_{h\ cr} \tag{2}$$

In equation 2, $Re_{h\ cr}$ denotes the value of Re_h where the step just begins to have an influence on transition. This is commonly referred to as the critical Reynolds number. Also, s_{tr} is the streamwise distance to transition with the step in place and $s_{tr\ nat}$ is the natural transition distance without the step.

In Type II transition, the step causes premature transition. The transition location and step Reynolds number for the Type II flow are described in equation 3.

$$s_h < s_{tr} < s_{tr\ nat} \text{ and } Re_{h\ cr} < Re_h < Re_{h\ fl} \tag{3}$$

The step causes the transition location to move somewhere between the natural transition location and the location of the step (s_h). In equation 3, $Re_{h\,fl}$ is the Reynolds number where transition takes place at the location of the step.

In Type III transition, the influence of the step is so strong that transition takes place at the step location. The transition location and step Reynolds number for the Type III flow are described in equation 4.

$$s_{tr} = s_h \text{ and } Re_h > Re_{h\,fl} \tag{4}$$

For the Type III flow, the flow is fully turbulent behind the step.

The main focus of this study is on finding the critical step height Reynolds number $Re_{h\,cr}$. This is found when transition of Type II is detected.

CHAPTER 3

Review of Previous Literature

A literature search revealed three pertinent studies. All of which are based on wind tunnel data. These studies are used for comparison to the flight test data gathered in this experiment. Two of these studies tested for critical Reynolds numbers on aft facing steps and one study tested the influence of pressure gradients on a wire trip.

The most widely used criteria for step and gap tolerances came from the USAF/Northrop X-21 flight program conducted in the early sixties (Anon, 1967). In addition to flight testing, the program was supported by wind-tunnel and analytical studies. As an interesting note, the laminar flow control wings made for the X-21 were not very successful due to unmatched joints in the spanwise wing splices. These splices were similar to the ones tested in this study. Even though the program was canceled before a successful wing could be produced, quite a bit of useful research was accomplished.

Part of the X-21 research program included wind tunnel tests in which the Reynolds number which causes premature transition was determined for aft facing steps and other configurations. The excrescences were located on a flat plate at 25% chord. The report does not state what definition was used to determine step height Reynolds numbers for the surface imperfections. However, according to Dr. Werner Pfenninger, who conducted wind-tunnel experiments to develop these criteria, the step height Reynolds numbers were established based on the conditions where the first turbulent bursts occurred far downstream from the surface imperfection (Holmes et al., 1985). This is consistent with the transition criteria used

for critical Reynolds number, $Re_{h\,cr}$, used in this report. Results from the X-21 program found $Re_{h\,cr}$ to be approximately 1100.

Research on the critical Reynolds number for round wire trips was conduced in an Australian experiment by Stuper (Stuper 1949). This study focused on wind tunnel experiments with wire trips subject to a pressure gradient. The pressure gradient used was made to match that of a laminar flow airfoil. The experiment concluded that a favorable pressure gradient has only a slightly beneficial effect on transition. However, the wind tunnel used in this experiment had high levels of free stream turbulence and it was suggested by the author that further research was necessary with reduced turbulence.

The most pertinent study was conducted by Werner Lurz at the Helsinki University of Technology (Lurz 1980). Although this is a very thorough study, the main focus of this study is the analysis of the flow region behind an aft facing step and not in finding the critical step height Reynolds number. Most of the research was concentrated on flows where transition and separation was occurring at the step. Consequently, the $Re_{h\,cr}$ was determined to be approximately 540 $\pm$ 29% and $Re_{h\,fl}$ was found to be 1730 $\pm$ 3%. The value of $Re_{h\,fl}$ is much easier to determine accurately. The value for $Re_{h\,cr}$ found in this study is almost half of that found by the X-21 experiments.

With so few studies in this area and the lack of agreement on the value of $Re_{h\,cr}$, there was clearly a need for more research.

CHAPTER 4

Description of Apparatus

Aft Facing Steps

The aft facing steps were constructed of flat vinyl sheets and bonded to the wing surface with spray contact cement. Vinyl has the advantage of being able to conform to the surface curvature even around the leading edge. For the aft facing steps, the vinyl started on the bottom surface of the wing, covered the leading edge, and extended to the location of the step. This assures a joint free surface from the leading edge to the step. The vinyl step layer is shown in figure 4.

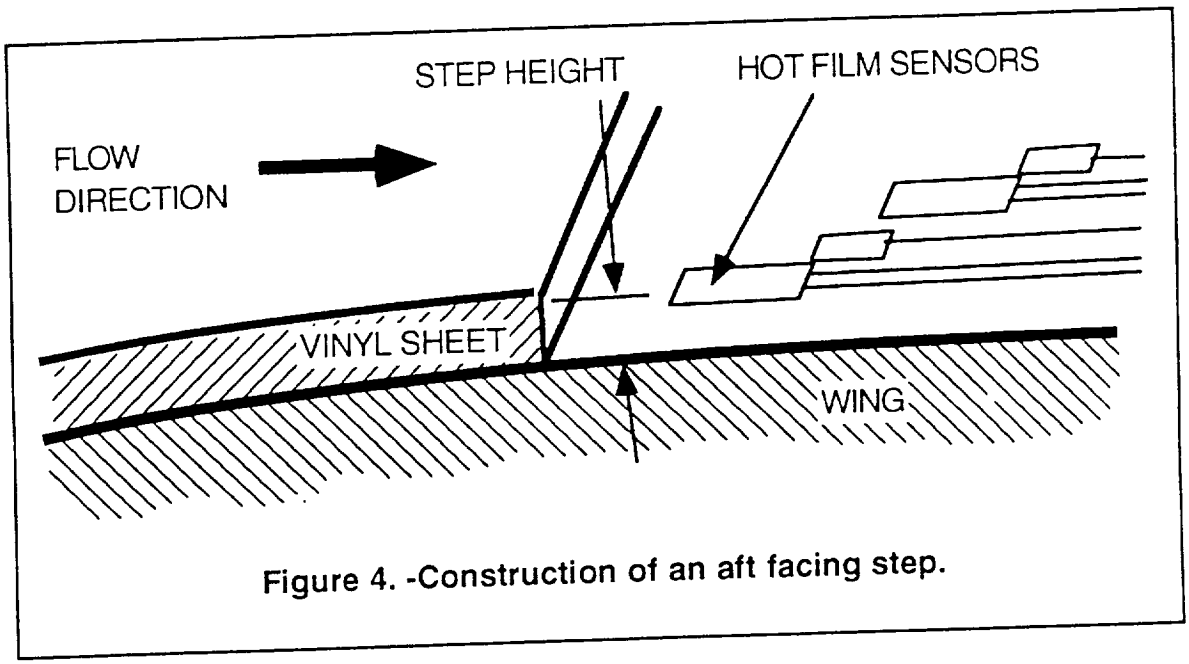

Figure 4. -Construction of an aft facing step.

Four thicknesses of vinyl sheeting were used in the flight tests. The nominal sizes were 0.012, 0.016, 0.020, and 0.030 inches. However, the actual thickness of each sheet varied from the nominal size. For the data analysis, the thickness at ten locations were measured and the values averaged. Table 1 contains the vinyl measurement data. All of the measurements were taken at one inch spacing.

Table 1. -Vinyl sheet thickness.

	Nominal Thickness			
	0.012	0.016	0.020	0.030
	Measured Thickness			
1	0.0117	0.0145	0.0197	0.0314
2	0.0116	0.0148	0.0196	0.0314
3	0.0116	0.0146	0.0196	0.0313
4	0.0114	0.0145	0.0195	0.0313
5	0.0117	0.0148	0.0194	0.0311
6	0.0117	0.0147	0.0197	0.0313
7	0.0118	0.0147	0.0197	0.0312
8	0.0115	0.0148	0.0196	0.0312
9	0.0116	0.0149	0.0194	0.0312
10	0.0117	0.0148	0.0195	0.0311
	Average Thickness			
	0.0116	0.0147	0.0196	0.0313
	Standard Deviation			
	0.00012	0.00014	0.00012	0.00011

There was a concern that the slight waviness of the vinyl might contribute to premature transition. The allowable waviness criteria was calculated from equation 5 (Fage 1943).

Eq. 5 $$\frac{h'}{d} = 9E6 \left[\frac{u * s_w}{\nu} \right]^{-1.5} \left[\frac{s_w}{d} \right]^{.5}$$

In equation 5, h' is the wave height, d is the distance between waves, u is the local velocity, s_w is the surface distance to the wave, and ν is the kinematic velocity. The standard method for measuring waviness is to measure three points in a line with one inch spacing between each point. The deviation of the center point is the wave height, h'. For the flight conditions, the resulting allowable wave height between a two inch measurement is approximately 0.020 inches. This is approximately 150 times the standard deviation of the vinyl sheet. Therefore the vinyl waviness was considered negligible.

Grit Transition Strip

In addition to the aft facing steps, a grit strip was flight tested in order to calibrate the hot film data. The grit strip was sized to cause boundary layer transition at the lowest test airspeed. The lowest airspeed case being the most difficult to transition. With a laminar boundary layer in front of the strip and a turbulent boundary layer aft of the strip, the resulting hot film data was used in order to distinguish the difference between laminar and turbulent hot film signals. The grit strip is shown in figure 5.

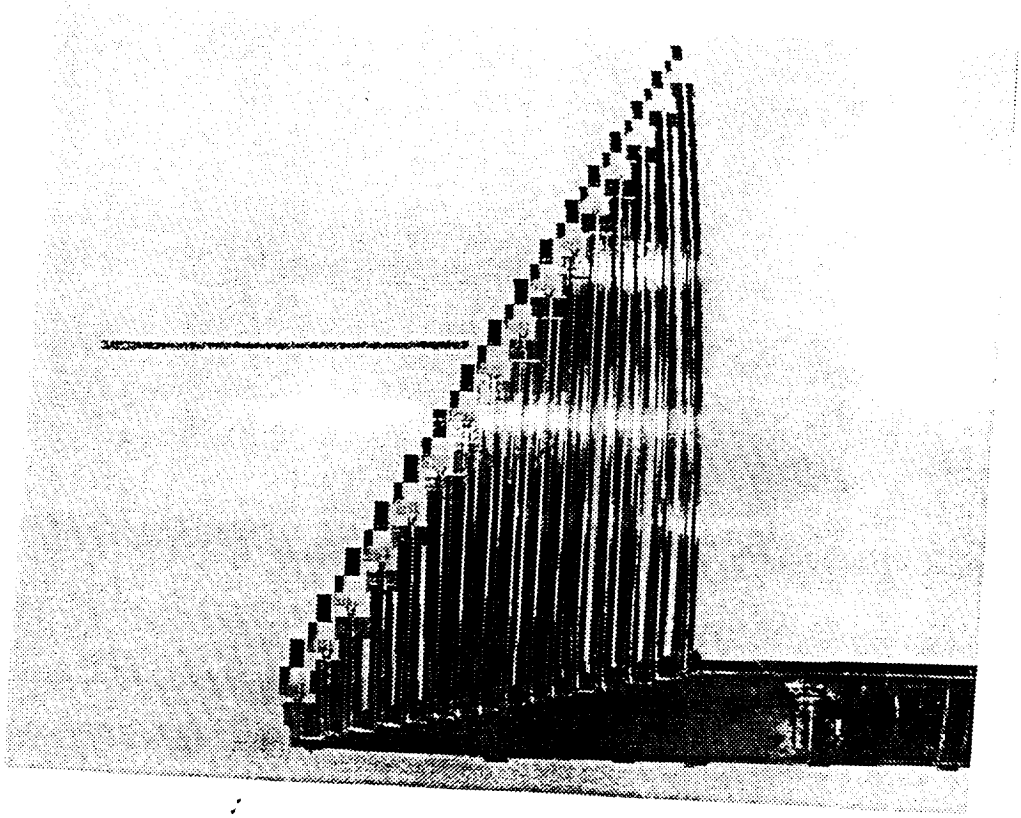

Figure 5. -Grit transition strip.

The use of a grit transition strip is a commonly used method to produce transition. The sizing of the grit transition strip is detailed in a paper by Braslow (Braslow and Know, 1958). According to Braslow, the critical grit transition Reynolds

should be 1200. For a transition strip at 42.6% chord and a velocity of 50 knots, the corresponding grit size is 0.020 inch.

For this experiment, glass beads of size 0.023 to 0.027 inch were used. This size guaranteed transition. The glass beads were glued on the wing in a 0.25 inch wide strip. A clear spray enamel was used to stick the beads to the wing surface.

PIK-20E Motor Glider

The test vehicle was a PIK-20E motor glider (Figure. 6). The PIK-20E is an all composite motorglider with composite sandwich wing surfaces. The wing surface is free of any joints or gaps. In addition, the wing has been resurfaced to remove any surface waviness or roughness. The physical dimensions of the wing are shown in figure 7 (Johnson, 1976).

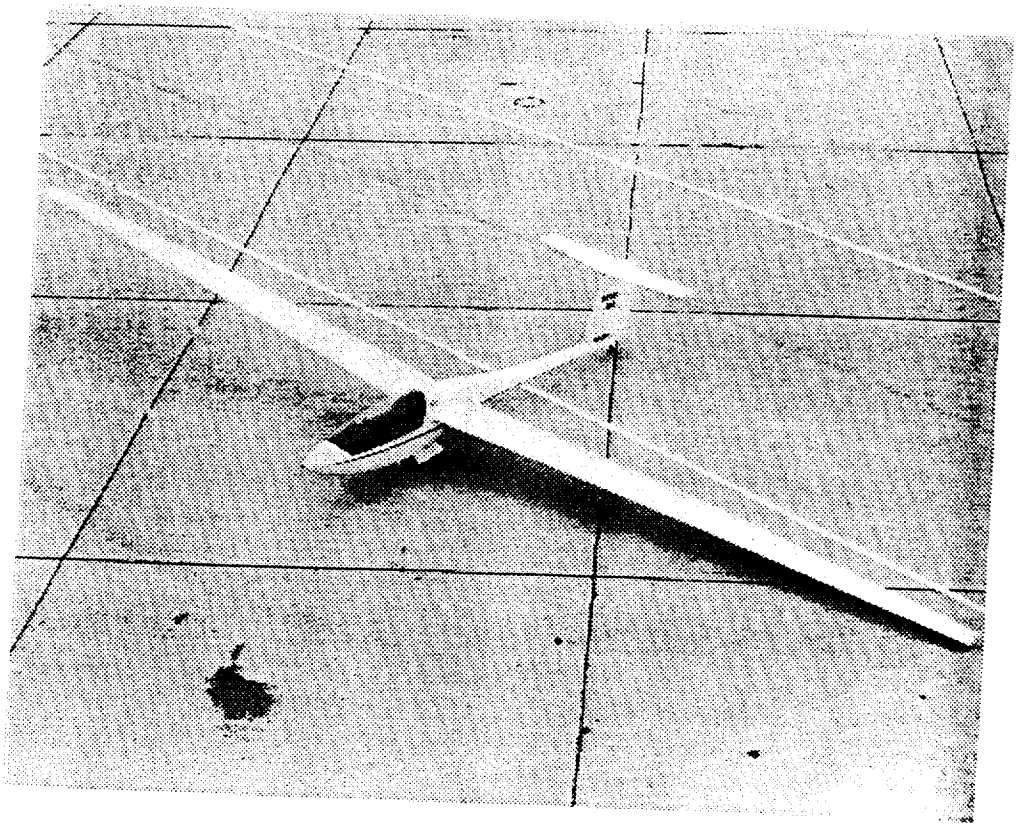

Figure 6. -PIK-20E motor glider.

The motor is used only for takeoff and climb out to the test altitude. When the test altitude is reached, the engine is retracted and stored in the fuselage. By testing while the aircraft is in the glider mode, the vibration and electronic interference from the engine is avoided.

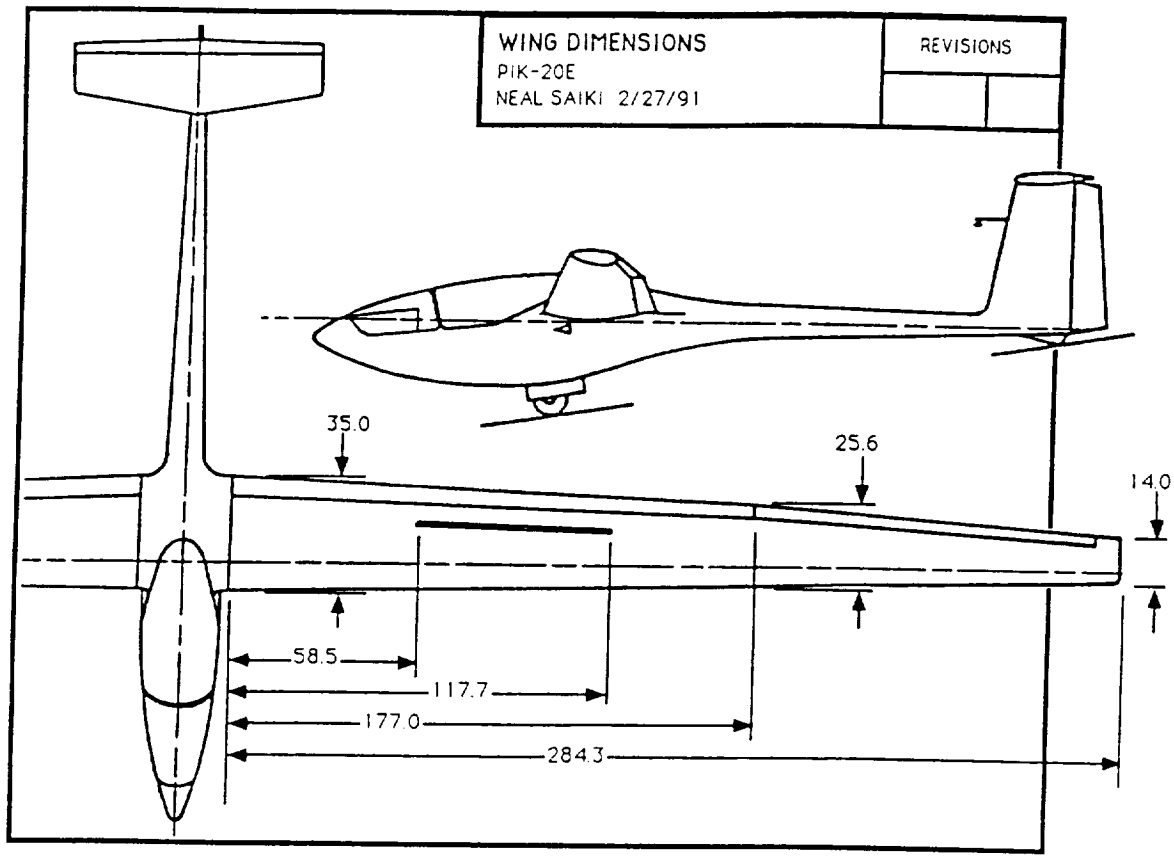

Figure 7. -Wing dimensions.

Hot Film Anemometry System

In the past, hot film anemometers have been successfully used in flight test experiments to detect boundary layer transition on low speed aircraft (Obara & Holmes, 1985; Holmes, et al, 1986; Manuel, et al, 1987). The anemometry system used in this flight experiment is a refinement over previous systems. It is temperature compensated which allows unattended operation during large speed or altitude changes (AS&M 1989; Chiles, 1988; Chiles & Johnson, 1985). More recently, this system has been used successfully in flight test on a F-16 airplane at the NASA Ames-Dryden Flight Research Facility and some of the hardware was used in this experiment.

The hot film anemometry system consisted of hot film sensors, cards for each sensor, an onboard computer, and battery. This is diagrammed in figure 8. Sixteen pairs of hot film sensors and temperature compensators were mounted on the wing.

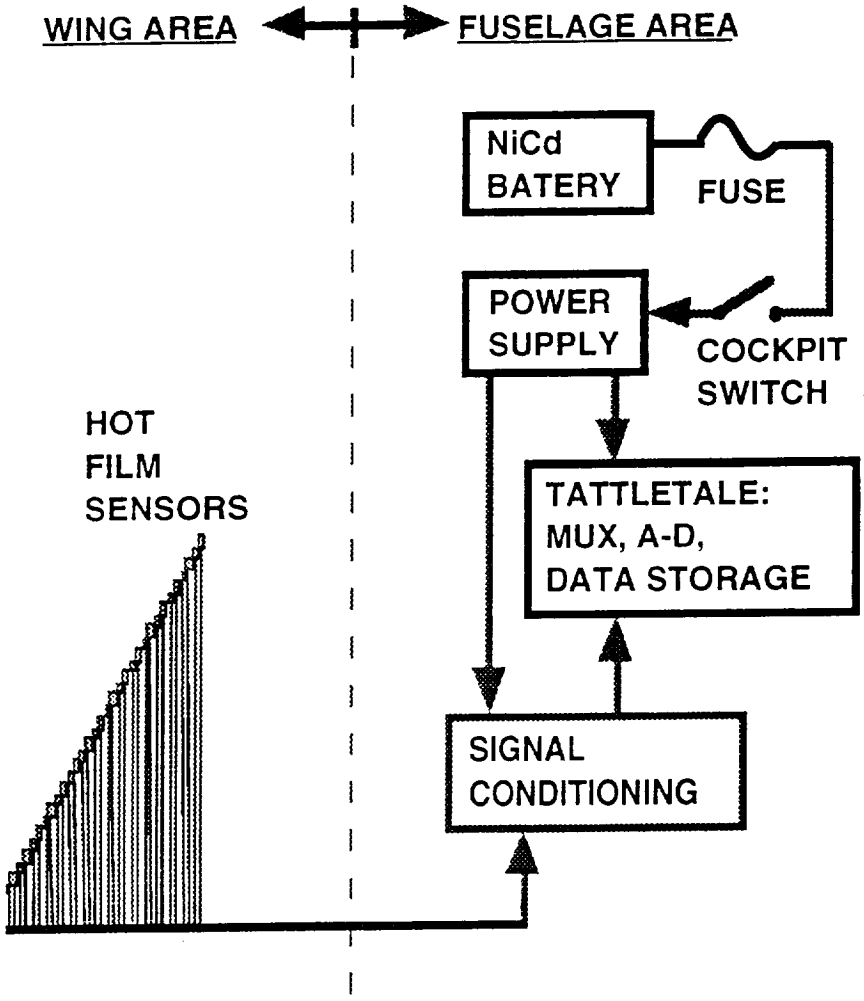

Figure 8. -Instrumentation diagram.

Hot film sensors are made of thin plastic with a tiny filament wire bonded onto the surface. The filament is heated at constant voltage by an amplifier circuit. The resistance change is measured as the filament wire is cooled by the air passing over it. A turbulent boundary layer, with higher surface velocities, cools the filament more then a laminar boundary layer. Each hot film sensor and card form a Wheatstone bridge with the analog output signal sent to the onboard computer. The details of each sensor are shown in figure 9.

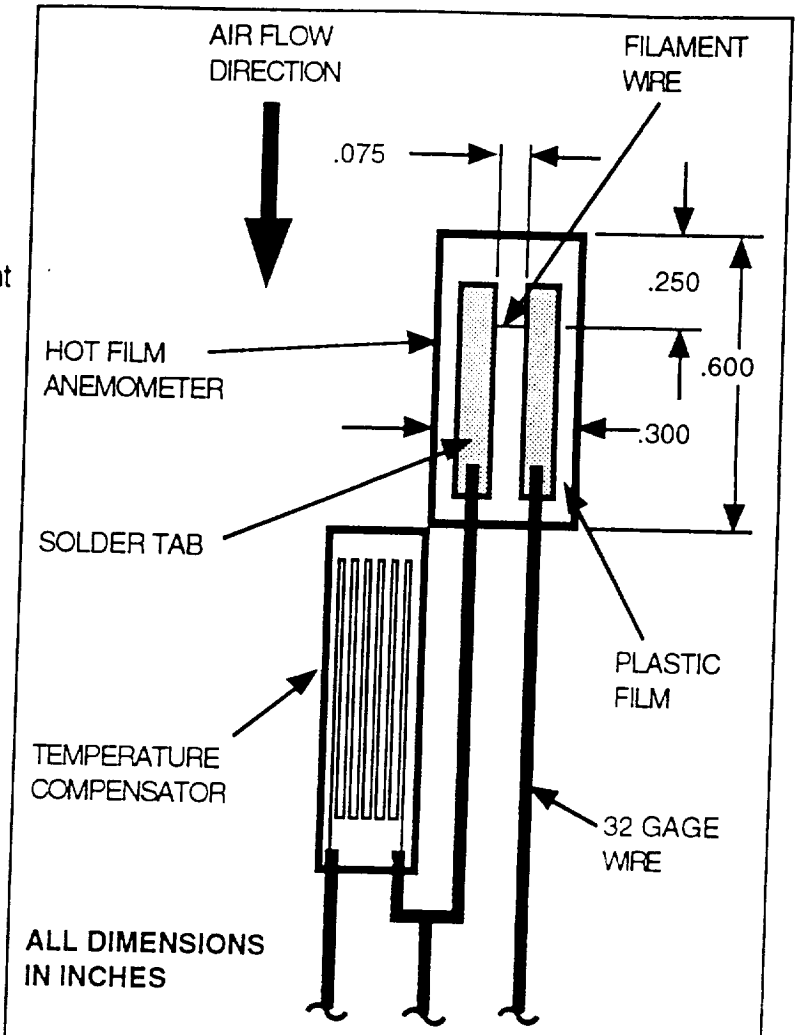

Figure 9. -Hot film sensor detail.

The hot films were glued onto the upper surface of the wing with spray contact cement. This allowed the hot films to be repositioned by softening the contact cement with a hot air gun. The sensors were positioned in order to cover the laminar zone of the wing. The chord locations of the sixteen sensors are shown in figure 10.

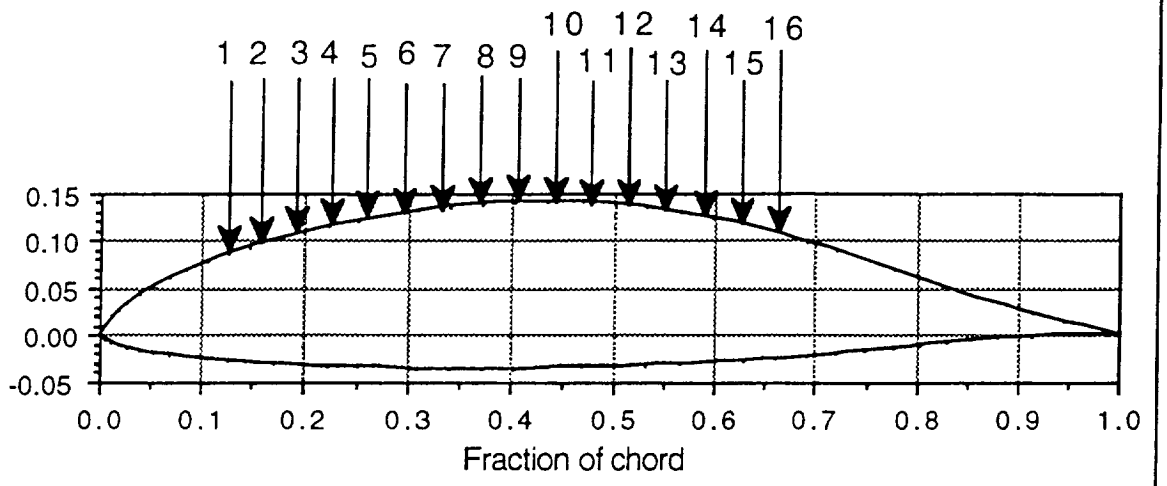

Figure 10. -Hot film chord locations.

The location of the test section on the wing planform is shown in figure 11. This location was chosen because it is outboard of the speed brakes, inboard of the ailerons, and outside of the fuselage influence. For a more complete description of the wing flow field refer to appendix A.

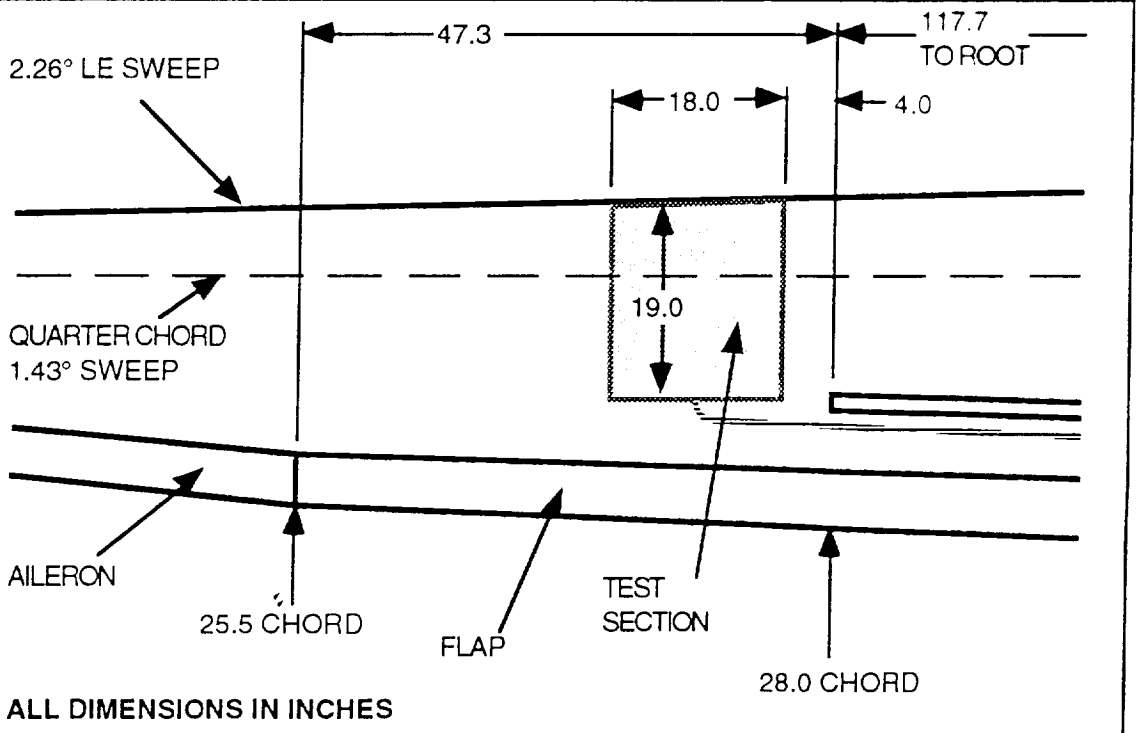

Figure 11. -Test section location.

The arrangement of the hot films is shown in figure 12. The hot films were arranged at an angle of 30° to the flow so that each film would not be disturbed by the ones in front of it. Since the disturbance half angle from a point source is approximately 7° (Schlicting 1987), the 30° angle is the smallest angle to the flow that can be used.

Although there were sixteen hot films, there were only eight anemometer cards and therefore only eight hot films could be recorded at a time. The eight active hot films were chosen based on the predicted location of transition. Analog data from the anemometer cards went to a multiplexer and then to the onboard computer which has an analog to digital converter. The digitized data was then stored in the computer's onboard RAM.

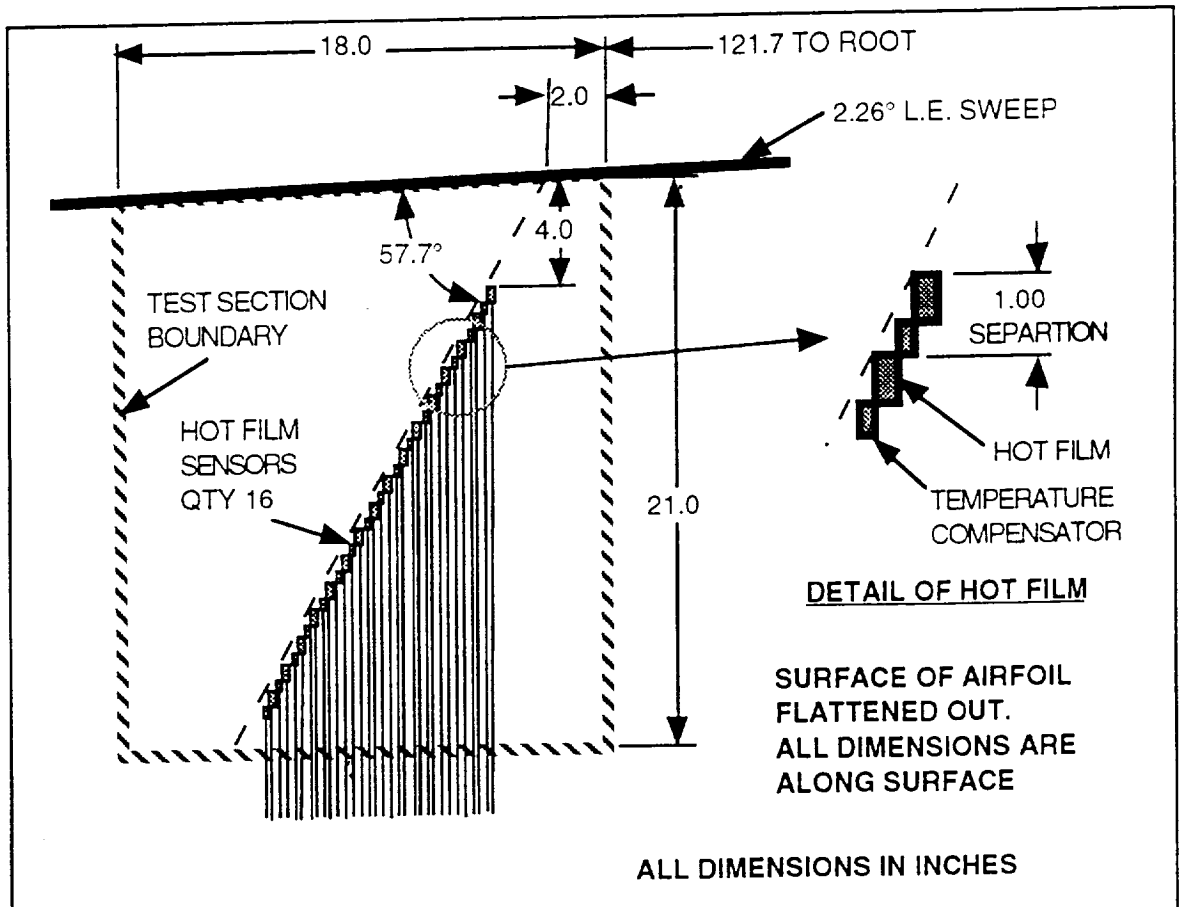

Figure 12. -Arrangement of hot films.

The inflight computer was a Tattletale Model 7 (TT7) made by the Onset Computer Corporation (figure 13). It is a single board computer and uses a MC68332 processor similar to an Apple Macintosh computer. For data storage, there is one megabyte of on-board memory. That is enough memory to record all of the flight data without an external data storage device. The 12-bit analog to digital converter is capable of sampling at speeds up to 100,000 Hz, but a sample rate of 1500 Hz was chosen as sufficient for this experiment. If the sample rate was any higher, then an external hard drive would be necessary.

Figure 13. -Onboard computer.

Cockpit Data

In addition to the computer recorded data, flight test conditions (airspeed, altitude, and temperature) were recorded by the pilot on a lap board. Airspeed and altitude were read from existing cockpit gauges. Outside air temperature was

measured with a digital readout thermometer with the temperature probe mounted on the underside of the fuselage. The accuracy of these instruments is listed in table 2.

Table 2. -Cockpit instrument accuracy.

Indicated Airspeed	±1 kt.
Indicated Pressure Altitude	±100 Ft.
Outside air temperature	± 2° F.

CHAPTER 5

Experimental Procedure

Flight Breakdown

Fifteen flight tests where data was recorded were accomplished for this study. A listing of the flights are contained in table 3. Not all of the flights had an aft facing step on the wing. The first two flights were made in the smooth wing configuration. The smooth wing configuration was used to determine the natural transition location and to identify a laminar flow hot film signal. Flights 3 through 8 tested aft facing steps at 24.4% and 42.6% chord. Flight 9 was done in the smooth wing configuration and tested the effect of side-slip. The side-slip was maintained with crossed aileron and rudder control. Flight 10 was flown with a grit transition strip which was used to identify a turbulent flow hot film signal. Flights 11 through 13 tested aft facing steps at the 10.5% chord location. Flight 14 was flown with a smaller step at the 24.4% chord in order to bracket the lower end of the critical Reynolds number. Finally, flight 15 was a repeat of flight 5 which had a problem with the data acquisition system.

Table 3. -Flight breakdown.

Flight	Configuration	Step Size	Location
1	Smooth		
2	Smooth		
3	Aft Step	.0313	24.4%
4	Aft Step	.0196	24.4%
5	Aft Step	.0147	24.4%
6	Aft Step	.0116	42.6%
7	Aft Step	.0147	42.6%
8	Aft Step	.0196	42.6%
9	Smooth, Slip		
10	Grit Trip Strip		42.6%
11	Aft Step	.0147	10.5%
12	Aft Step	.0116	10.5%
13	Aft Step	.0196	10.5%
14	Aft Step	.0116	24.4%
15	Aft Step	.0147	24.4%

Due to limitations in the data acquisition system, only eight of the hot films were recorded at a time. Table 4 lists the active hot films for each flight. The decision of which hot films to record was based on the location of transition.

Table 4. -Matrix of active hot film patches.

Flight	Active Hot Films															
	1	2	3	4	5	6	7	9	10	11	12	13	14	15	16
1				X	X		X		X		X	X	X	X	
2				X	X		X		X		X	X	X	X	
3					X	X	X	X		X		X	X	X	
4					X	X	X	X		X		X	X	X	
5					X	X	X	X		X		X	X	X	
6				X					X		X	X	X	X	
7					X			X	X	X	X	X	X	X	
8								X	X	X	X	X	X	X	
9	X			X		X	X	X	X	X	X	X	X	X	
10	X			X				X	X	X		X		X	
11	X	X		X			X	X	X	X		X		X	
12	X	X		X			X		X		X		X	X	
13	X	X		X			X		X		X		X	X	
14					X	X	X		X		X		X	X	
15					X	X	X	X		X		X	X	X	
								X		X		X	X	X	

Flight Envelope

Since the effects of altitude are adjusted for in the data analysis, the tests were performed anywhere within the altitude envelope of the glider. Data points were taken anywhere from approximately 10,000 to 5,000 feet above mean sea level (MSL). Flight velocity was varied from 50 knots to 110 knots in ten knot increments. The kinematic viscosity of air increases with altitude which tends to lower the Reynolds numbers. Therefore the data points were taken in order of increasing airspeed as the glider descends, thus producing the largest range of Reynolds numbers.

Flight Profile

The typical flight profile consisted of the following steps.

- **Takeoff and climb out** This was accomplished with the internal engine.
- **Level out at test altitude** The test altitude was approximately 9,000 feet MSL. The test altitude was determined by the pilot based on turbulence and air traffic. Since turbulence is usually greater near the ground, sometimes it was necessary to climb higher then 9,000 feet MSL. Once the test altitude is reached, the engine is stored.
- **Warm up hot film system** Prior to flying the first test point, power was applied to the anemometer cards to allow them to warm for two minutes.
- **Stabilize airspeed** The airspeed was held at the test velocity.
- **Record data point**. To record the point, the data record button was pressed. Immediately after the data point, the airspeed, altitude, and outside air temperature was recorded on the pilot's lap board.
- **Repeat** Repeat for next velocity until all points are completed.
- **Land** The landing were done in glider mode with the engine retracted.

This procedure was repeated for fifteen flights over the course of three months. One or two flights were accomplished per flight day.

CHAPTER 6

Theoretical Modeling of the Airfoil

Theoretical modeling of the airfoil was necessary in order to determine such factors as velocity distribution, pressure gradient, and boundary layer thickness. Determination of these factors were necessary in order to evaluate the influence on step induced transition. Since physical measurement of the airfoil flow field was not feasible, theoretical prediction of the boundary layer was required. These factors were then compared to the test data in order to discern any possible correlation with transition.

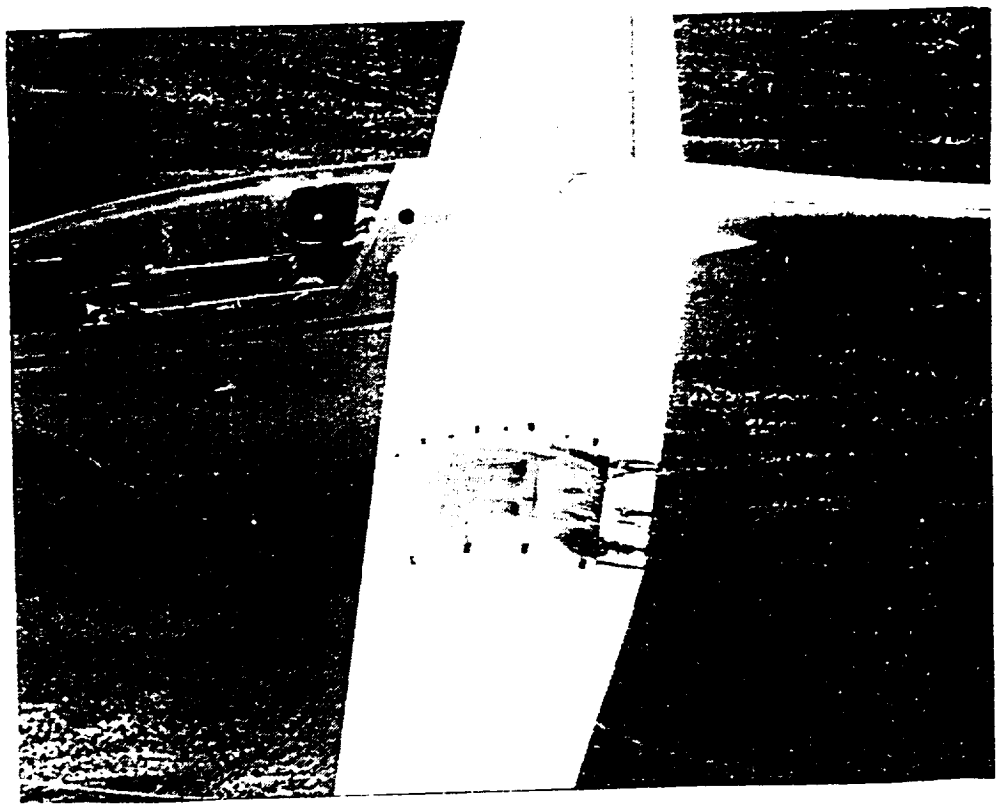

Figure 14. -Oil flow on wing.

The airfoil on the PIK-20E is designed to have extensive regions of laminar flow. Previous unpublished NASA Dryden flow visualization experiments with the PIK-20E have shown laminar flow to exist to approximately 57% of the airfoil chord with a laminar separation bubble occurring at transition. Figure 14 shows the test aircraft with a mixture of oil and graphite on the left wing. The dark band at 58% chord indicates laminar separation and the light band at 62% indicates turbulent reattachment. This transition mechanism is consistent with the low chord Reynolds numbers flown in this experiment. The chord Reynolds number at the test section varied from a maximum of 2,400,000 to 850,000 depending on altitude and airspeed. At these low Reynolds numbers, a laminar separation bubble is assumed to be the mechanism for transition. Therefore, it became a matter of locating the point of laminar separation to determine the transition location.

In order to better define the flow field over the upper surface of the airfoil it was necessary to model the flow field using two theoretical techniques. Both techniques are integral techniques. A program named Profile was used for the analysis. This program was created by Eppler and Sommers (Eppler, 1980). Profile is a combination of an inviscid panel method and integral boundary layer program. In addition to the Profile analysis, a second analysis using Karmen Pohlhausen integral equations was performed. These equations were programmed on a personal computer. The results of these procedures are provided here and the details of these techniques are explained further in appendices B and D.

Before either of these analysis techniques could be implemented, an accurate airfoil contour had to be mapped out. On sailplanes, it is very common for the actual aircraft airfoil to be very different then the specified airfoil. This was the case with the PIK-20E airfoil. The procedure for measuring the airfoil involved making a plaster cast of the airfoil, measuring the coordinates, and smoothing the coordinates with a computer program. This procedure is described and detailed in appendix C.

For determining separation and transition on laminar flow airfoils, the most important factor is pressure gradient. Using an inviscid panel method, Profile calculates the pressure gradient for a given angle of attack, α. A plot of chordwise pressure gradients are shown in figure 15. In order to have a good sampling of pressure gradients, the step locations were chosen at x/C=10.5%, 24.4%, and 42.6%.

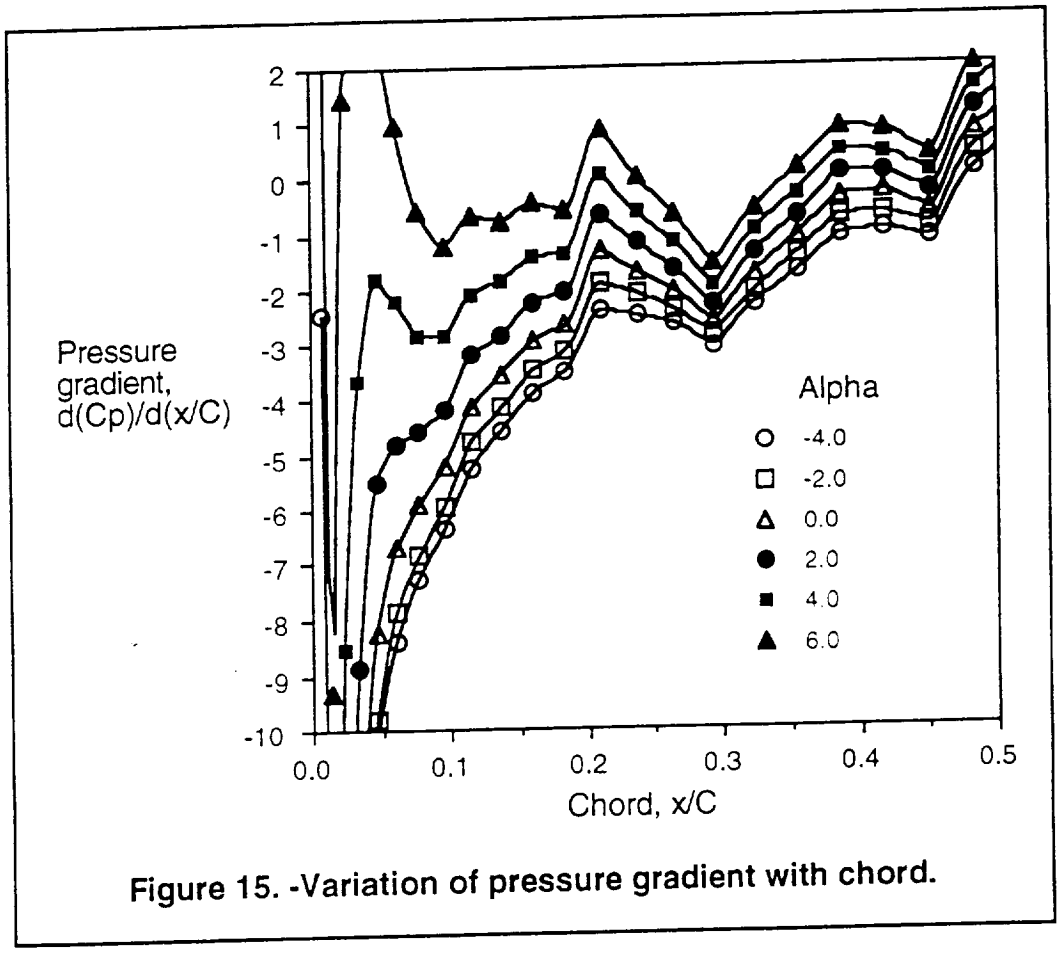

Figure 15. -Variation of pressure gradient with chord.

With the pressure gradient known, the boundary layer shape factor can be calculated using a Karmen Pohlausen (K&P) analysis. This process is detailed in appendix D. Shape factor is a useful measurement of boundary layer stability. The shape factor, H_{12} is defined in equation 6.

$$H_{12} = \frac{\delta_1}{\delta_2} \tag{6}$$

In equation 6, δ_1 is the displacement thickness and δ_2 is the momentum thickness. Figure 16 shows the variation of shape factor H_{12} with chord location. Separation is likely to occur when the shape factor H_{12} reaches 3.5. This corresponds to the criteria for separation in the K&P analysis (Schlicting, 1979).

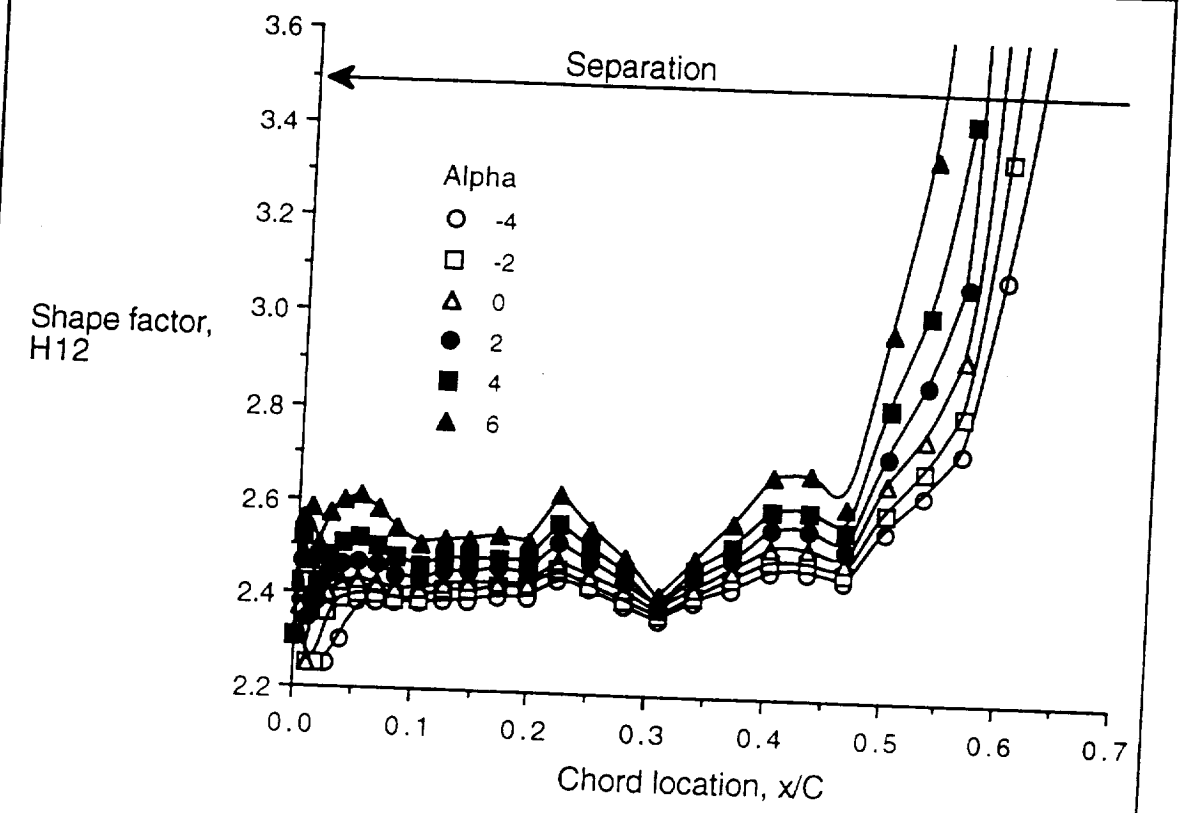

Figure 16. -Variation of shape factor H_{12} with chord.

In the K&P analysis, the separation point is used as the location of the start of the laminar separation bubble. Using this criteria, the transition location was plotted and is shown in figure 17. Overlaid on this figure is a plot of transition location as predicted by Profile. The criteria for transition in the Profile program is an empirical relationship based on shape factor and momentum thickness Reynolds number.

Both methods agree within 3% chord except when $\alpha = 6°$. At $\alpha = 6°$ the aircraft is at stall speed. At this angle of attack, the airfoil would most likely have separation over most of the upper surface.

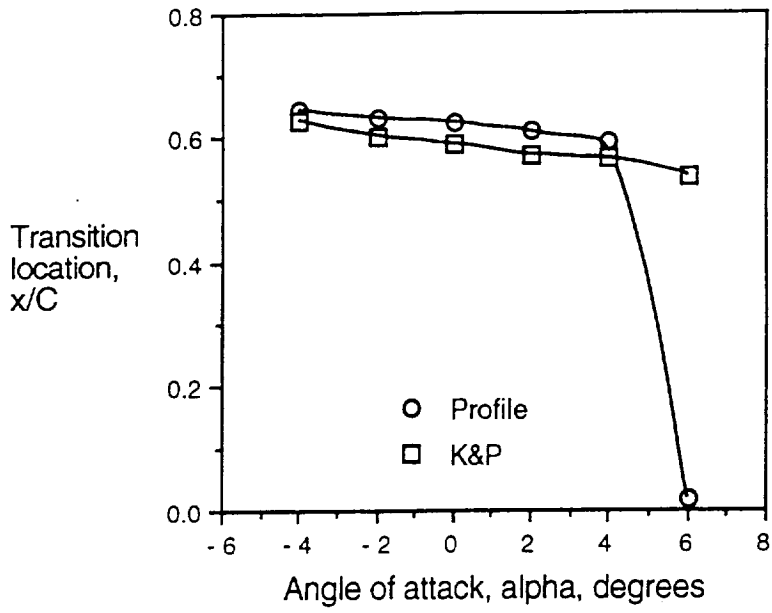

Figure 17. -Variation of predicted transition location with angle of attack.

CHAPTER 7

Reduction of Flight Data

Calculating Local Velocity

For each of the data points, the airspeed, altitude, and outside air temperature (OAT) were recorded by the pilot on a lap board. What follows in this section is a description of how these quantities were used to determine the boundary layer conditions over the test section. In addition, a brief error analysis of the procedure is presented.

There are many steps involved in determining the local flow velocity over the test steps, u. The local velocity is derived from indicated airspeed, V_i, outside air temperature, and altitude. This process is diagramed in figure 18.

First the indicated velocity, V_i, is converted to true velocity, V_t. This is accomplished with the following equations 7 through 13 (Roberts, 1980).

Equation 7 corrects for instrument error.

$$V_{ic} = V_i + \Delta V_{ic} \tag{7}$$

In equation 7, V_{ic} is the airspeed corrected for instrument error and ΔV_{ic} is the instrument correction. A laboratory calibration for the airspeed indicator was not available. Previous flight test experiments have shown ΔV_{ic} to be negligible and therefore it is assumed zero.

Equation 8 corrects for position error.

$$V_c = V_{ic} + \Delta V_{pc} \tag{8}$$

In equation 8, V_c is the calibrated airspeed and ΔV_{pc} is the position error correction.

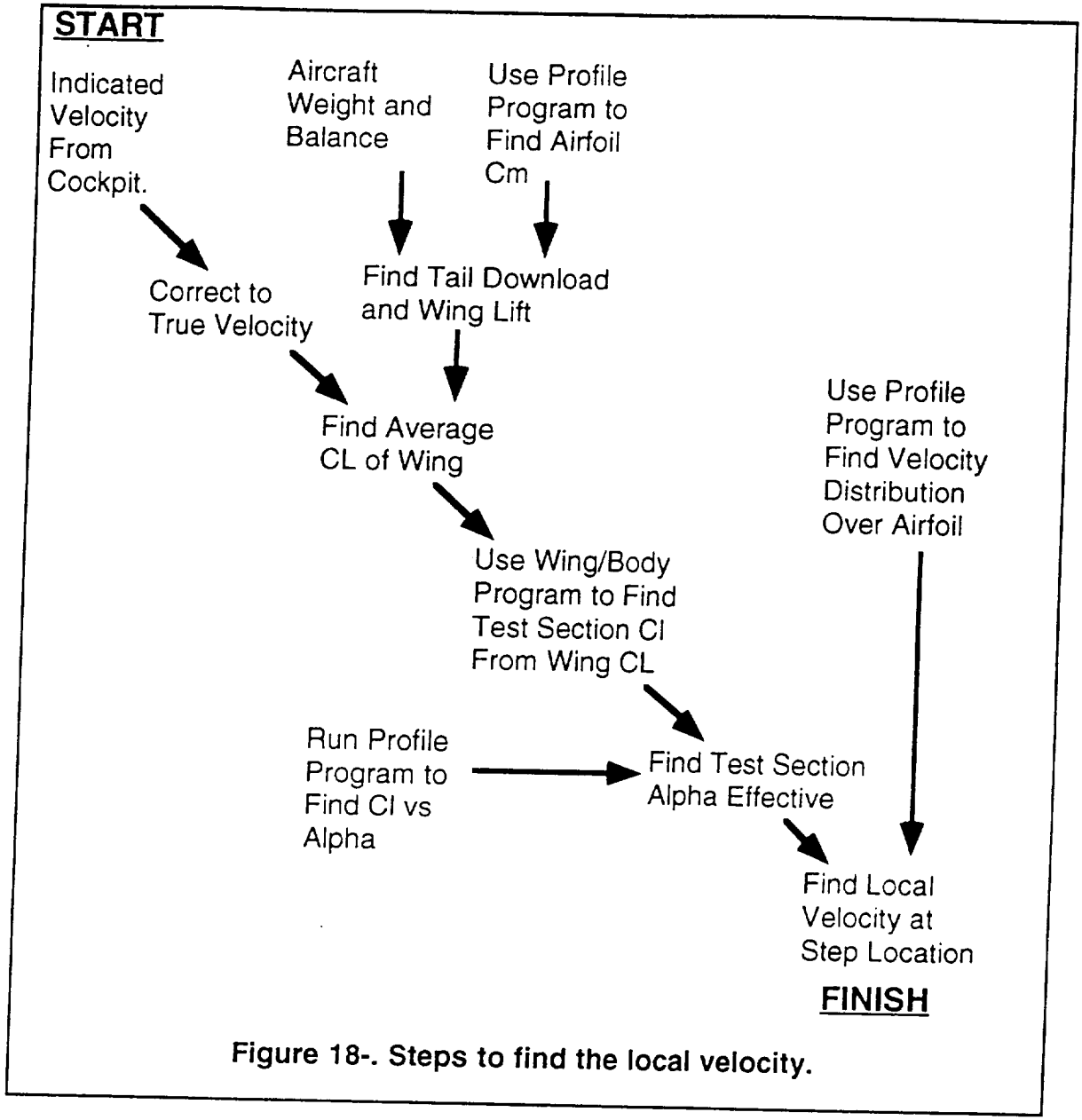

Figure 18-. Steps to find the local velocity.

The flight manual for the PIK-20E shows a graph of ΔV_{pc} verses Vic. For the range of airspeeds tested in this experiment the correction can be closely approximated by Equation 9.

$$\Delta V_{pc}'' = -0.010500 * V_{ic} + 1.5173 \text{ Knots} \quad (9)$$

Next the calibrated airspeed is corrected for scale altitude correction in equation 10.

$$V_e = V_c + \Delta V_c \tag{10}$$

In equation 10, V_e is the equivalent airspeed and ΔV_c is the scale altitude correction. The effect compressibility is negligible for this experiment and therefore ΔVc is assumed zero.

Next the equivalent airspeed is corrected for air density in equation 11.

$$V_t = \frac{V_e}{\sqrt{\sigma}} \tag{11}$$

In equation 11, the density ratio, σ, can be defined by the following two equations:

$$P_a = P_o * (1\text{-}6.87335E\text{-}6*H_i)^{5.2561} \tag{12}$$

$$\sigma = \frac{P_a / P_o}{T / T_o} \tag{13}$$

In equation 12, P_a is the ambient air pressure, H_i is the indicated pressure altitude, P_o is the standard atmosphere sea level pressure, T is the outside air temperature and T_o is the standard atmosphere sea level temperature.

With these equations, the aircraft true velocity can be determined. Calculations of aircraft true velocity for the flight data were performed and the results are contained in table E.1 in Appendix E.

The next process was to weigh the aircraft and determine the aircraft center of gravity (CG). Finding the aircraft CG is necessary in order to calculate the tail download verses velocity so that the total wing lift verses velocity can be determined. This defines the relationship between the aircraft lift coefficient, $Cl_{A/C}$ and equivalent velocity, V_e. The aircraft moment arms are shown in figure 19.

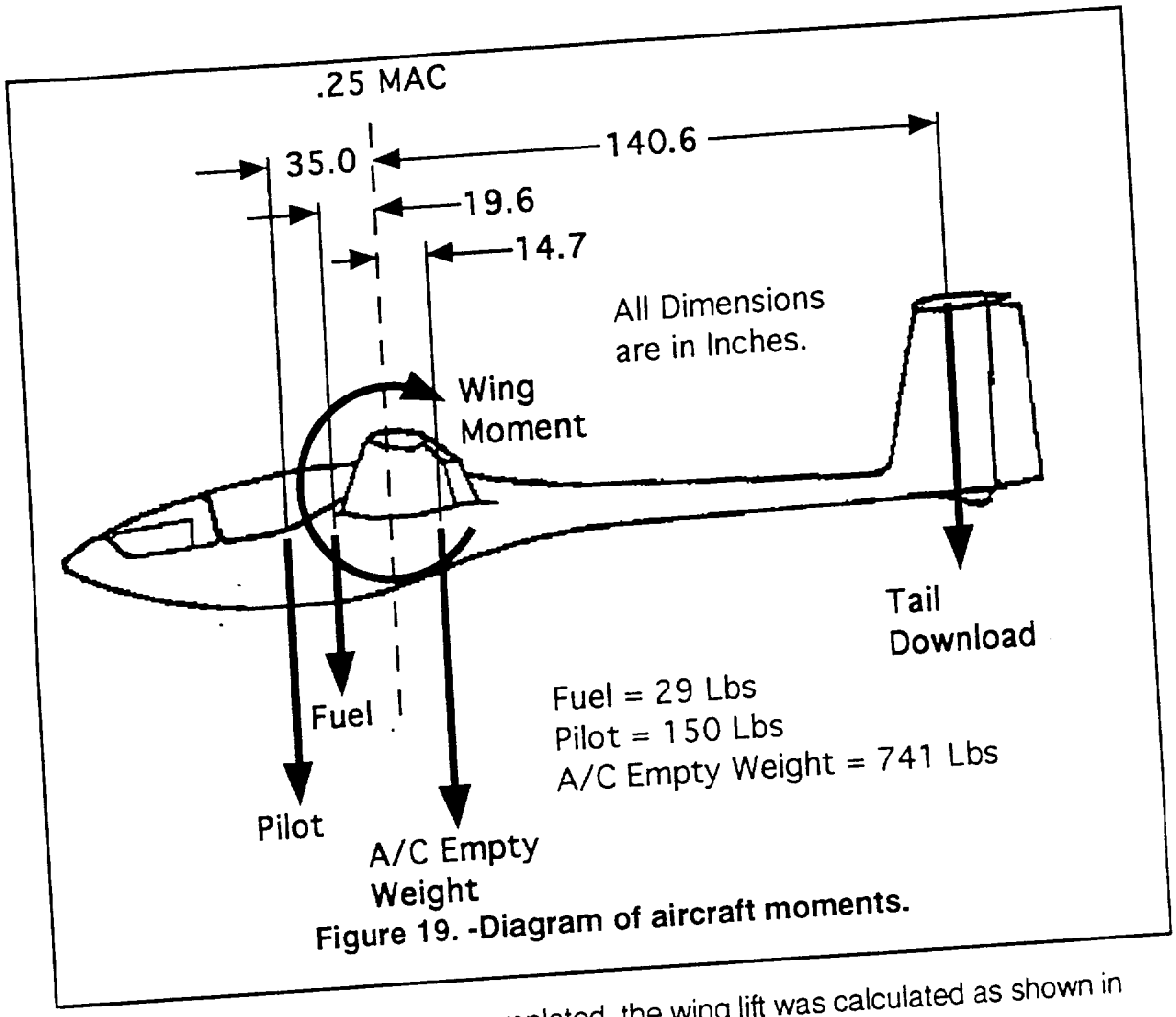

Figure 19. -Diagram of aircraft moments.

With the CG calculation completed, the wing lift was calculated as shown in table 5. Two simplifying assumptions were made in this analysis. First, the fuselage moment is negligible. A reasonable assumption for sailplane fuselages. Second, an average fuel weight was assumed since the fuel variation does not significantly effect the weight or CG.

Table 5. -Calculation of tail downloads.

All moments taken about the quarter MAC.
Pitch up is positive.

Weights (Lbs)	Moment Arms (In)	Moments (Ft-Lbs)
Fuel = 29	Fuel = -19.6	Fuel = -47.4
Pilot = 150	Pilot = -35.0	Pilot = -437.5
A/C = 741	A/C = 14.7	A/C = 907.7
	Tail = 140.6	

Airfoil Cm = -0.135
Wing Area = 107.6 Ft^2
MAC = 2.30 Ft

V e	V e	q	Wing Momt	Total Momt	Tail Load	Wing Lift
Knots	ft/s	PSF	Ft-Lbs	Ft-Lbs	Lbs	Lbs
50	84.4	8.48	-283.2	139.7	-11.9	908
60	101.3	12.20	-407.7	15.1	-1.3	919
70	118.2	16.61	-555.0	-132.1	11.3	931
80	135.1	21.70	-724.9	-302.0	25.8	946
90	152.0	27.46	-917.4	-494.6	42.2	962
100	168.9	33.90	-1132.6	-709.8	60.6	981
110	185.8	41.02	-1370.5	-947.6	80.9	1001
120	202.7	48.82	-1631.0	-1208.1	103.1	1023

With the amount of wing load determined, the angle of attack at the test section can be determined. The results are shown in table 6. The calculations for table 6 use equations 14 through 16. Plots of the airfoil Cl verses α relationship are found in Appendix B. The relationship between section and wing lift coefficient is developed in Appendix A.

$$q = 0.5 * \rho_o * V_{eq}^2 \quad (14)$$

$$Cl_{A/C} = \frac{\text{Wing Lift}}{q * S} \quad (15)$$

$$Cl_{TS} = \frac{Cl_{A/C}}{0.9496} \quad (16)$$

In the above equations, q is the dynamic pressure, ρ_o is standard sea level air density, S is the projected wing area, and Cl_{TS} is the test section lift coefficient.

Table 6. -Calculation of test section angle of attack.

Wing Area = 107.6 ft^2
Wing Chord at Test Section = 27.4 in
Approximate Value For Kinematic Viscosity = 2.1E-06 ft^2/s

V e Knots	V e ft/s	q PSF	Wing Lift Lbs	$Cl_{A/C}$	Re	Cl_{TS}	T.S. Alpha degrees
50	84.4	8.48	908	1.00	9.2E+5	1.05	4.4
60	101.3	12.20	919	0.70	1.1E+6	0.74	2.3
70	118.2	16.61	931	0.52	1.3E+6	0.55	-0.1
80	135.1	21.70	946	0.41	1.5E+6	0.43	-1.4
90	152.0	27.46	962	0.33	1.7E+6	0.34	-2.3
100	168.9	33.90	981	0.27	1.8E+6	0.28	-2.8
110	185.8	41.02	1001	0.23	2.0E+6	0.24	-3.2
120	202.7	48.82	1023	0.19	2.2E+6	0.21	-3.3

The values from table 6 were plotted in figure 20 to show the relationship between test section angle of attack and equivalent velocity.

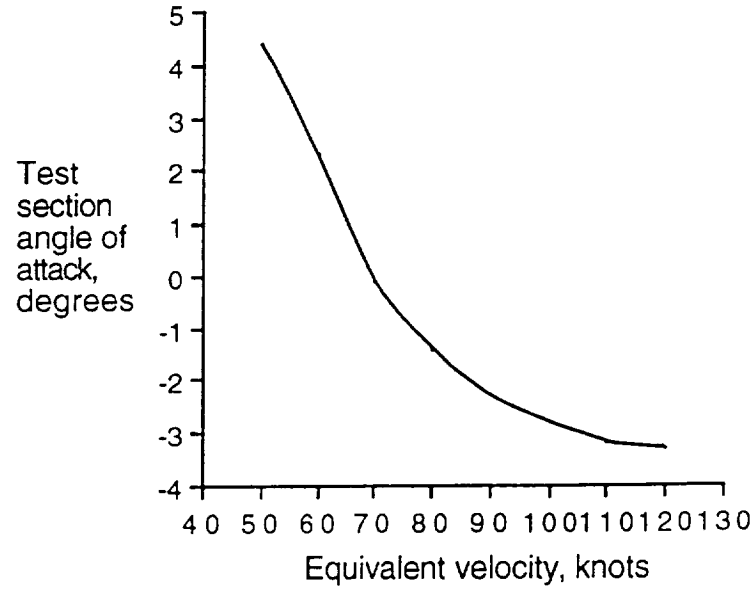

Figure 20. -Variation of test section angle of attack with velocity.

The final step is to determine the airflow velocity over the step. The local step velocity is plotted verses angle of attack in figure 21. The velocity distribution over the airfoil was found from the Profile airfoil analysis (see figure B.1 in appendix B). The test steps were located at 10.5%, 24.4%, and 42.6% chord on the wing. The relationship between the local airflow velocity, u, and angle of attack, can be closely approximated by the linear relationships given in equations 17 through 19. The angle of attack, α, is in degrees.

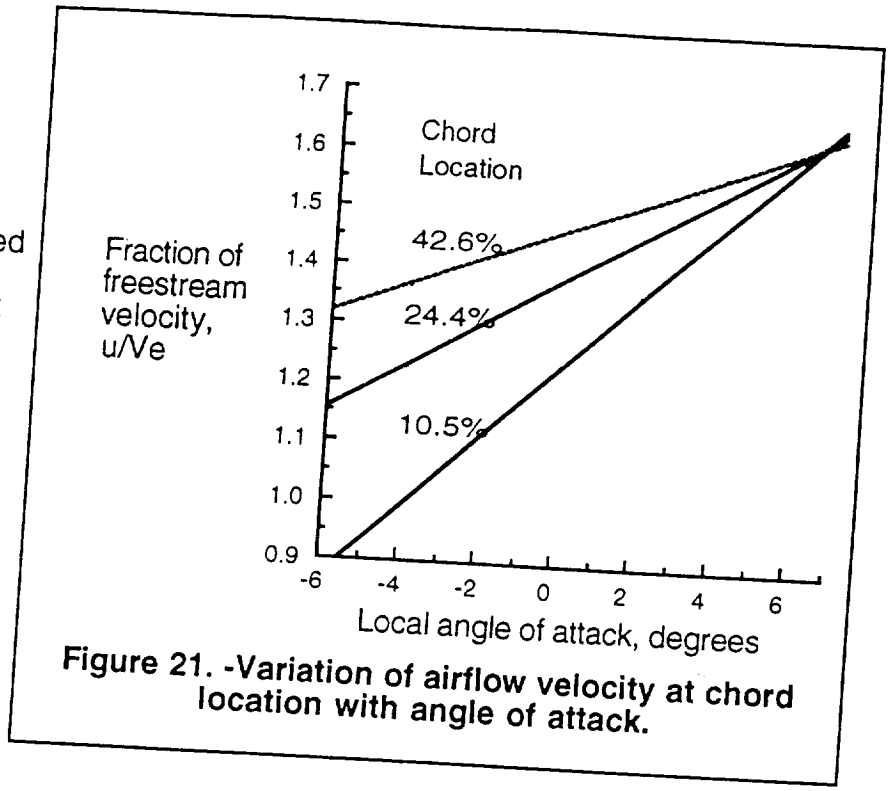

Figure 21. -Variation of airflow velocity at chord location with angle of attack.

$$\frac{u}{V_e} = 1.235 + 0.06056 * \alpha \quad @ \ 10.5\% \text{ chord} \tag{17}$$

$$\frac{u}{V_e} = 1.381 + 0.03797 * \alpha \quad @ \ 24.4\% \text{ chord} \tag{18}$$

$$\frac{u}{V_e} = 1.467 + 0.02500 * \alpha \quad @ \ 42.6\% \text{ chord} \tag{19}$$

With the local flow velocity defined in figure 21, the step Reynolds number can be calculated from equation 20. The step Reynolds numbers for the flight data are contained in table D.2 in appendix D. Graphs of the step Reynolds numbers are contained in the Results and Discussion section.

$$Re_h = \frac{u * h}{\nu} \tag{20}$$

Error Estimate in Velocity Calculation

Since the calculation of the local velocity at the step involves eight main calculation procedures, the local velocity estimation has a relatively large margin of error. Table 7 lists the steps and their estimated.contribution to this error. The estimated total possible error is approximately 18.1%.

Table 7. -Contributions to velocity error.

Cockpit Instrument reading error	1.6%
Instrument error	3.0%
Calculation of air density	2.0%
Calculation of aircraft lift coefficient	5.5%
Calculation of test section lift coefficient from Wing Body	2.0%
Calculation of test section angle of attack from Profile	2.0%
Calculation of local velocity from Profile	2.0%
Total possible error	18.1%

A better way to find the local velocity would have been to directly measure the pressure distribution over the airfoil surface. Unfortunately, the aircraft could not be instrumented for pressure within the time and budget constraints. Typical pressure instrumentation of a wing provides good results with error of less than 2% in reading the pressure field. This would have been a great improvement in accuracy over the estimation technique used in this study.

CHAPTER 8

Hot Film Data Analysis

Reading the Hot Film Signals

The analysis of hot film signals is an established method of determining laminar, transitional, and turbulent flow on low speed aircraft (Holms, 1984; Obra & Holmes, 1985; Manuel, et al, 1987; Croom, et al, 1987). The hot film data from this experiment is generally easy to interpret, however there are a few unexpected results.

Transition has been traditionally determined by one or more of the following methods: the amplitude of raw signals, root mean square (RMS) average of the raw signals, spectral content of the signals, and intermittency factor of the signals (Flight Instrumentation.., 1989). For this experiment, the first method of signal amplitude proved to be the most useful. Signal amplitude was quantified by taking the standard deviation of the signal. RMS values of each signal also proved valuable for analysis. However, analysis of the spectral content of the signal provided no usable results. Finally, intermittency factor proved to be too cumbersome and not very illustrative.

Every flow regime has a characteristic signal. A laminar boundary layer signal is typically characterized by a low amplitude signal. During transition the signal has high intermittence and peak RMS values. When the flow becomes completely turbulent the output is characterized by large amplitude, broad-band frequency spectrum signals (Flight Instrumentation.., 1989). The hot film data from this experiment generally follows these trends, however in this experiment it is not easy to discern the difference between a transitional and fully turbulent signal. This is

probably due to the complex transition mechanism that occurs in a laminar separation bubble.

Figure 22 shows the five main types of signals that were produced from the flight data. The laminar and turbulent signals are easy to distinguish. However, there is an unusual signal found at the theoretical location of separation. The signal is unusually quiet (low amplitude, low RMS intensity). This signal can only be explained as being produced by separation were the surface velocity is zero. Ahead of the separation point, the signal is very quiet with small spikes that can best be described as upward facing teeth. Aft of the separation point, the signal is very quiet with downward facing teeth. This is most likely caused by the flow forming a separation bubble with reversed flow inside the bubble. After the separation bubble, the signal is fully turbulent which would indicate turbulent reattachment aft of the separation bubble.

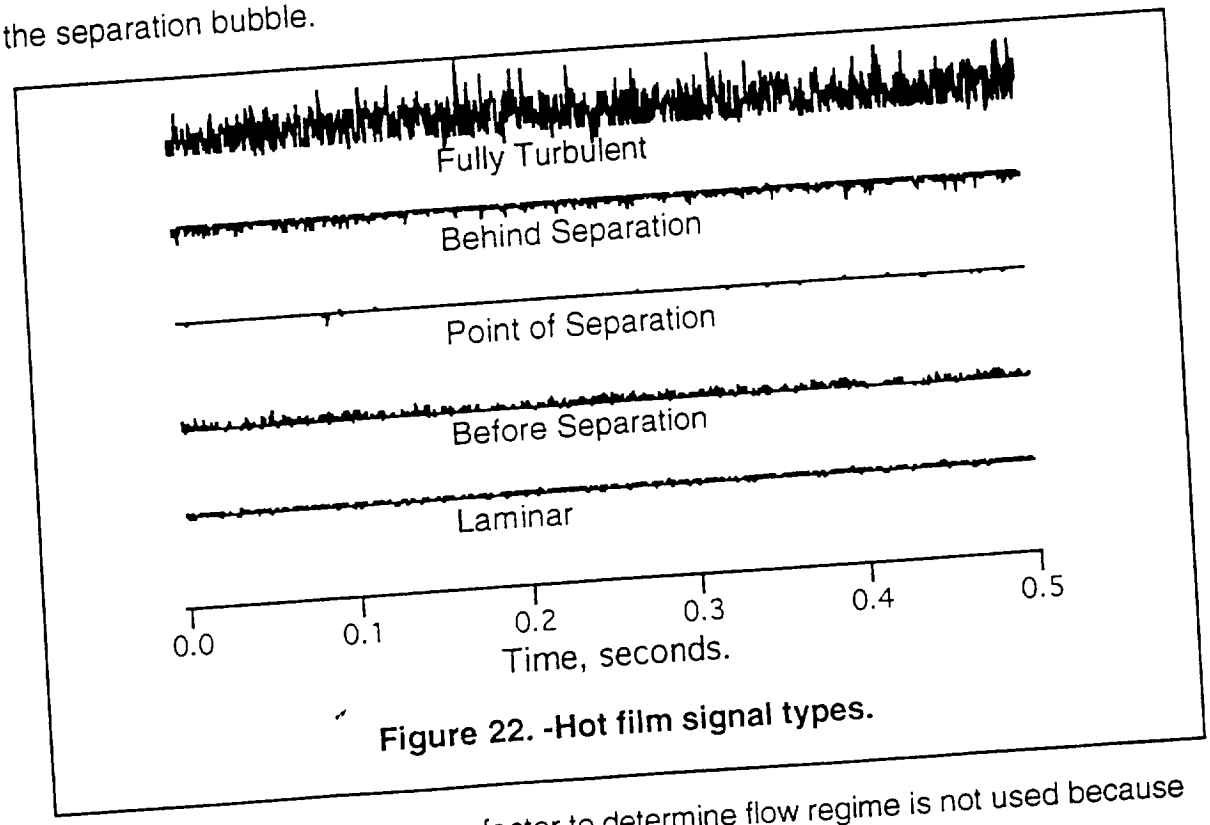

Figure 22. -Hot film signal types.

The use of intermittency factor to determine flow regime is not used because it requires that the time between turbulent bursts be manually counted from a signal

time plot. With the amount of flight data produced in this experiment, this would be very time consuming. Intermittency factor was forgone in favor of more automated methods.

In other hot film studies, the flow separation point has been successfully determined using the phase reversal signal (PRS) technique (Stack, et al 1987). The flow separation point was detected by observing a phase reversal in signals from sensor elements across the separation point. This could be seen when the signals were passed through a 300 Hz or lower filter. The resulting signals were seen to be approximately 180 degrees out of phase around the separation point.

In this experiment, the flight data was passed through filters ranging from 1000 Hz to 10 Hz without a phase reversal being evident. A phase reversal could not be found even where a separation was known to exist. The relatively large spacing between sensors is the most likely the reason that the PRS technique was not successful. The previously cited study used a 0.250 inch sensor spacing while the spacing is this experiment was 1.00 inch.

After the first nine flights, a trip strip test was flown in order to check the interpretation of the hot film signals. With a trip strip placed on the wing, a turbulent signal was produced. This signal was used in order to differentiate between a transitional and fully turbulent signal. Figure 23 contains a 0.10 second sample from each of the eight active hot films. At the left of each signal is the chord location of each sensor and the bottom axis shows the velocity in knots indicated airspeed. It is easy to differentiate the laminar and turbulent signals from this flight.

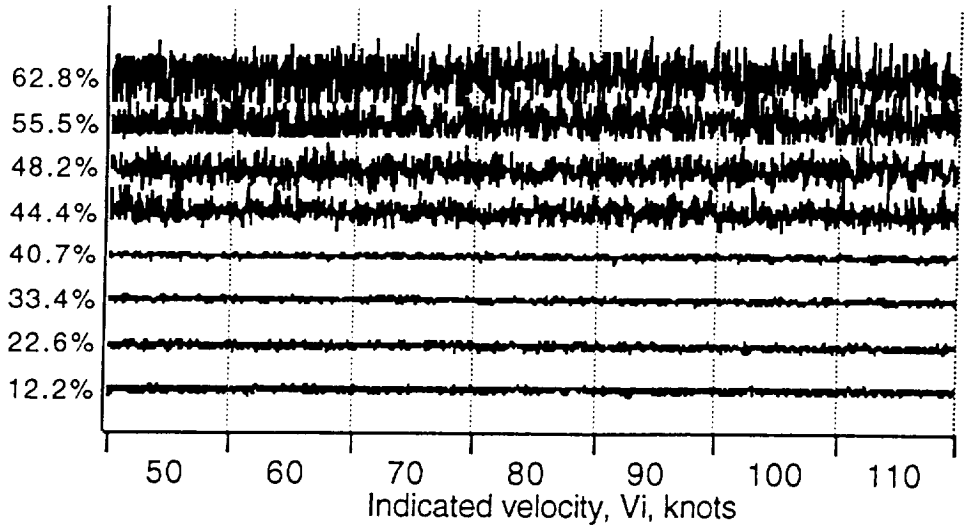

Figure 23. -Samples from each airspeed, trip strip at 42.6%.

Figure 24 contains a graph of RMS signal intensity for the trip strip flight. The units on the left of the plot are uncalibrated signal counts. There is a small peak in RMS value at the 44.4% sensor followed by a dip in RMS value across all of the airspeeds. The peak RMS value indicates peak transition. This characteristic peak and dip is repeated in other flights where transition occurs.

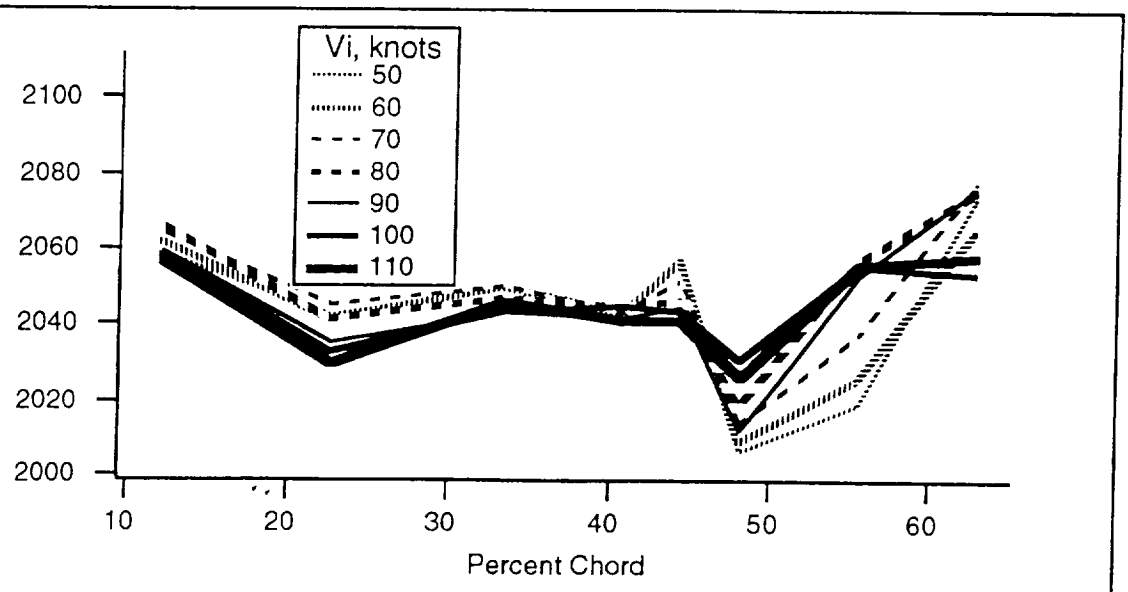

Figure 24. -Variation of RMS signal Intensity with chord, trip strip at 42.6%.

Figure 25 contains a graph of signal standard deviation. The large jump in standard deviation from around 23 to 85 signal counts clearly marks the transition location. This increase in standard deviation is found in all of the step transition data flights.

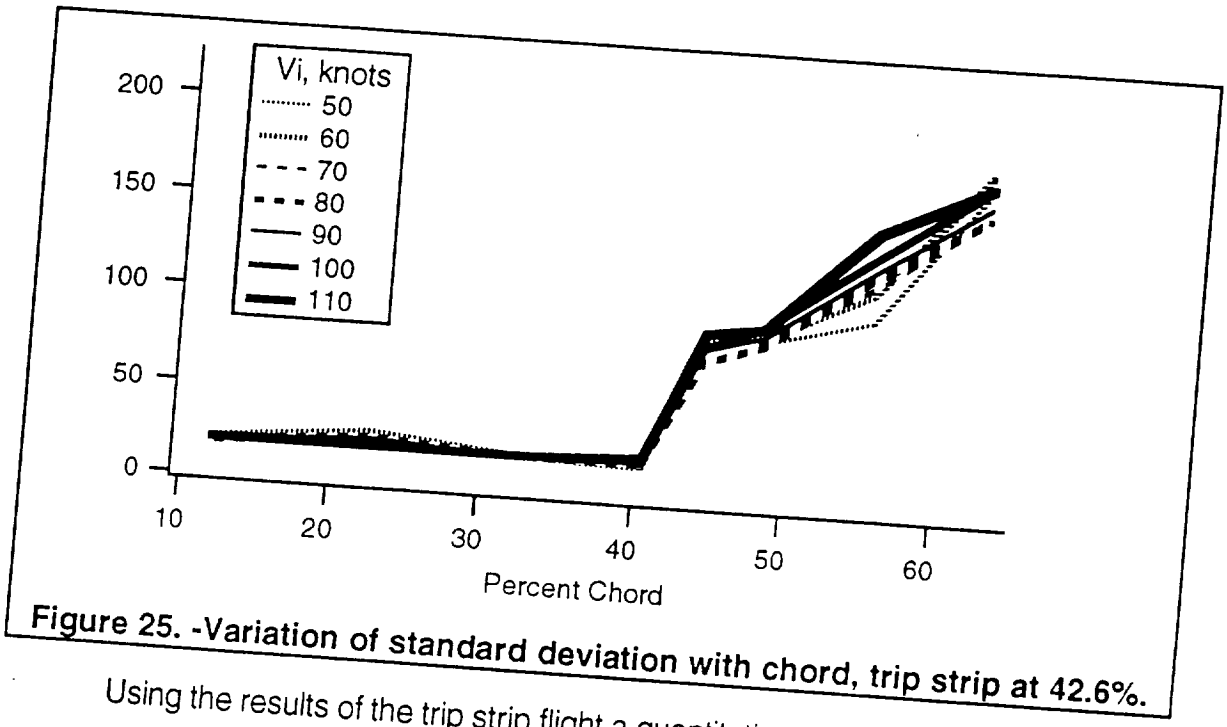

Figure 25. -Variation of standard deviation with chord, trip strip at 42.6%.

Using the results of the trip strip flight a quantitative method of differentiating signals was developed. In this study, signals with a standard deviation of less then 50 signal counts are considered laminar. Signals in the 50 to 85 range are considered a turbulent burst, and signals over 85 are defined as transition.

The resulting signals from the trip strip flight were consistent with the signal interpretation up to this flight. With confidence that the hot film data was correct, the flight tests were continued.

Determination of the Natural Transition Location

In order to illustrate the method of interpreting the hot film signals, the procedure for analyzing the data from flight 1 will be illustrated in the following section. In flight 1, the wing was in the smooth configuration. Figure 26 shows a 0.10 second sample from each of the eight hot films.

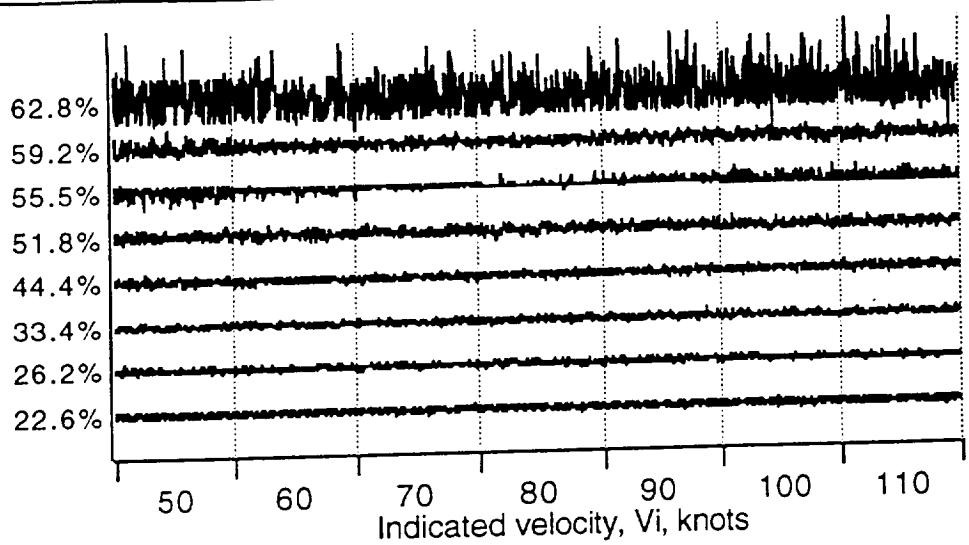

Figure 26. -Samples from each airspeed, smooth wing.

The quiet signal at the 55.5% chord sensor between 70 and 80 knots airspeed indicates the movement of the laminar separation bubble over the sensor. Transition in a laminar separation bubble is further supported by the higher RMS signal intensity at the 55.5% location for the 70 and 80 knots airspeed. This is demonstrated in figure 27.

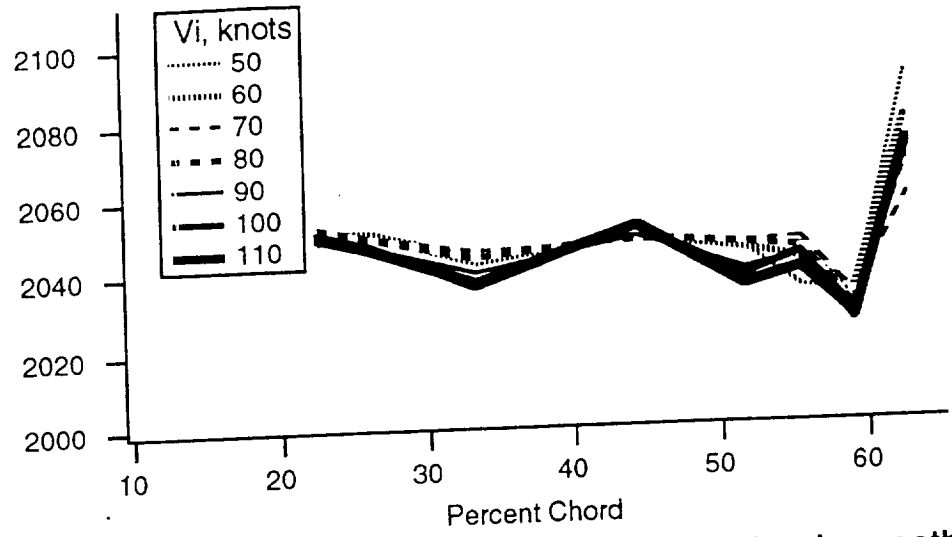

Figure 27. -Variation of RMS signal intensity with chord, smooth wing.

However, the standard deviation of the signal is still small at the 59.2% chord sensor leading to the conclusion that it is within the laminar separation bubble. The standard deviation is shown in figure 28. This would size the laminar separation bubble to between 4% and 7% chord.

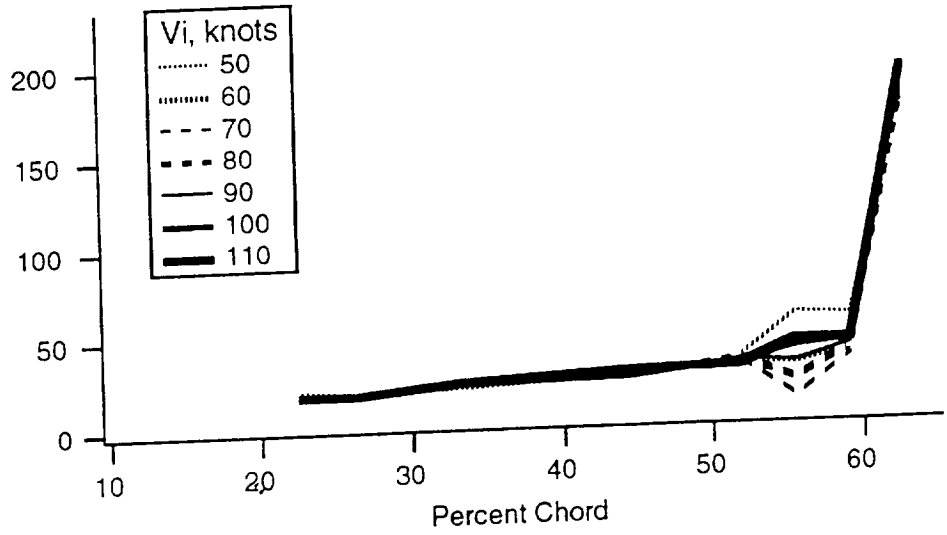

Figure 28. -Variation of standard deviation with chord, flight 1, smooth wing.

Problems with the Hot Film Data

The hot film data in this experiment suffered from three problems. One constant problem was contamination of the wing surface. Dirt and insect strikes had probably caused some premature transition. Also, atmospheric moisture had caused premature transition during at least one of the flights. The second problem was an intermittent electronics error in the data acquisition system which showed itself on four of the test flights. Finally, the most serious problem was one of transition caused by the corner of the vinyl sheet used to form the step.

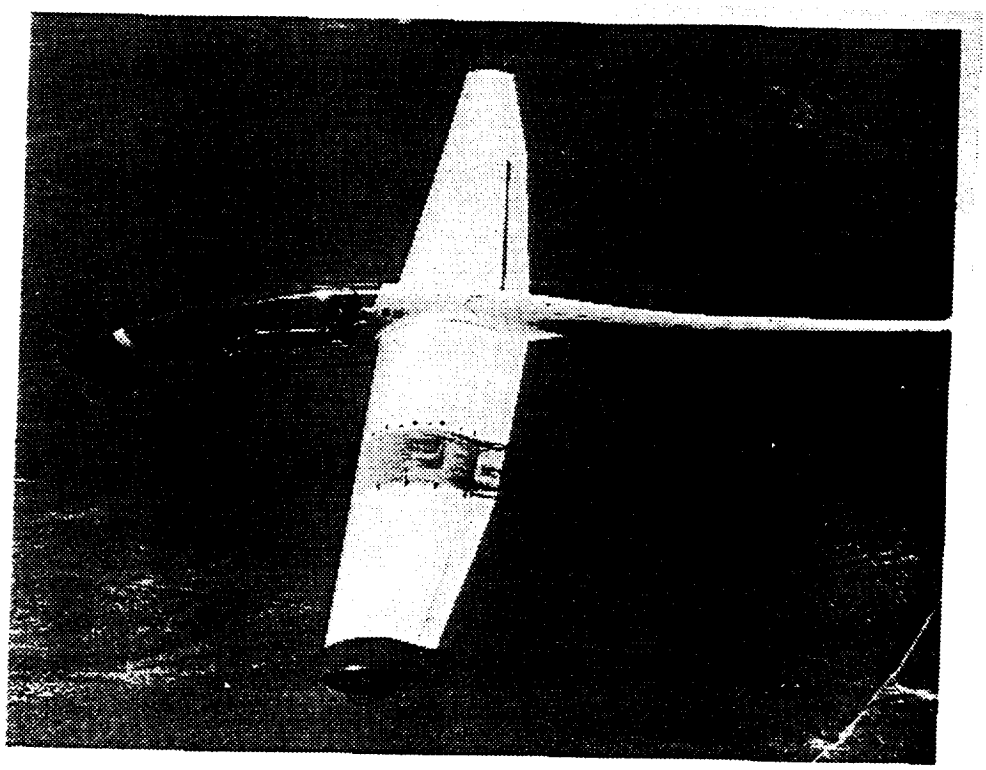

Figure 29. -PIK-20E oil flow experiment.

Contamination of the wing surface is a common problem when trying to maintain extensive laminar flow. In a previous oil flow experiment on the PIK-20E, a dark oil was put on the wing to show transition. Figure 29 shows a premature transition wedge obviously caused by some contamination on the wing surface. The

flight data from the hot film sensors tends to support the conclusion that extensive regions of laminar flow are difficult to maintain.

Other flight experiments have documented premature transition caused by atmospheric moisture (Flight Instrumentation.., 1989). During flight 9, some of the data indicates premature transition. Flight 9 also encountered a small amount of rain during the flight. The rain is the most likely cause of the premature transition. Figure 30 shows a sampling of hot film data from flight 9. This flight tested the effect of aircraft side-slip on the hot film data. In the figure, C = Center, L/2 = Half Left Rudder, L = Full Left Rudder, etc.

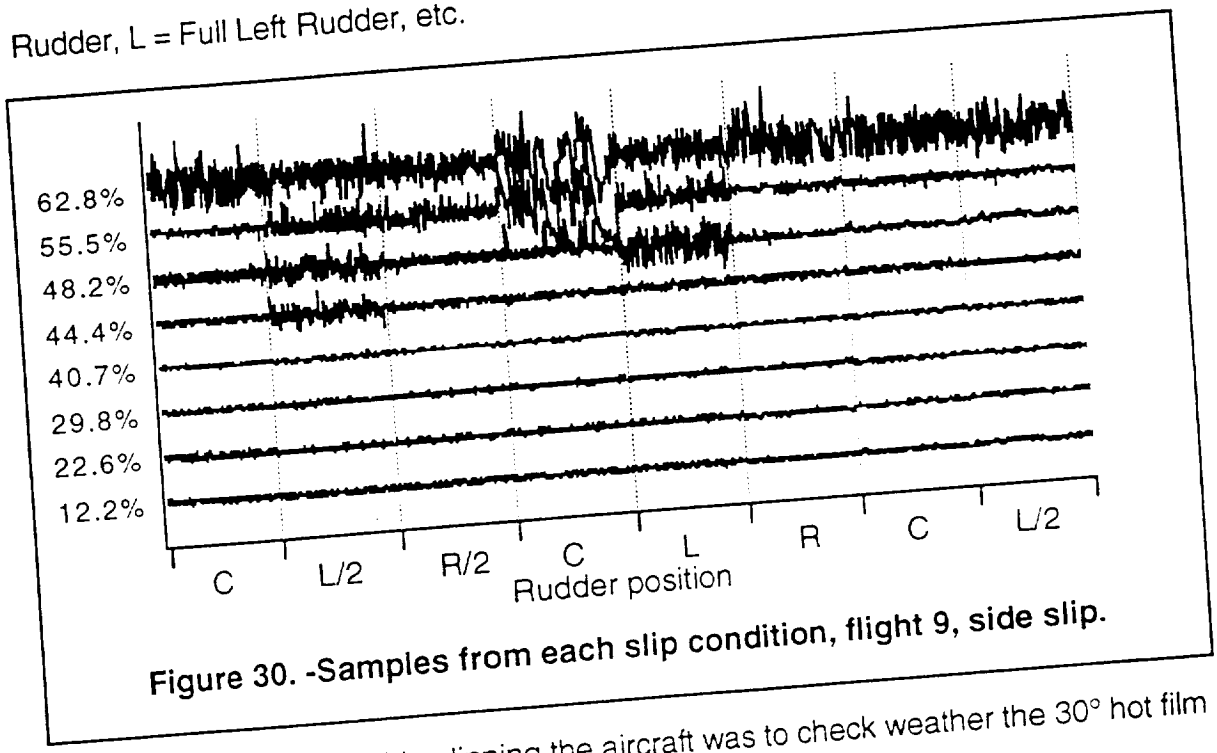

Figure 30. -Samples from each slip condition, flight 9, side slip.

The purpose of side-slipping the aircraft was to check weather the 30° hot film mounting angle was large enough to avoid causing hot film contamination. If the angle was insufficient then a hot film patch would be in the wake of the hot film patch ahead of it. Any interference would be aggravated by left side slip. The results of this flight are inconclusive. Although both of the left rudder test points shown in figure 30 show premature transition, contamination may not be the problem. The eighth data point, which is not shown, is a repeat of half left rudder and shows no premature

transition. This and the fact that there was premature transition in the no slip case, leads to the conclusion that the scattered rain during this flight test was the probable cause of the premature transition during flight 9.

Intermittent electronic noise was another problem encountered during the flight tests. The noise would occur only during flight test and could not be repeated on the ground despite much effort. The most common effect on the data was to cause the hot film signal to become filled with very high amplitude noise. Fortunately, the noise would rarely last more the a second or two. During the four seconds of data recording there would still be at least a second of good data. All of the obviously bad data has been omitted from the plots of the flight data whenever possible. However there was an unexplainable saw-toothed wave on three of the test points. This saw-toothed wave lasted all four seconds. This can be seen in flights 5, 9, and 11 (Figures E.5, E.9, E.11 in Appendix E). The erroneous signals from flight 5 were so bad that the entire test was repeated in flight 14.

The most serious problem with the flight data was inconsistent premature transition on only some of the sensors. The effect of this on the data was to cause sensors in the 20% to 45% chord range to show turbulent signals while sensors further aft would read laminar. This is best seen in the flight four data shown in figure 31. Since it is impossible for a turbulent boundary layer to become laminar, there must be a cone shaped turbulent wake behind the corner of the vinyl step.

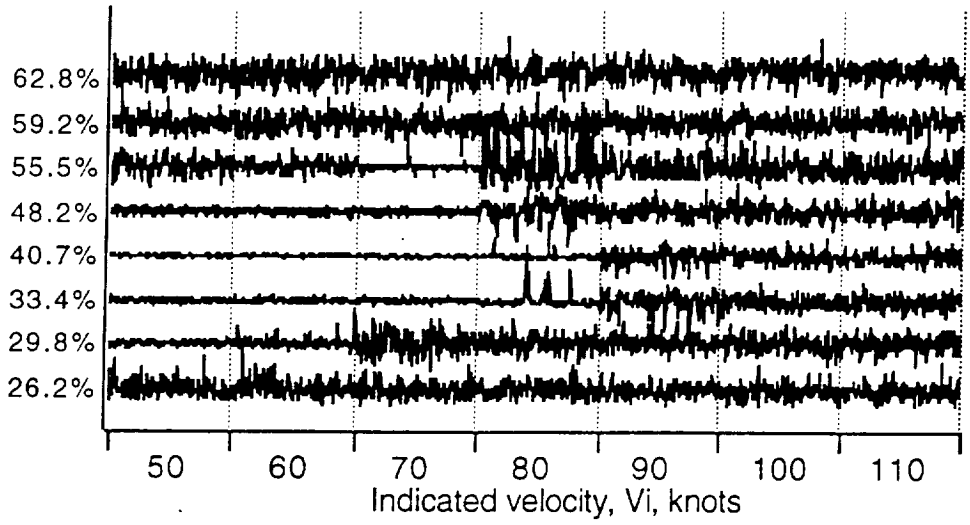

Figure 31. -Samples from each airspeed, flight 4, 0.0196 aft step at 24.4%.

The most probable cause of a turbulent cone would be from disturbances propagated by the corner of the vinyl sheet. Figure 32 shows a drawing of how the vinyl was placed on the wing. The vinyl was cut at an angle so as to avoid the hot films in front of the steps. In this way the step height could be changed without moving the hot films for each flight. This was a good solution considering that the hot film sensors could not be removed without being destroyed.

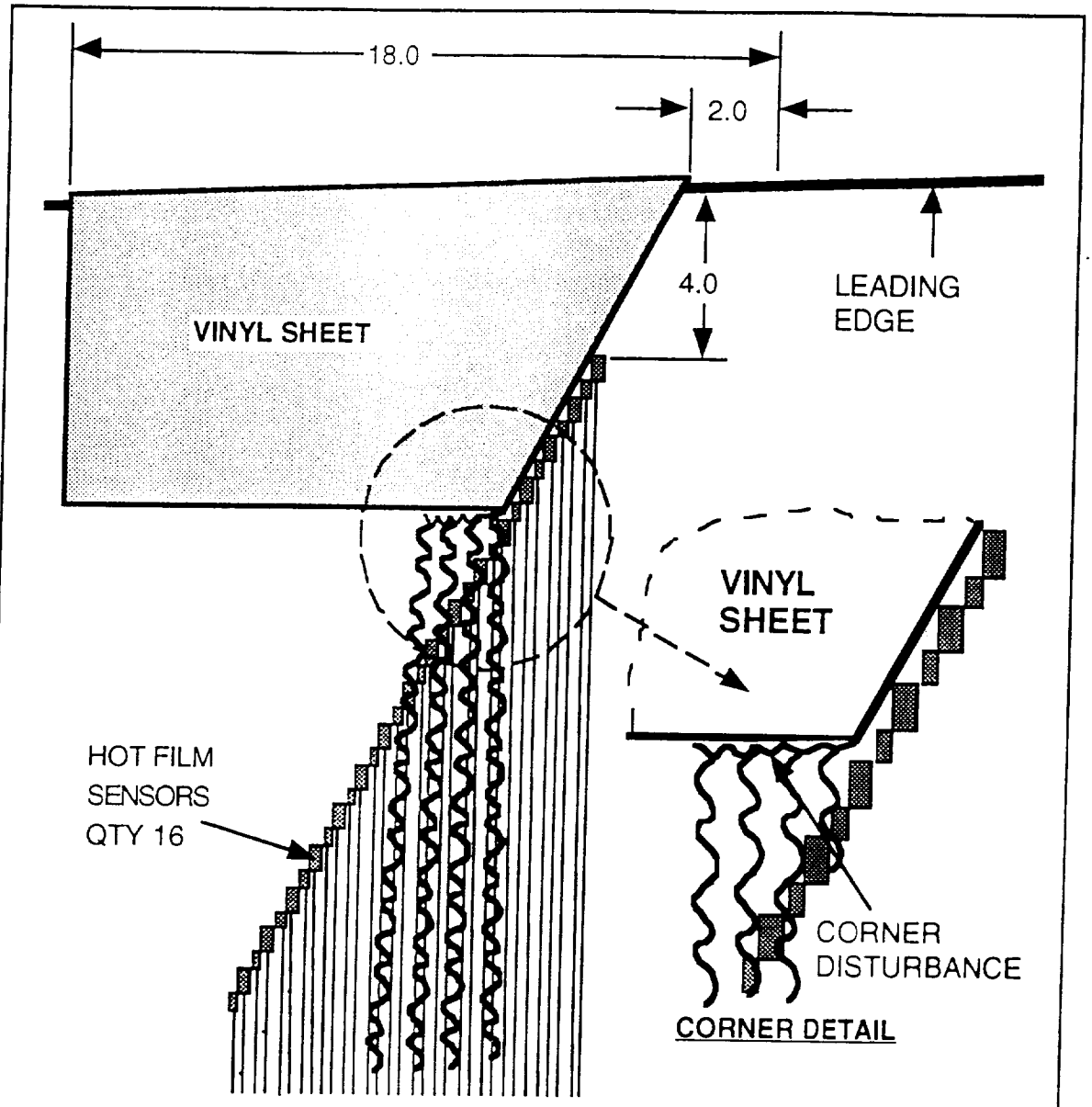

Figure 32. -Corner disturbance.

Unfortunately, the turbulence caused by the corner of the vinyl sheet did not leave the corner at the typical seven degree disturbance angle. The disturbance most likely propagated chordwise in the stagnation zone behind the step. This is similar to the disturbance propagation which causes leading edge transition. The result of this was to cause the six sensors behind the corner to be in the disturbance wake. For

instance, a step located at 24% chord caused erroneous data up to the sensor at 44% chord.

Unfortunately, all of these problems were intermittent and difficult to trace. Despite these problems, there was plenty of good data to analyze. Only one of the fifteen data flights was totally unusable.

CHAPTER 9

Results and Discussion

Natural Transition Location

Flights 1 and 2 were performed in order to determine the natural transition location. Results from these flight are in excellent agreement with theoretically predicted results. These flights prove the accuracy of using the hot film system.

Figure 33 contains a plot of the laminar separation bubble location and the turbulent reattachment location from the flight data.

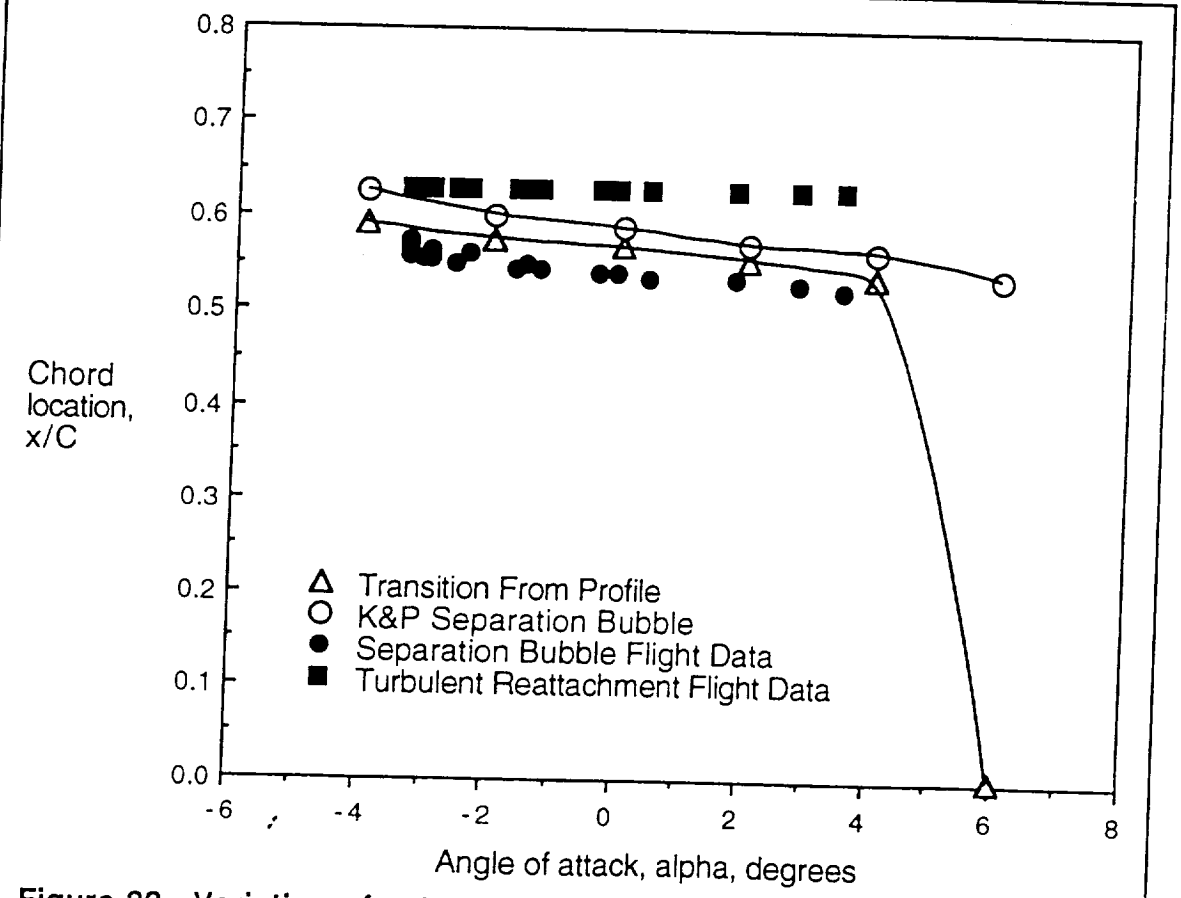

Figure 33. -Variation of natural transition location with angle of attack.

Overlaid upon this data are the theoretically predicted values from the Karmen Pohlhaussen analysis (Appendix D) and the Profile analysis (Appendix B). The actual separation bubble is consistently located slightly ahead of the location predicted by the Karmen Pohlhaussen analysis, although it is within an acceptable range of three percent chord. The predicted value for transition from Profile was also in good agreement. Profile predicted the transition location to be inside of the laminar separation bubble. The beginning of the laminar separation bubble is the point of separation and the end of the bubble is the point of turbulent reattachment. This is consistent with the transition mechanism of a laminar separation bubble.

The first two data flights show excellent correlation and consistency. Unfortunately, later flights proved not so consistent.

Step Transition

Two values of step height Reynolds number were determined from the step transition flights: critical step height Reynolds number ($Re_{h\,cr}$), and fully turbulent step height Reynolds number ($Re_{h\,fl}$). The critical step height Reynolds number is when the step first causes intermittent turbulent bursts downstream of the step. The fully turbulent step height Reynolds number is when transition takes place at the step.

Determination of when a hot film signal indicates laminar flow, turbulent bursts, or transition is indicated from the signal standard deviation as detailed in the previous chapter. The results of the step transition flights are presented in order of chord location: 10.5%, then 24.4%, and finally 42.6% chord.

Flights 11, 12, and 13 tested an aft facing step at the 10.5% chord location. Step height Reynolds numbers are plotted versus percent chord in figure 34.

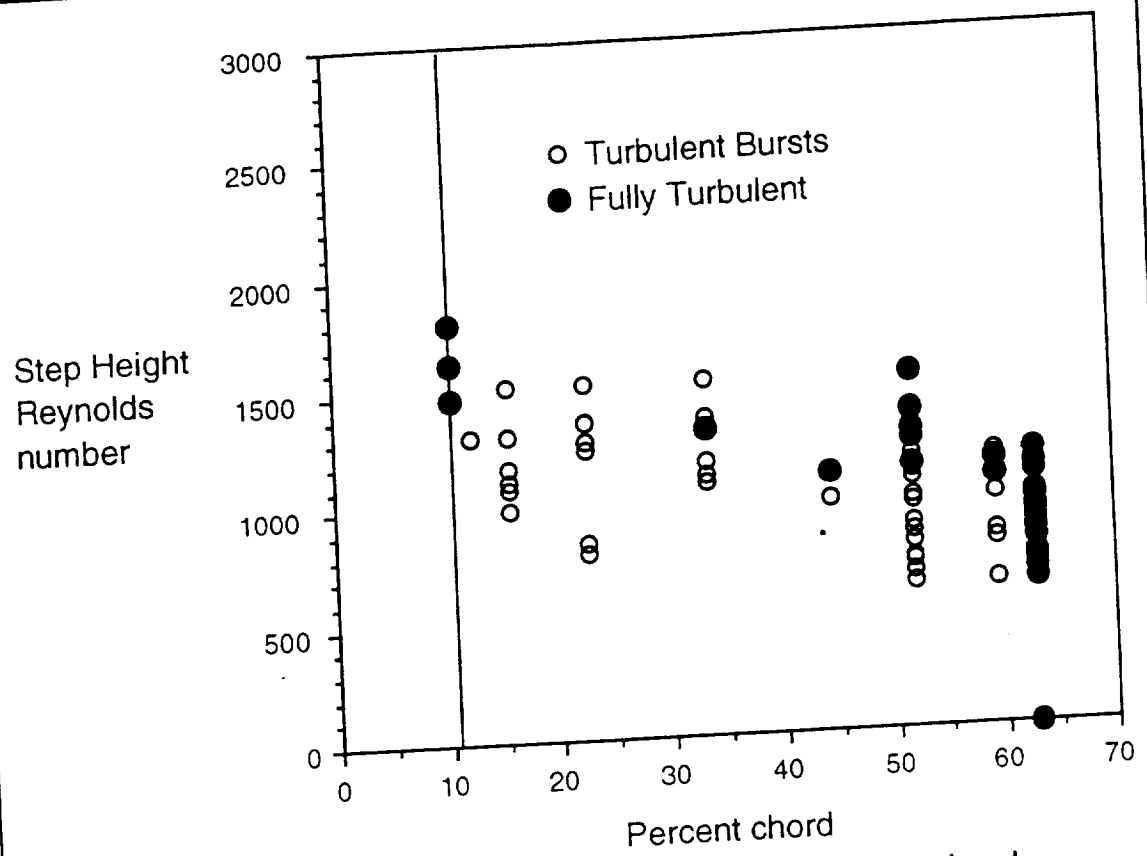

Figure 34. -Transition data plot for a step at 10.5% chord.

From the plot, $Re_{h\,fl}$ is in the range of 1400 to 1600. The value of $Re_{h\,cr}$ is not as easily determined as the value of $Re_{h\,fl}$ since the Reynolds number range does not extend below $Re_h = 628$ in order to bracket the lower value of $Re_{h\,cr}$. However, there is not an increase in turbulence until $Re_h = 800$ indicating that $Re_{h\,cr}$ is close to $Re_{h\,cr} = 628$.

Flights 3, 4, 14, and 15 tested an aft facing step at the 24.4% chord location. Flight 5 also tested a step at this location, but the signals contained an excessive amount of interference. Flight 15 was a repeat of flight 5. $Re_{h\,cr}$ and $Re_{h\,fl}$ are plotted versus percent chord in figure 35.

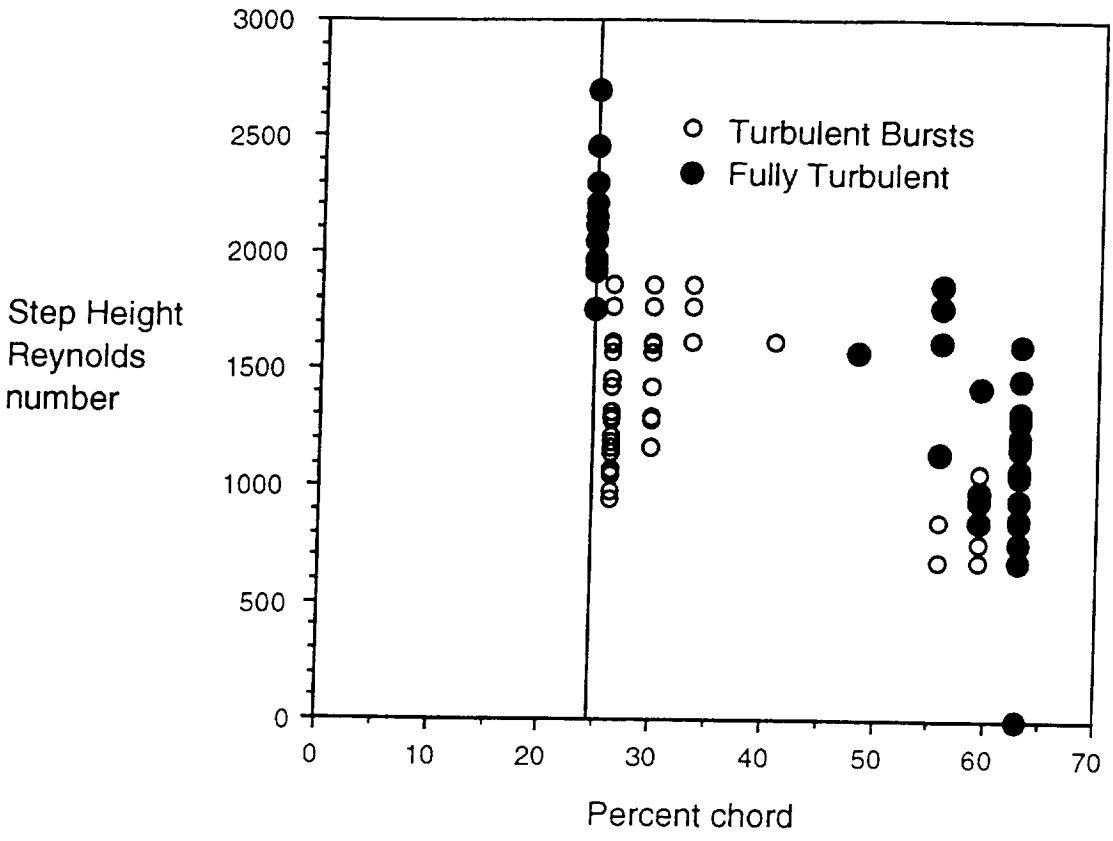

Figure 35. -Transition data plot for a step at 24.4% chord.

From the plot, $Re_{h\ fl}$ is in the range of 1650 to 1850. Again, the value of $Re_{h\ cr}$ is not as easily detrmined as value of $Re_{h\ fl}$ since the Reynolds number range does not extend below $Re_h = 686$ in order to bracket the lower value of $Re_{h\ cr}$. However, there is not an increase in turbulence until $Re_h = 900$ indicating that $Re_{h\ cr}$ is close to $Re_{h\ cr} = 686$.

Flights 6, 7, and 8 tested an aft facing step at the 42.6% chord location. The values of $Re_{h\ cr}$ and $Re_{h\ fl}$ are plotted verses percent chord in figure 36.

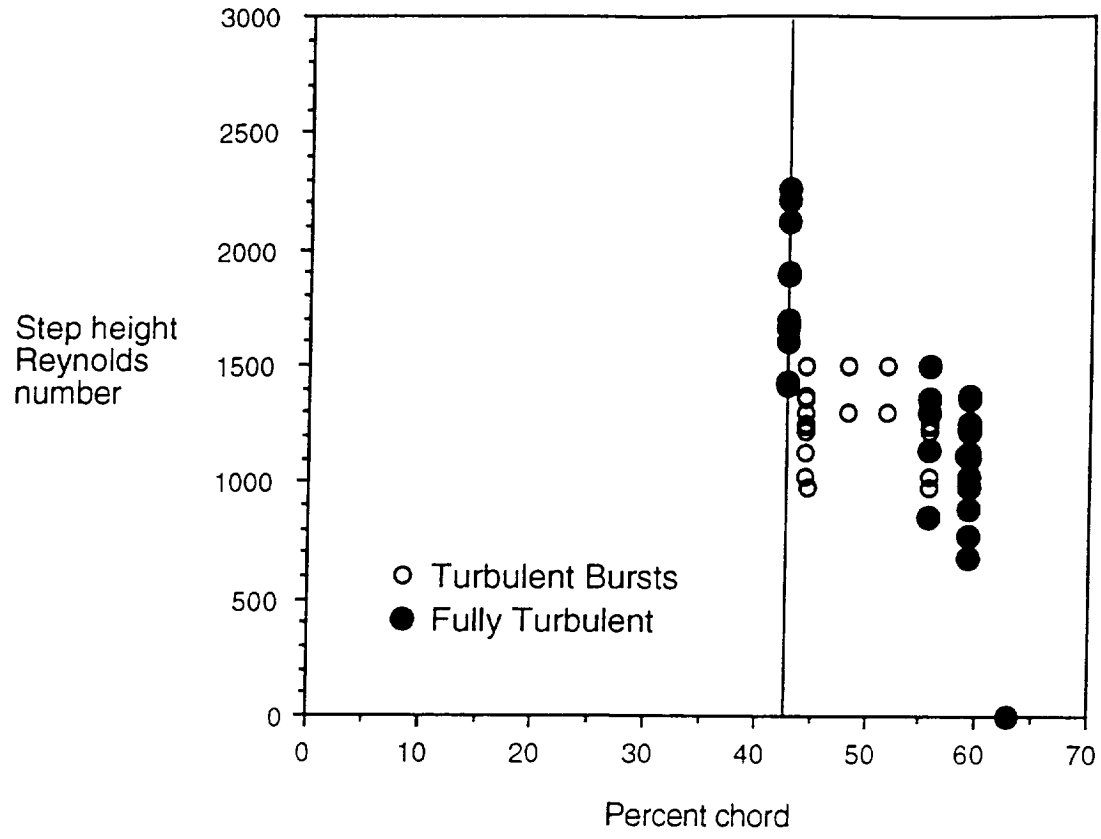

Figure 36. -Transition data plot for a step at 42.6% chord.

From the plot, $Re_{h\,fl}$ is in the range of 1350 to 1550. Again, the value of $Re_{h\,cr}$ is not as easily determined as value of $Re_{h\,fl}$ since the Reynolds number range does not extend below $Re_h = 680$ in order to bracket the lower value of $Re_{h\,cr}$. At the lowest value of $Re_h = 680$ the transition location has already moved forward slightly to the 59% chord sensor. However, there is not an increase in turbulence until $Re_h = 850$ indicating that $Re_{h\,cr}$ is close to $Re_{h\,cr} = 680$.

From the three step locations, the value of $Re_{h\,fl}$ is in the range of 1350 to 1800 which results in a nominal value of $Re_{h\,fl} = 1600 \pm 250$. The average value of $Re_{h\,cr}$ is approximately 665. Unfortunately, there was insufficient data at lower Reynolds numbers in order to determine a tolerance for $Re_{h\,cr}$. Further flight tests with smaller step heights are needed.

The values of $Re_{h\,fl}$ and $Re_{h\,cr}$ agree well with the values of $Re_{h\,fl}$ = 1730±3% and $Re_{h\,cr}$ = 540±29% found by Lurz at the Helsinki University of Technology (Lurz, 1980). However, in the X-21 study (Final Report.., 1967), the value of $Re_{h\,cr}$ was found to be approximately 1100 . This value is significantly larger then the value of $Re_{h\,cr}$ = 665 determined in this study.

The indication that testing of steps smaller then 0.011 inches tends to support the generalization that laminar flow is very difficult to maintain over an aft facing step. Given that most aircraft fly a great deal faster that a glider, the allowable step size for most airplanes is very small. The typical sheet metal junctures or de-icing boots found on aircraft wings would obviously cause a loss of laminar flow.

Effect of Shape Factor and Pressure Gradient

In a boundary layer, shape factor and pressure gradient are important parameters in determining boundary layer stability. The effect of shape factor and pressure gradient on step induced transition is harder to discern. Unfortunately, a large amount of test data would be required to determine the relationship. From the limited test data, the effect of shape factor could not be determined. However, there may be a slight correlation on the effect of pressure gradient.

Only the effects of shape factor and pressure gradient on $Re_{h\,fl}$ are presented. The effect on $Re_{h\,cr}$ could not be determined. From the flight data, the value of $Re_{h\,fl}$ is better defined then $Re_{h\,cr}$ and can be bracketed with more confidence. The influence of shape factor and pressure gradient on $Re_{h\,cr}$ is better suited for wind tunnel study where large amounts of data can be easily gathered. Many more flight tests would have been necessary in order to determine a relationship.

Figure 37 shows the variation of shape factor, H_{12}, with angle of attack. For most of the data flights, the angle of attack varied from -2.1° to 3.3°. In this range there is little overlap in shape factor at the three test locations. Therefore the values of $Re_{h\,fl}$ for each step location can be compared with shape factor to determine any correlation.

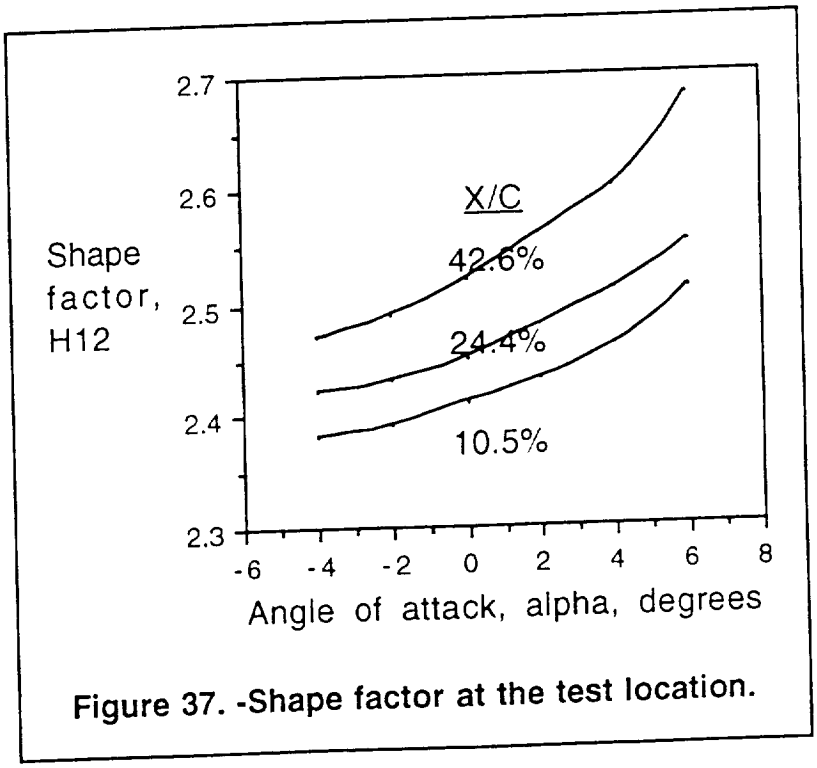

Figure 37. -Shape factor at the test location.

Figure 38 contains a plot of $Re_{h\,fl}$ versus shape factor H_{12}. The data points chosen were the ones that were within the range of $Re_{h\,fl}$ for the step location. For example, at the 10.5% chord location, the $Re_{h\,fl}$ value was determined to be between 1400 and 1600. Therefore the data points were taken that had a step height Reynolds number between 1400 and 1600. The shape factor at the test point is shown in figure 37.

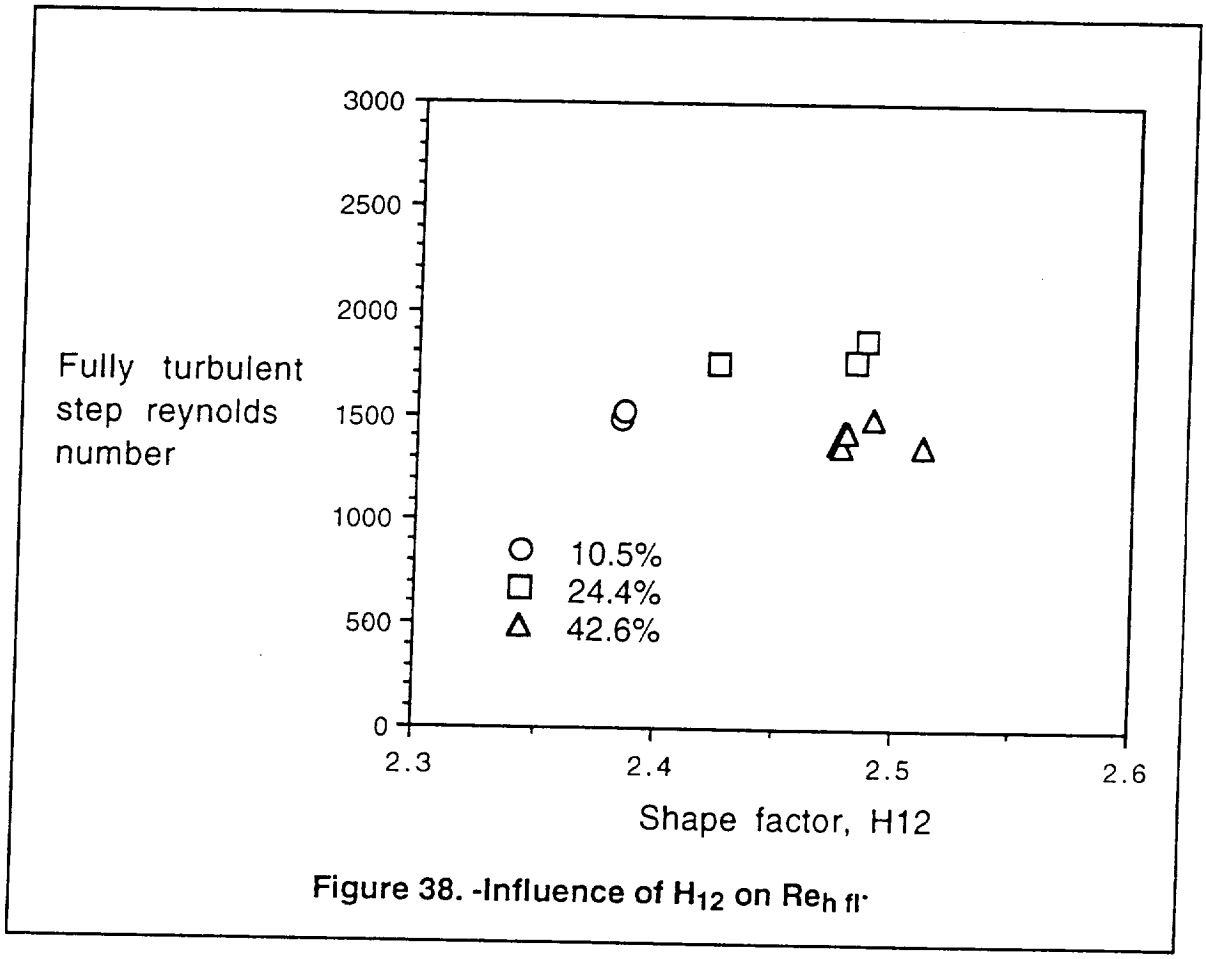

Figure 38. -Influence of H_{12} on $Re_{h\,fl}$.

Unfortunately there is not much that can be determined from figure 38. The points have little correlation. With only three step locations it is not possible to determine any relationship.

Figure 39 shows the variation of dimension-less pressure gradient with α. Again for most of the data flights, the α varied from -2.1° to 3.3°. In this range there is little overlap in pressure gradient at the three test locations. The more positive values of pressure gradient are more adverse to boundary layer stability.

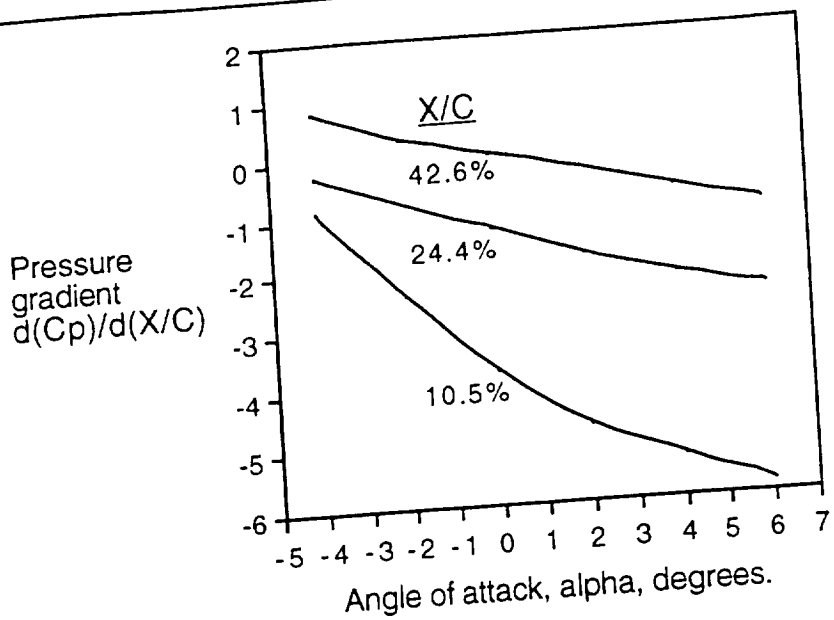

Figure 39. -Pressure gradient at the test location.

Using the same criteria for test points in the previous example, the values of $Re_{h\,fl}$ versus pressure gradient are plotted in figure 40.

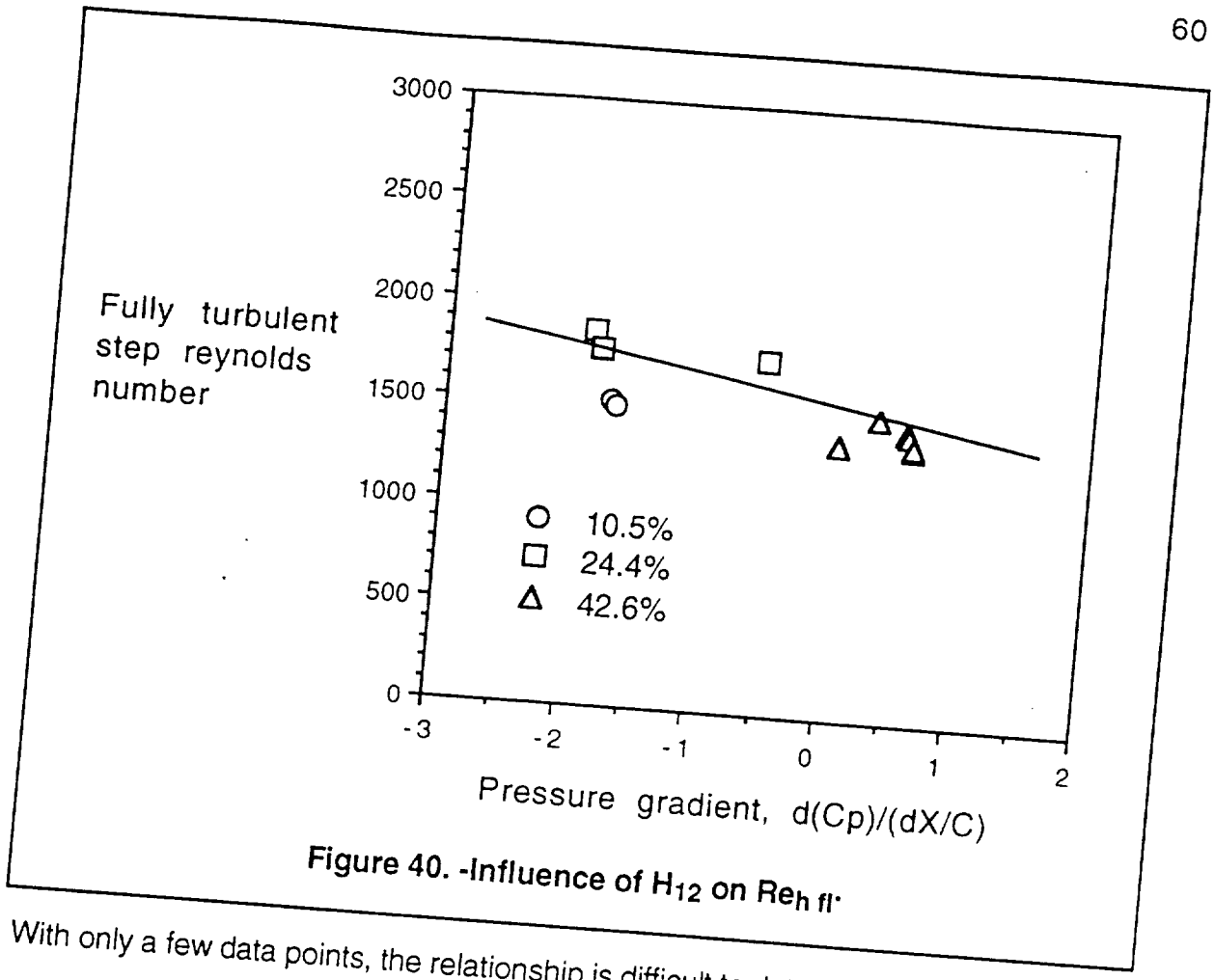

Figure 40. -Influence of H_{12} on $Re_{h\,fl}$.

With only a few data points, the relationship is difficult to determine. However, there seems to be a slight influence of pressure gradient on $Re_{h\,fl}$. As the pressure gradient becomes more adverse, the value of $Re_{h\,fl}$ reduces. This would be consistent with theoretical prediction.

CHAPTER 10

Conclusions

The use of hot film sensors was an accurate and reliable method of determining laminar, transitional, and turbulent flow. However there were a few problems with the data acquisition system. Surface contamination and electrical interference were the main problems. Fortunately, the quantity and redundancy of the flight test data in this experiment was sufficient to work around these problems.

The flight test experimental data were not in agreement with the results from a commonly used wind tunnel study. The value of critical Reynolds number was found to be approximately 665. This is much lower then the value of 1100 found in the previous study. Unfortunately, there was insufficient data at lower Reynolds numbers in order to determine a tollerance for $Re_{h\,cr}$. Further flight tests with smaller step heights are needed.

However, there was excellent agreement with the wind tunnel study by Lurz (Lurz, 1980). The results from the wind tunnel study proved valid in flight test. The free stream turbulence inherent in a wind tunnel did not cause disagreement with flight test data.

The value for step height Reynolds number for full transition was found to be 1600±250. The wide tolerance is partially due to its dependence on pressure gradient.

Step height Reynolds number for full transition was found to be a weak function of pressure gradient. The more adverse pressure gradient causes the step height Reynolds number to decrease Unfortunately, this experiment did not have sufficient data to fully determine this relationship. Only the influence of pressure gradient could be detected.

Shape factor, H_{12} could not be correlated to step transition. This experiment did not have sufficient data to determine this relationship. A wind tunnel study would be better suited to determine the influence of shape factor.

Premature transition was achieved with the smallest step size of 0.011 inches. This tends to support the generalization that laminar flow is very difficult to maintain over an aft facing step. Given that most aircraft fly a great deal faster that a glider, the allowable step size for most aircraft is very small. The typical sheet metal junctures or de-icing boots found on aircraft wings would obviously cause a loss of laminar flow.

REFERENCES

Althaus, Dieter: Stuttgarter Proflikatalog I (Stuttgart Airfoil Catalog 1). Braunscheig, Wiesbaden, Vieweg, 1981.

Anderson, Bianca T.; and Meyey, Robert R.: Effects of Wing Sweep on Boundary-Layer Transition for a Smooth F-14A Wing at Mach Numbers From 0.700 to 0.825. NASA TM 101712, 1990.

Anderson, John D.: Introduction to Flight. Second ed. McGraw-Hill, Inc., 1985, pp. 138.

Beyer, William H.: Standard Mathematical Tables. 24th ed. Cleveland, CRC Press, 1976.

Bowers, Albion H.;Sim, Alex G.: A Comparison of Wortmann Airfoil Computer-Generated Lift and Drag Polars With Flight and Wind Tunnel Results. NASA TM 86035 1984.

Braslow, Albert L.; and Knox, Eugene C.: Simplified Method for Determination of Critical Height of Distributed Roughness Particles for Boundry Layer Transition at Mach Numbers from 0 to 5. NASA TN 4363, 1958.

Braslow, Albert L.; and Muraca, Ralph J.: A Perspective of Laminar-Flow Control. AIAA conference paper, Los Angeles CA., Aug. 21-24 1978.

Chiles, H. R.: The Design and use of a Temperature-Compensated Hot-Film Anemometer System for Boundary-Layer Transition Detection on a Supersonic Aircraft. NASA TM-100421, 1988.

Chiles, H. R.; and Johnson, J. B.: Development of a Temperature-Compensated Hot-Film Anemometer System for Transition Detection on High-Performance Aircraft. NASA TM-86732, 1985.

Eppler, Richard; and Somers, Dan M.: A Computer Program for the Design and Analysis of Low-Speed Airfoils. NASA TM 80210, 1980.

Fage, A.: The Smallest Size of Spanwise Surface Corragation Which Affects Boundry Layer Transition on an Airfoil. R&M No. 2120 Brit. A.R.C., 1943.

Final Report on LFC Aircraft Design Data Laminar Flow Control Demonstration Program. NOR 167-136, Northrop Corp., June 1967.

Flight Instrumentation for Simultaneous Detection of Flow Separation and Transition. (NASA SBIR Phase 1 89-1-03.05-7093.) Analytical Services and Materials Inc., 1989.

Holmes, B. J.; Croom, C. C.;Gall, P. D.; Manuel, G. S.; and Carraway, D. L.: Advanced Transition Measurement Methods for Flight Applications. AIAA Paper 86-9786, 1986.

Holmes, Bruce J.; Obara, Clifford J.; and Yip, Long P.: Natural Laminar Flow Experiments on Modern Airplane Surfaces. NASA TP 2256, 1984.

Holmes, Bruce J.; Obara, Clifford J.; Martin, Glenn L.; and Domack, Christopher S.: Manufacturing Tollerences for Natural Laminar Airframe Surfaces. SAE Paper No. 850863, April 1985.

Johnson, Richard H., A Flight Test Evaluation of the PIK-20E. Soaring, Sept 1976, pp 42-44.

Lighthill, M. J.: A New Method of Two-Dimensional Aerodynamic Design. R. & M. No. 2112, British A.R.C., 1945.

Lurz, Warner: An Experimental Study of the effect of a backward Facing Step in the Flat Plate Upon the Laminar Boundary Layer. Ph. D. Thesis, Helsinki University of Technology, Finland, 1980.

Manuel, G. S.; Carraway, D. L.; and Croom, C.C.: The Laminar Separation Sensor: An Advanced Transition Measurement Method for Use in Wind Tunnel Tests and Flight. SAE TP 871018, 1987.

Obara, C. J.; and Holmes, B. J.: Flight-Measured Laminar Boundary-Layer Transition Phenomena Including Stability Theory Analysis. NASA TP-2417, 1985.

Roberts, Sean C.: Light Aircraft Performance. Flight Research Inc., 2nd Ed., 1980.

Schlichting, H.: Boundary Layer Theory. McGraw-Hill Book Co., 7th Ed., 1979.

Stack, J. P.; Mangalam, S. M.; and Berry, S. A.: A Unique Measurment Technique to Study Laminar-Separation Bubble Characteristics on an Airfoil. AIAA Paper 87-1271, June 1987.

Stuper, J.: The Influence of Surface Irreguralities on Transistion with Various Pressure Gradients. Aeronautical Laboratory, Fisherman's Bend, Melbourne Australia, May 1949.

Wheatley, Patrick, O.; Gerald, Curtis, F.: Applied Numerical Analysis. 4th Ed. Cal Poly State Univ San Luis Obispo, Addison-Wesley Publishing Co 1989.

APPENDIX A

Computation of Wing Flow Field

There are two reasons why it is necessary to calculate the aircraft flow field. The primary reason is to find the relationship between the wing section lift coefficient and the total aircraft lift coefficient. Determining this relationship is necessary in order to find the relationship between airspeed and wing section angle of attack. The secondary reason was to find where the test section should be located on the wing. The panel method program Wing/Body was used to answer both of these questions.

The Wing/Body program was develop by Ralph Carmichael through a contract with the Boeing Aircraft company and made available at NASA through Steve Seato in 1975. Because complete documentation is not available, this description is preferred. The program is written in FORTRAN IV and was run on an Elxsi mainframe computer.

Wing/Body calculates steady pressure distributions on wing and body combinations of arbitrary planform. The flow is assumed incompressible and the analysis uses a source panel method. This results in an invicid flow solution which is sufficient to render the lift distribution of a wing and body combination. The PIK-20E was represented with a total of 196 panels.

The wing was represented as a flat sheet of 100 trapezoidal panels making the correct wing planform, but having no section thickness. From this model the lift distribution at moderate angle of attacks can be found. The PIK-20E wing is double tapered. The inner taper was modeled with 75 panels while the outer panel was modeled with 25 panels. This uneven paneling was done to better define the inner region of the wing which is in the influence of the body. The fuselage was

represented with a twenty-four inch diameter cylinder with tapered ends. The input file for the program is shown in figure A.1.

```
$FIRST   ICTRL=2 ICECHO=1 IWING=1 IBDY=1  NPUNCH(1)=1 $
$TITLE   PIK 20E MOTOR-GLIDER
$BODY    BCODE=0 NB=3 NROWS=16 XSTART=0. LBODY=250.0
       LNOSE=75.0 RADIUS=12.0 $
$WING    M=15 N=5
        MACH=0.0 OC=6 ISYM=.TRUE. PER=0.85
       SREF=15494.4
       ROOTLE=75.0 ROOTTE=110.0 TIPLE=81.26 TIPTE=106.88
       YROOT=12.0 YTIP=177.0
       ZROOT=0.0 ZTIP=5.88 $
$WING    M=5 N=5
       ROOTLE=81.26 ROOTTE=106.88 TIPLE=86.0 TIPTE=101.0
       YROOT=177.0 YTIP=296.0
       ZROOT=5.88 ZTIP=12.11 $
$ENDI   $
$INCR    DELTA=0. $
$INCR    DELTA=1. $
```

Figure A.1. -Wing/Body input file.

The program outputs the difference in top and bottom pressure coefficient for each wing panel. By summing the chordwise panels at each span station, the section lift coefficient at the span station, Cl_S, can be found from Equation A.1.

$$Cl_S = \sum \Delta Cp_{panel} \qquad (A.1)$$

Results from the Wing/Body program are shown in Table A.1 for an angle of attack of 1 degree. The resulting lift coefficient distribution is graphed in Figure A.2. The Wing/Body program integrates the pressure distribution around the wing and derives a lift coefficient for the wing based on wing area. The resulting lift coefficient is 0.098283. With the assumptions that the fuselage lift and tail down load are negligible on a sailplane, this produces a lift slope of 0.098283 /degree for the aircraft.

Table A.1. -PIK-20E spanwise Cl distribution.

Data From Program "WING/BODY"
Alpha = 1 degree

Num	Y (inches)	Δ Cp 1	Δ Cp 2	Δ Cp 3	Δ Cp 4	Δ Cp 5	Cl
1	17.48	.2936	.0993	.0706	.0446	.0258	.107
2	28.48	.2864	.1013	.0699	.0461	.0264	.106
3	39.48	.2816	.1012	.0702	.0465	.0266	.105
4	50.48	.2789	.1007	.0701	.0466	.0267	.105
5	61.48	.2776	.1003	.0699	.0465	.0267	.104
6	72.48	.2768	.1000	.0698	.0464	.0267	.104
7	83.48	.2763	.0999	.0697	.0464	.0267	.104
8	94.48	.2761	.0998	.0696	.0463	.0267	.104
9	105.48	.2760	.0997	.0696	.0463	.0267	.104
10	116.48	.2758	.0997	.0695	.0463	.0266	.104
11	127.47	.2757	.0996	.0694	.0462	.0266	.104
12	138.47	.2754	.0995	.0694	.0462	.0266	.103
13	149.47	.2751	.0994	.0693	.0461	.0265	.103
14	160.47	.2747	.0991	.0691	.0460	.0264	.103
15	171.47	.2739	.0988	.0688	.0457	.0262	.103
16	188.72	.2739	.0988	.0688	.0458	.0263	.103
17	212.51	.2742	.0989	.0689	.0458	.0263	.103
18	236.29	.2722	.0980	.0682	.0453	.0260	.102
19	260.06	.2648	.0950	.0659	.0436	.0249	.099
20	283.83	.2377	.0831	.0568	.0369	.0209	.087

NOTES
Y = distance from the panel centroid to A/C centerline
Δ Cp = difference in top to bottom pressure coefficient
Cl = Σ ΔCp = section lift coefficient

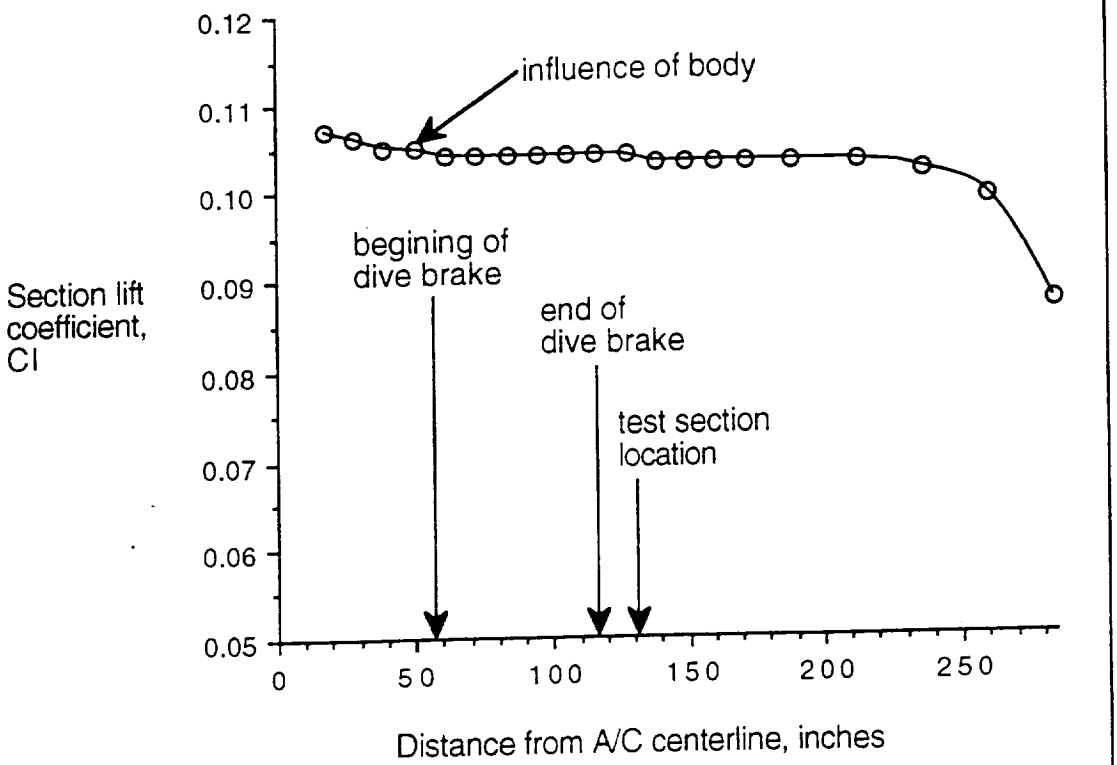

Figure A.2. -Spanwise Cl distribution.

Using the graph in Figure A.2, it was determined that the test section needed to be placed 130 inches from the aircraft centerline. The graph indicates that the fuselage influences the flow out to sixty inches from the aircraft centerline, however this is where the dive brake starts. Since the airflow is disturbed by the retracted dive brakes, the test section was located just outboard of the dive brakes.

From the spanwise lift distribution, the relationship between the aircraft lift coefficient, $Cl_{A/C}$, and the test section lift coefficient ,Cl_{TS}, can be determined. When the aircraft $Cl_{A/C}$ = 0.09828 the test section Cl_{TS} = 0.1035 which renders the relationship:

$$\frac{Cl_{A/C}}{Cl_{TS}} = \frac{0.09828}{0.1035} = 0.9496 \qquad (A.2)$$

APPENDIX B

Airfoil Analysis Using Profile Code

Profile is a computer program used to design and analyze low-speed airfoils. It is a combination of an inviscid panel method program and an integral boundary layer analysis program. The Profile code was used to analyze the PIK-20E airfoil section for three purposes. First, it was used to derive the inviscid flow solution around the airfoil. Second, the boundary layer characteristics were determined. Third, the airfoil section characteristics (i.e. Cl_s, Cm, Cd) were derived.

Most of the information about Profile comes from the paper (which is also the user's manual) by Eppler and Sommers (Eppler, 1980). The program is written in FORTRAN IV and was run on an Elxsi mainframe computer at NASA Dryden. For a better description of the program it is suggested to consult the user's manual, but what follows here is a brief description of the program method.

The flow about an airfoil can be thought of as a thin viscous layer near the surface and an inviscid potential flow everywhere else. First, the potential flow problem is solved by using a method similar to that of Lighthill (Lighthill, 1945), and then the boundary layer is solved for using integral momentum and energy equations.

The program begins the analysis with a set of airfoil coordinate points. These points are then curve fitted to form the airfoil surface. Profile does the curve fit with a cubic B-spline and then conformally maps the airfoil surface. Unfortunately, Profile is unusually sensitive to surface waviness and therefore the airfoil coordinates must be smoothed in order to produce a realistic solution. This smoothing process is somewhat involved and is detailed further in Appendix C.

The input file contains the following information:

-X-Y coordinates for the upper and lower surfaces.

-angles of attack

-Reynolds numbers

-type of transition (natural or forced)

-choice of output.

After running the program the output file contains the following information:

-pressure distributions for each angle of attack

-section lift, drag, and moment coefficients

-listings of shape factor, H_{32}, and momentum thickness, δ_2, for each angle of attack and Reynolds number

-transition locations for each condition.

With the airfoil coordinates determined, the inviscid panel solution from Profile provides the velocity distribution as shown in figure B.1. This is for the airfoil at the test section on the wing.

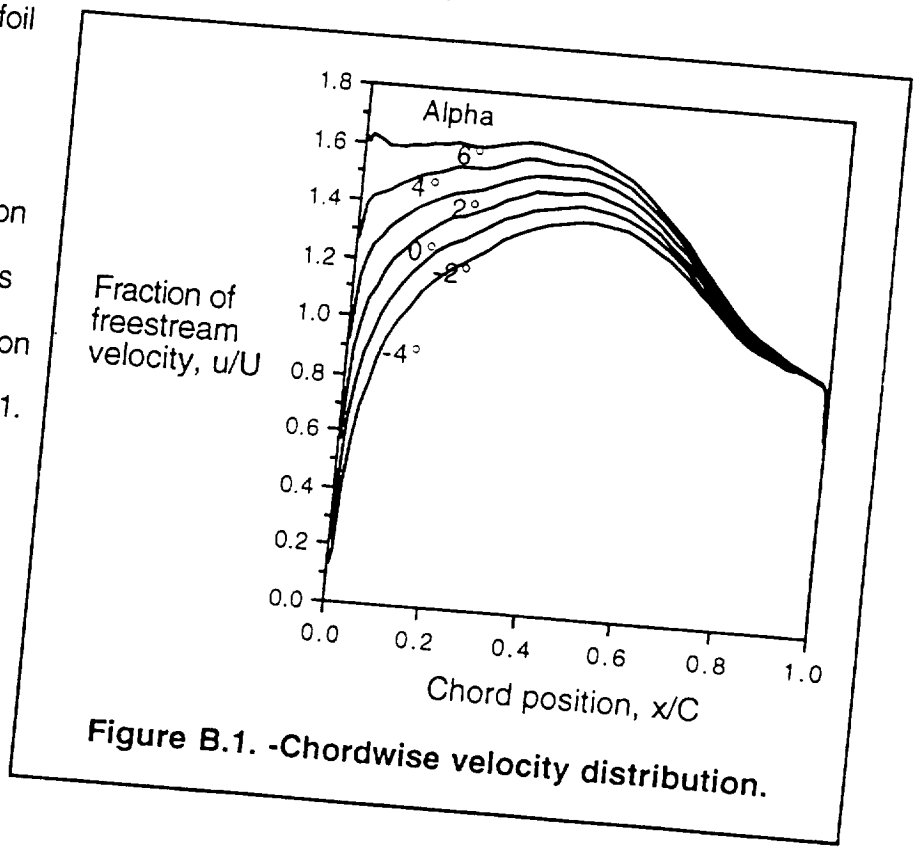

Figure B.1. -Chordwise velocity distribution.

From the velocity distribution, the pressure distribution is determined in figure B.2. The point of minimum pressure is approximately at 45% chord for most angles of attack with an adverse pressure gradient further aft.

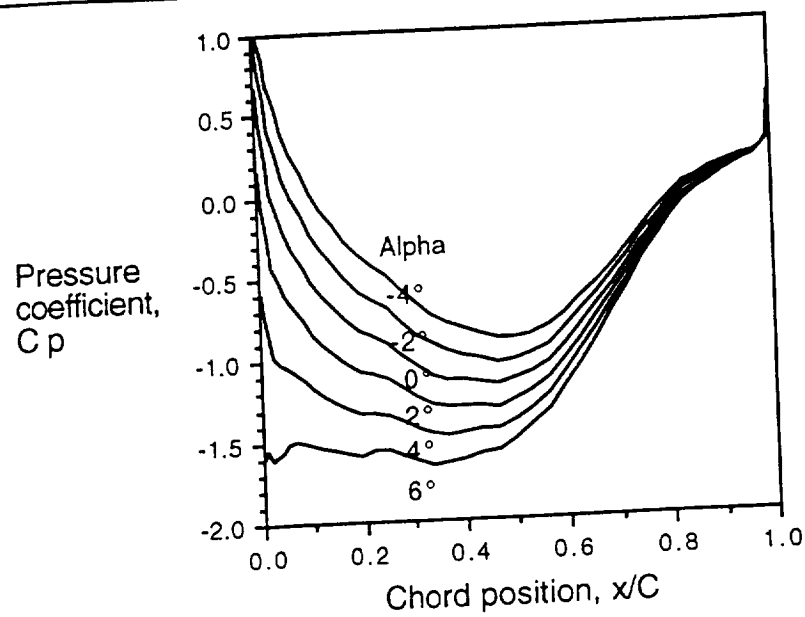

Figure B.2. -Variation of pressure coefficient with chord.

The variation of Cl versus α is given in figure B.3. Since lift coefficient is a function of Reynolds numbers at high angles of attack, there are curves that cover the range of test Reynolds numbers.

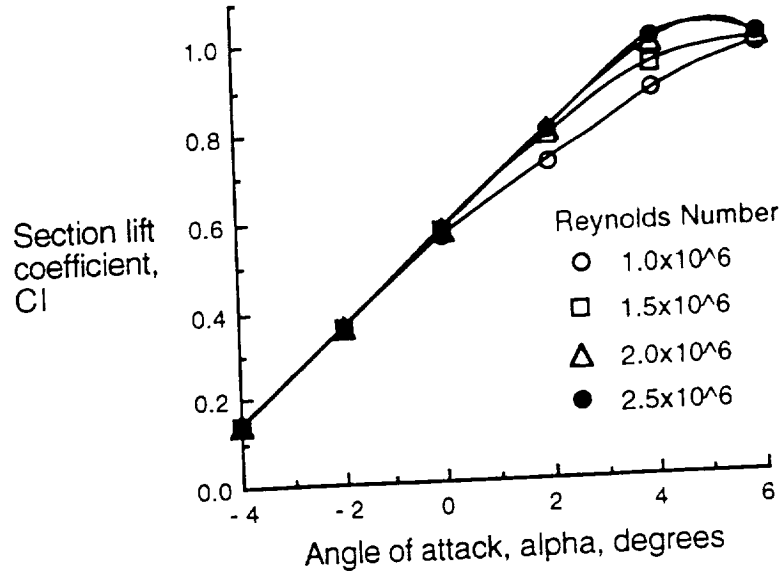

Figure B.3. -Variation of lift coefficient with alpha.

The variation of Drag coefficient versus α is presented in figure B.4.

The variation of pitching moment coefficient versus α is given in figure B.5. Both the Cl-Alpha and Cm-Alpha curves are necessary in order to find the test section angle of attack given the aircraft velocity.

A sample run of the input and output files are contained in tables B.1 and B.2. In order to save space, only the boundary layer shape factors for α=2° are given. All output data pertaining to the lower surface has been omitted. In the output section, the distances are in surface distance from the trailing edge. Since chord location is easier to work with, table B.3 was used to convert surface distance to chord location.

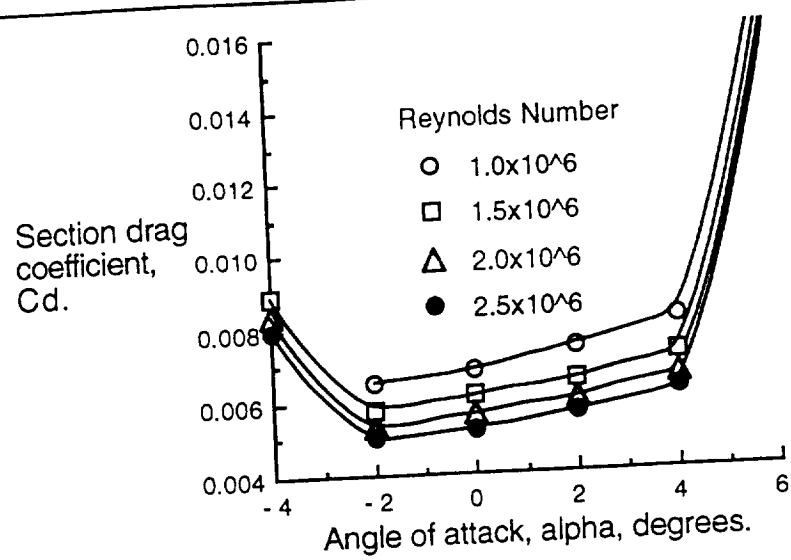

Figure B.4. -Variation of section drag coefficient with alpha.

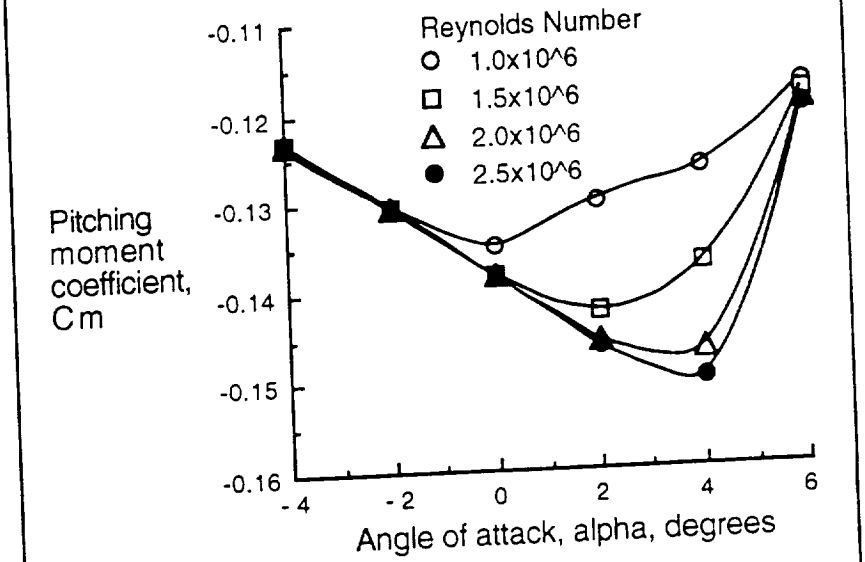

Figure B.5. -Variation of pitching moment coefficient with alpha.

Table B.1. -Profile input file.

```
FXPR
PIK-20E sss
  44  44
 .00000  .00198  .00533  .01066  .01807  .02755  .03905  .05252
 .06792  .08516  .10417  .12489  .14720  .17104  .19627  .22280
 .25049  .27925  .30902  .33961  .37086  .40266  .43488  .46737
 .50000  .53264  .56512  .59734  .62914  .66038  .69093  .72066
 .74946  .77719  .80373  .82906  .85401  .88162  .91376  .94473
 .96943  .98632  .99569 1.00000
 .00000  .00659  .01313  .02013  .02767  .03556  .04364  .05190
 .06036  .06895  .07754  .08597  .09413  .10192  .10923  .11592
 .12209  .12773  .13272  .13674  .13965  .14139  .14200  .14143
 .13942  .13600  .13119  .12495  .11754  .10917  .09996  .09019
 .08015  .07013  .06047  .05148  .04313  .03434  .02474  .01616
 .00971  .00537  .00289  .00150
 .00000  .00198  .00533  .01066  .01807  .02755  .03905  .05252
 .06792  .08516  .10417  .12489  .14720  .17104  .19627  .22280
 .25049  .27925  .30902  .33961  .37086  .40266  .43488  .46737
 .50000  .53264  .56512  .59734  .62914  .66038  .69093  .72066
 .74946  .77719  .80373  .82906  .85401  .88162  .91376  .94473
 .96943  .98632  .99569 1.00000
 .00000 -.00245 -.00517 -.00796 -.01061 -.01320 -.01575 -.01821
-.02056 -.02276 -.02482 -.02673 -.02847 -.03002 -.03136 -.03250
-.03342 -.03413 -.03462 -.03487 -.03489 -.03468 -.03423 -.03353
-.03260 -.03143 -.03000 -.02832 -.02640 -.02420 -.02167 -.01880
-.01566 -.01242 -.00930 -.00649 -.00409 -.00212 -.00051  .00056
 .00080  .00051  .00018  .00000
ALFA 3 6 -400 -200 000 200 400 600
RE       3 1000   3 2000   3 3000
DIAG 0
CDCL
ENDE
```

Table B.2. -Profile output file.

1PANEL METHOD AIRFOIL PIK-20E CA = .66010, 7.14814 ALPHA0 = 5.28 DEGREES
AIRFOIL PIK-20E sss 17.63% THICKNESS .00% FLAP .00 DEGREES DEFLECTION

N	X	Y	-4.00	-2.00	.00	2.00	4.00	6.00
			PRESSURE DISTRIBUTIONS FOR THE ABOVE ANGLES OF ATTACK RELATIVE TO THE CHORD LINE					
0	1.0000	.00150	.513	.514	.517	.520	.525	.531
1	.99569	.00289	.247	.245	.246	.248	.252	.258
2	.98632	.00537	.217	.213	.211	.211	.213	.217
3	.96943	.00971	.183	.176	.171	.168	.167	.169
4	.94473	.01616	.162	.152	.144	.137	.133	.131
5	.91376	.02474	.131	.117	.104	.094	.086	.080
6	.88162	.03434	.090	.072	.055	.041	.029	.019
7	.85401	.04313	.047	.024	.004	-.014	-.030	-.043
8	.82906	.05148	.006	-.021	-.045	-.066	-.085	-.102
9	.80373	.06047	-.070	-.199	-.350	-.389	-.425	-.458
12	.72066	.09019	-.369	-.421	-.470	-.517	-.561	-.602
13	.69093	.09996	-.476	-.537	-.596	-.652	-.705	-.755
14	.66038	.10917	-.581	-.653	-.722	-.788	-.851	-.911
15	.62914	.11754	-.670	-.752	-.832	-.909	-.983	-1.054
16	.59734	.12495	-.756	-.850	-.942	-1.031	-1.118	-1.200
17	.56512	.13119	-.835	-.990	-1.107	-1.221	-1.333	-1.442
19	.50000	.13942	-.894	-1.023	-1.151	-1.278	-1.403	-1.526
20	.46737	.14143	-.897	-1.038	-1.178	-1.317	-1.455	-1.591
21	.43488	.14200	-.860	-1.009	-1.158	-1.308	-1.457	-1.604
22	.40266	.14139	-.829	-.987	-1.148	-1.309	-1.470	-1.631
23	.37086	.13965	-.795	-.964	-1.136	-1.310	-1.484	-1.659
24	.33961	.13674	-.741	-.920	-1.102	-1.287	-1.474	-1.663
25	.30902	.13272	-.671	-.857	-1.049	-1.245	-1.444	-1.645
26	.27925	.12773	-.580	-.773	-.972	-1.177	-1.386	-1.599
27	.25049	.12209	-.504	-.704	-.913	-1.129	-1.352	-1.579
28	.22280	.11592	-.435	-.646	-.866	-1.096	-1.334	-1.579
29	.19627	.10923	-.372	-.595	-.831	-1.078	-1.335	-1.602
30	.17104	.10192	-.284	-.516	-.764	-1.026	-1.301	-1.587
31	.14720	.09413	-.191	-.433	-.694	-.973	-1.267	-1.576
32	.12489	.08597	-.089	-.340	-.615	-.910	-1.226	-1.559
33	.10417	.07754	.020	-.241	-.529	-.844	-1.183	-1.545
34	.08516	.06895	.141	-.128	-.328	-.685	-1.080	-1.512
36	.05252	.05190	.395	.111	-.225	-.611	-1.046	-1.527
37	.03905	.04364	.532	.243	-.114	-.537	-1.022	-1.569
38	.02755	.03556	.684	.399	.025	-.435	-.980	-1.608
39	.01807	.02767	.841	.584	.207	-.288	-.899	-1.622
40	.01066	.02013	.969	.786	.440	-.066	-.732	-1.553
41	.00533	.01313	.982	.953	.678	.159	-.602	-1.601
42	.00198	.00659	.754	.986	.933	.595	-.025	-.925
43	.00000	.00000	-3.189	-.697	.690	.964	.125	-1.824

Table B.2. -Continued.

1BOUNDARY LAYER AIRFOIL PIK-20E ALPHA = 2.00 DEGREES RELATIVE TO THE CHORD LINE

UPPER SURFACE		R = 1000000 MU = 0		R = 2000000 MU = 0	
S	U	H32	DELTA2	H32	DELTA2
.00144	.189	1.6200	.000025	1.6200	.000018
.00832	.636	1.6200	.000036	1.6200	.000025
.01566	.917	1.6172	.000045	1.6172	.000032
.02446	1.033	1.6037	.000064	1.6037	.000045
.03503	1.135	1.6055	.000076	1.6055	.000054
.04737	1.198	1.5983	.000092	1.5983	.000065
.06142	1.240	1.5936	.000109	1.5936	.000077
.07722	1.269	1.5906	.000125	1.5906	.000088
.09479	1.298	1.5920	.000140	1.5920	.000099
.11406	1.328	1.5946	.000153	1.5946	.000108
.13492	1.358	1.5962	.000165	1.5962	.000117
.15729	1.382	1.5938	.000178	1.5938	.000126
.18104	1.404	1.5938	.000191	1.5938	.000135
.20612	1.423	1.5921	.000204	1.5921	.000144
.23239	1.442	1.5925	.000216	1.5925	.000153
.25975	1.448	1.5837	.000233	1.5837	.000165
.28812	1.459	1.5861	.000246	1.5861	.000174
.31743	1.475	1.5919	.000255	1.5919	.000180
.34761	1.498	1.5999	.000260	1.5999	.000184
.37847	1.512	1.5956	.000272	1.5956	.000192
.40985	1.520	1.5891	.000286	1.5891	.000202
.44170	1.520	1.5797	.000304	1.5797	.000215
.47392	1.519	1.5756	.000320	1.5756	.000226
.50642	1.522	1.5774	.000332	1.5774	.000235
.53911	1.509	1.5591	.000359	1.5591	.000254
.57193	1.490	1.5375	.000390	1.5375	.000276
.60476	1.466	-1.5571	.000433	-1.5730	.000308
.63758	1.425	-1.6425	.000520	-1.6783	.000383
.67023	1.382	-1.6777	.000631	-1.7114	.000481
.70258	1.337	-1.6906	.000762	-1.7210	.000595
.73448	1.285	-1.6885	.000929	-1.7181	.000736
.76578	1.232	-1.6784	.001129	-1.7093	.000903
.79628	1.178	-1.6618	.001365	-1.6958	.001098
.82576	1.125	-1.6369	.001653	-1.6763	.001333
.85401	1.075	-1.6050	.001987	-1.6522	.001601
.88088	1.033	-1.5685	.002347	-1.6264	.001885
.90719	1.007	-1.5475	.002612	-1.6141	.002091
.93617	.979	-1.5168	.002950	-1.5967	.002347
.96971	.952	-1.4766	.003359	-1.5770	.002644
1.00185	.929	-1.4600	.003728	-1.5577	.002932
1.02738	.912	-1.4600	.004001	-1.5412	.003169
1.04482	.888	-1.4600	.004441	-1.4988	.003558
1.05451	.867	-1.4600	.004875	-1.4600	.003957
1.05904	.693	-1.4600	.011708	-1.4600	.009503

Table B.2. -Continued.

```
1BOU1SUMMARY  AIRFOIL PIK-20E sss   ANGLE OF ATTACK RELATIVE TO THE
CHORD LINE      ALPHA0 = 5.28 DEGREES
 * INDICATES VELOCITY REDUCTION WITHIN BUBBLE BELOW .94
0       R =  1000000  MU = 0    R =  2000000  MU = 0
0 ALPHA = -4.00 DEGREES
      1 S TURB   S SEP    CD    2 S TURB   S SEP    CD
  UPPER   .4286   .0033  .0040     .4286   .0023  .0033
  LOWER  1.0053  1.0036  .0057*   1.0053   .0020  .0051*
  TOTAL   CL =  .415 CD = .0097    CL =  .139 CD = .0084
       CM = -.1235 AC =  1.28    CM = -.1232 AC =  1.28
0 ALPHA = -2.00 DEGREES
      1 S TURB   S SEP    CD    2 S TURB   S SEP    CD
  UPPER   .4396   .0042  .0046     .4396   .0030  .0037
  LOWER   .3384   .0000  .0019     .3384   .0000  .0016
  TOTAL   CL =  .357 CD = .0065    CL =  .358 CD = .0053
       CM = -.1304 AC =  3.28    CM = -.1306 AC =  3.28
0 ALPHA =  .00 DEGREES
      1 S TURB   S SEP    CD    2 S TURB   S SEP    CD
  UPPER   .4492   .0185  .0052     .4492   .0038  .0042
  LOWER   .3015   .0000  .0016     .3015   .0000  .0014
  TOTAL   CL =  .563 CD = .0068    CL =  .577 CD = .0056
       CM = -.1351 AC =  5.28    CM = -.1384 AC =  5.28
0 ALPHA =  2.00 DEGREES
      1 S TURB   S SEP    CD    2 S TURB   S SEP    CD
  UPPER   .4635   .0765  .0059     .4635   .0069  .0048
  LOWER   .2799   .0000  .0014     .2799   .0000  .0012
  TOTAL   CL =  .722 CD = .0074    CL =  .793 CD = .0060
       CM = -.1301 AC =  7.28    CM = -.1457 AC =  7.28
0 ALPHA =  4.00 DEGREES
      1 S TURB   S SEP    CD    2 S TURB   S SEP    CD
  UPPER   .4813   .1258  .0068     .4813   .0334  .0055
  LOWER   .2675   .0000  .0013     .2675   .0000  .0011
  TOTAL   CL =  .878 CD = .0081    CL =  .983 CD = .0066
       CM = -.1267 AC =  9.28    CM = -.1469 AC =  9.28
0 ALPHA =  6.00 DEGREES
      1 S TURB   S SEP    CD    2 S TURB   S SEP    CD
  UPPER  1.0539   .2164  .0181    1.0539   .2022  .0163*
  LOWER   .2541   .0000  .0012     .2541   .0000  .0010
  TOTAL   CL =  .971 CD = .0193    CL =  .989 CD = .0172
       CM = -.1176 AC = 11.28    CM = -.1195 AC = 11.28
1WARNING - SUBROUTINE SMOOTH HAS SLOPES -.254 AND -.667 BETWEEN POINTS
43 AND 44
0WARNING - SUBROUTINE SMOOTH HAS SLOPES -.403 AND -.191 BETWEEN POINTS
44 AND 45
```

Table B.3. -Chord location and surface distance.

N	X/C	Y/C	dS/C	S/C
1	.00000	.00000		0.000
2	.00533	.01313	.014	0.014
3	.01066	.02013	.009	0.023
4	.01807	.02767	.011	0.034
5	.02755	.03556	.012	0.046
6	.03905	.04364	.014	0.060
7	.05252	.05190	.016	0.076
8	.06792	.06036	.018	0.093
9	.08516	.06895	.019	0.113
10	.10417	.07754	.021	0.133
11	.12489	.08597	.022	0.156
12	.14720	.09413	.024	0.180
13	.17104	.10192	.025	0.205
14	.19627	.10923	.026	0.231
15	.22280	.11592	.027	0.258
16	.25049	.12209	.028	0.287
17	.27925	.12773	.029	0.316
18	.30902	.13272	.030	0.346
19	.33961	.13674	.031	0.377
20	.37086	.13965	.031	0.408
21	.40266	.14139	.032	0.440
22	.43488	.14200	.032	0.472
23	.46737	.14143	.032	0.505
24	.50000	.13942	.033	0.538
25	.53264	.13600	.033	0.570
26	.56512	.13119	.033	0.603
27	.59734	.12495	.033	0.636
28	.62914	.11754	.033	0.669
29	.66038	.10917	.032	0.701
30	.69093	.09996	.032	0.733
31	.72066	.09019	.031	0.764
32	.74946	.08015	.030	0.795
33	.77719	.07013	.029	0.824
34	.80373	.06047	.028	0.853
35	.82906	.05148	.027	0.879
36	.85401	.04313	.026	0.906
37	.88162	.03434	.029	0.935
38	.91376	.02474	.034	0.968
39	.94473	.01616	.032	1.000
40	.96943	.00971	.026	1.026
41	.98632	.00537	.017	1.043
42	.99569	.00289	.010	1.053
43	1.00000	.00150	.005	1.058

APPENDIX C

Airfoil Surface Coordinates

Transferring the true wing airfoil shape into the Profile program resulted in a multi-step process. First a mold of the airfoil section was made, then the coordinates were taken from the mold, and finally the coordinates were smoothed out. The coordinate smoothing was necessary in order to use the Profile program.

The PIK-20E wing airfoil is listed as a Wortman FX67-K-170 at the root and a FX67-K-150 at the tip (figures C.1 and C.2, coordinates from Althaus, 1981). However it is very common for the actual wing section to vary from the theoretical and this was the case for the PIK-20E. The last three digits of the airfoil designation indicate that the root section is supposed to be 17.0% thick and the tip section 15.0% thick. However, the test section thickness measured 18.27% thick.

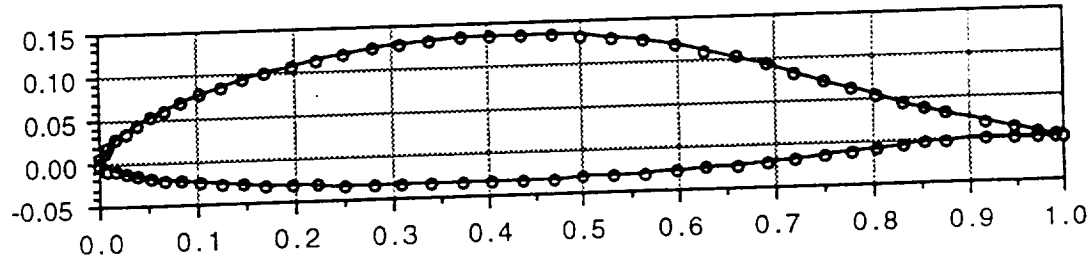

Figure C.1. -Wortman FX67-K-170 root section.

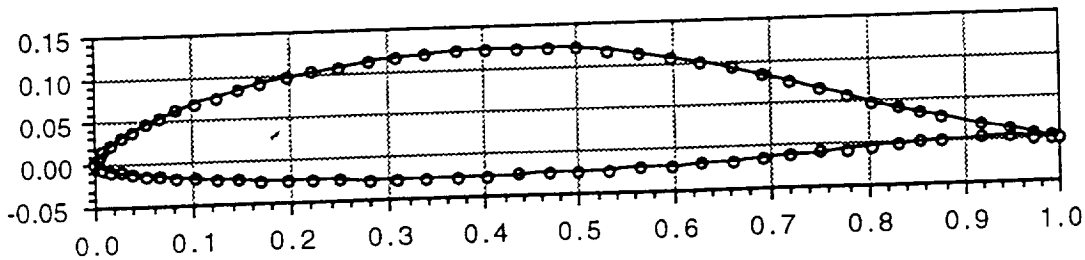

Figure C.2. -Wortman FX67-K-150 tip section.

Since this experiment depends on knowing the exact airfoil shape, a wing section mold (called a splash) was made from putty and plywood (Fig. C.3). A piece of half inch plywood was cut to the approximate airfoil shape and plastic putty was applied to the bottom edge. The airfoil was then covered in Teflon tape and the splash placed over the tape. Finally the splash was allowed to dry to the airfoil shape. After drying, the coordinates of the splash were then measured on a milling machine with a digital readout. The splash coordinates are listed in table C.1.

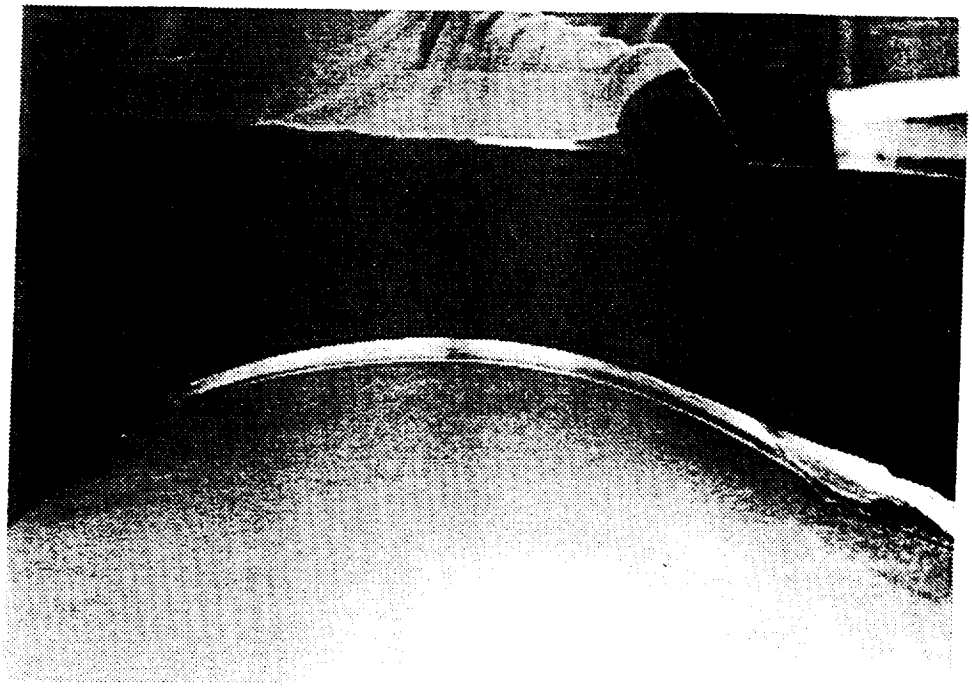

Figure C.3. -Wing splash.

The Profile airfoil analysis program has an unusual sensitivity to surface waviness. This sensitivity is documented in the paper by Bowers, 1984. When the raw splash data is run through Profile the resulting velocity distribution is full of small velocity spikes and is unrealistically jagged. Because of this problem, the FORTRAN program Smoother was written to smooth out the tiny surface waves that produce the velocity spikes. With very small adjustments to the coordinates, most of the spikes can be removed. Figure C.4 shows the velocity profile without smoothing and figure C.5 shows it with smoothing.

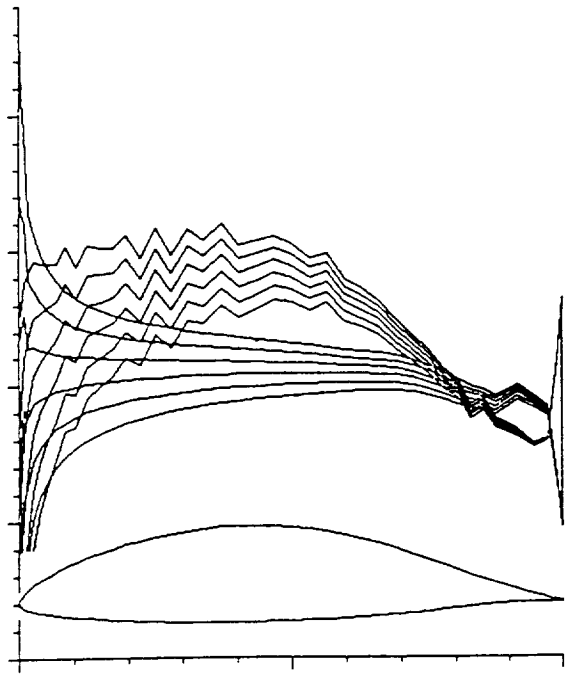

Figure C.4. -Unsmoothed airfoil.

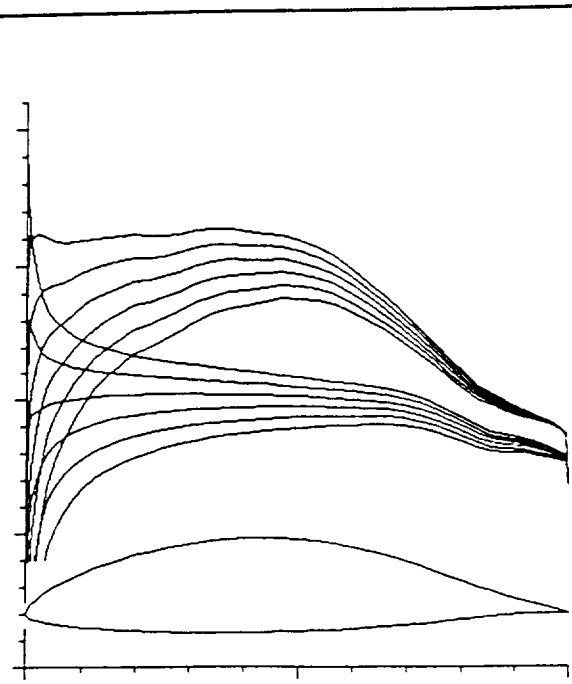

Figure C.5. -Smoothed airfoil.

The Smoother program works by using a weighted averaging scheme similar to the one used in a cubic B-spline curve fit (Wheatley, 1989). This works well since Profile also uses a cubic B-Spline to construct the airfoil surface from the coordinate points. Equation C.1 is the equation used to average each point.

$$X_{smoothed} = \frac{1}{6}X_{i-1} + \frac{2}{3}X_i + \frac{1}{6}X_{i+1} \qquad (C.1)$$

For the splash airfoil it was necessary to do three iterations of this scheme in order to achieve sufficient smoothness. The program listing for Smoother is given in figure C.8.

After all of the points are smoothed the airfoil becomes about one percent thinner. This is because Smoother tries to smooth the arch of the airfoil into a straight line. The program corrects this by scaling the airfoil in the y axis in order to restore the original height.

One of the main concerns in using a smoothing routine is that the surface should not be smoothed so much as to cause the basic shape to change. Smoother is very successful at this in that the height above the surface is adjusted not more then 0.015 inch. This is acceptable considering that the measurement of the original splash was only accurate to 0.010 inch. The method of measuring the amount of adjustment perpendicular to the surface is shown in figure C.6 and calculated in equations C.2 (Beyer, 1976). Figure C.6 shows three points and their corresponding three smoothed points.

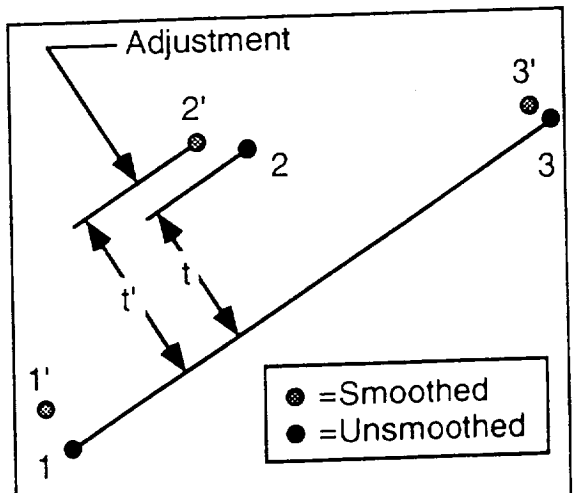

Figure C.6. -Measurement of point adjustment.

$$t = \begin{vmatrix} x_1 & y_1 & 1 \\ x_2 & y_2 & 1 \\ x_3 & y_3 & 1 \end{vmatrix} \frac{1}{\sqrt{(x_1-x_3)^2+(y_1-y_3)^2}} \qquad (C.2)$$

$$t' = \begin{vmatrix} x_1 & y_1 & 1 \\ x_2 & y_2 & 1 \\ x_3' & y_3' & 1 \end{vmatrix} \frac{1}{\sqrt{(x_1-x_3)^2+(y_1-y_3)^2}}$$

$$\text{Adjustment} = t' - t$$

In addition to smoothing, an adjustment to the trailing edge was necessary. When the trailing edge is defined as a sharp point, the velocity profile near the trailing edge is unrealistically jagged. This is due to the necessity for closure of the pressure envelope at the trailing edge. The velocity distribution has much more realistic closure when a finite trailing edge of 0.040 is used (as shown in figures C.4 and C.5). On the real aircraft airfoil the trailing edge is a radius of approximately 0.020 of an inch.

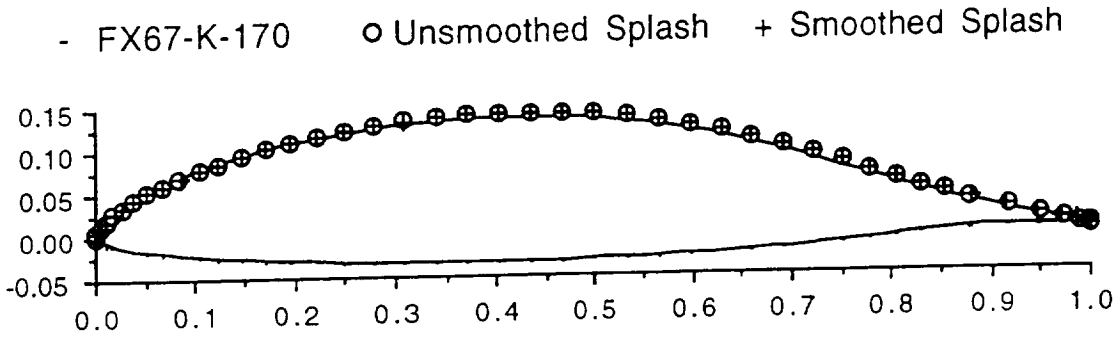

Figure C.7. -Comparison of FX67-K-170, unsmoothed, and smoothed airfoils.

Table C.1. -Splash and smoothed splash airfoil.

Splash Chord = 26.270 inches

#	X/C	Raw Splash X (Inches)	Raw Splash Y Up Act (Inches)	Raw Splash Y/C Up	Smoothed X/C	Smoothed Y/C
1	1.0000	26.270	0.000	0.0000	1.00000	0.00150
2	0.9989	26.242	0.060	0.0023	0.99569	0.00289
3	0.9904	26.018	0.110	0.0042	0.98632	0.00537
4	0.9735	25.573	0.230	0.0088	0.96943	0.00971
5	0.9484	24.916	0.390	0.0148	0.94473	0.01616
6	0.9157	24.056	0.620	0.0236	0.91376	0.02474
7	0.8759	23.010	0.935	0.0356	0.88162	0.03434
8	0.8536	22.423	1.135	0.0432	0.85401	0.04313
9	0.8297	21.795	1.330	0.0506	0.82906	0.05148
10	0.8044	21.131	1.575	0.0600	0.80373	0.06047
11	0.7778	20.433	1.830	0.0697	0.77719	0.07013
12	0.7500	19.703	2.100	0.0799	0.74946	0.08015
13	0.7211	18.944	2.365	0.0900	0.72066	0.09019
14	0.6913	18.162	2.625	0.0999	0.69093	0.09996
15	0.6607	17.357	2.870	0.1093	0.66038	0.10917
16	0.6294	16.535	3.090	0.1176	0.62914	0.11754
17	0.5976	15.698	3.285	0.1250	0.59734	0.12495
18	0.5653	14.849	3.460	0.1317	0.56512	0.13119
19	0.5327	13.994	3.575	0.1361	0.53264	0.13600
20	0.5000	13.135	3.670	0.1397	0.50000	0.13942
21	0.4673	12.276	3.725	0.1418	0.46737	0.14143
22	0.4347	11.421	3.730	0.1420	0.43488	0.14200
23	0.4025	10.572	3.710	0.1412	0.40266	0.14139
24	0.3706	9.735	3.680	0.1401	0.37086	0.13965
25	0.3393	8.913	3.595	0.1368	0.33961	0.13674
26	0.3087	8.108	3.490	0.1329	0.30902	0.13272
27	0.2787	7.320	3.345	0.1273	0.27925	0.12773
28	0.2500	6.568	3.215	0.1224	0.25049	0.12209
29	0.2222	5.837	3.035	0.1155	0.22280	0.11592

TABLE C.1. -Continued.

30	0.1956	5.139	2.870	0.1093	0.19627	0.10923
31	0.1703	4.475	2.675	0.1018	0.17104	0.10192
32	0.1465	3.847	2.470	0.0940	0.14720	0.09413
33	0.1241	3.260	2.255	0.0858	0.12489	0.08597
34	0.1033	2.714	2.020	0.0769	0.10417	0.07754
35	0.0843	2.214	1.810	0.0689	0.08516	0.06895
36	0.0670	1.760	1.580	0.0601	0.06792	0.06036
37	0.0516	1.354	1.355	0.0516	0.05252	0.05190
38	0.0381	1.000	1.140	0.0434	0.03905	0.04364
39	0.0265	0.697	0.930	0.0354	0.02755	0.03556
40	0.0170	0.448	0.720	0.0274	0.01807	0.02767
41	0.0096	0.252	0.520	0.0198	0.01066	0.02013
42	0.0043	0.112	0.330	0.0126	0.00533	0.01313
43	0.0011	0.028	0.180	0.0069	0.00198	0.00659
44	0.0000	0.000	0.000	0.0000	0.00000	0.00000

```
      PROGRAM SMOOTHER
c     Program SMOOTHER takes airfoil coordinates in the PROFILE
c     format and smooths them using weighted averaging.  Run as
c     many times as necessary to smooth the airfoil.
c ...
c     By NEAL SAIKI  2/4/91
c ...
      REAL  XU(100),XL(100),YU(100),YL(100),
     *NXU(100),NXL(100),NYU(100),NYL(100),AXU(10),AYU(10),
     HOLD
      INTEGER ADDPTS,N,I,NU,NL
C ----------AIRFOIL TO BE WORKED ON IS SAVED AS FILE ROUGH
      OPEN(1,FILE='ROUGH',STATUS='OLD',ACCESS='DIRECT')
      OPEN(2,FILE='SMOOTH',STATUS='OLD',ACCESS='DIRECT')
C ------- READS THE NUMBER OF UPPER AND LOWER COORDINATES
      FIND(1,3)
      READ(1,101)NU,NL
      101 FORMAT(2I5)
C ------------------READS IN UPPER AND LOWER COORDINATES
      READ(1,102)(XU(I),I=1,NU)
      READ(1,102)(YU(I),I=1,NU)
      READ(1,102)(XL(I),I=1,NL)
      READ(1,102)(YL(I),I=1,NL)
      102  FORMAT(8F10.5)
C -------------TRANSFER THE LE AND TE POINTS W/O ALTERATION
      NXU(1)=XU(1)
      NYU(1)=YU(1)
      NXL(1)=XL(1)
      NYL(1)=YL(1)
      NXU(NU)=XU(NU)
      NYU(NU)=YU(NU)
      NXL(NL)=XL(NL)
      NYL(NL)=YL(NL)
C ------------------------- SMOOTH THE UPPER SURFACE POINTS
      195 DO 200 I=2,NU-1
      NXU(I)=1./6.*XU(I-1)+2./3.*XU(I)+1./6.*XU(I+1)
      NYU(I)=1./6.*YU(I-1)+2./3.*YU(I)+1./6.*YU(I+1)
      200 CONTINUE
C ------------------------- SMOOTH THE LOWER SURFACE POINTS
      DO 300 I=2,NL-1
      NXL(I)=1./6.*XL(I-1)+2./3.*XL(I)+1./6.*XL(I+1)
      NYL(I)=1./6.*YL(I-1)+2./3.*YL(I)+1./6.*YL(I+1)
      300 CONTINUE
C ------------------------- FIND THE HIGH POINT OF OLD AND NEW
      DO 500 I=1,NU
      IF (YU(I).LE.RHIGH) GO TO 400
      RHIGH=YU(I)
      400 IF (NYU(I).LE.SHIGH) GO TO 500
      SHIGH=NYU(I)
```

Figure C.8. -Smoother program listing.

```
      500 CONTINUE
C ---------- RESTORE THE SMOOTHED AIRFOIL HEIGHT
      DO 600 I=1,NU
      NYU(I)=NYU(I)*RHIGH/SHIGH
      600 CONTINUE
C ---------- WRITE THE SMOOTHED COORDINATES TO SMOOTH FILE
      FIND(2,4)
      WRITE(2,102)(NXU(I),I=1,NU)
      WRITE(2,102)(NYU(I),I=1,NU)
      WRITE(2,102)(NXL(I),I=1,NL)
      WRITE(2,102)(NYL(I),I=1,NL)
      END
```

Figure C.7: -Continued.

APPENDIX D

Karman and Pohlhausen Boundary Layer Analysis

The Karman and Pohlausen boundary layer analysis is an integral method to solve for the boundary layer. Integral methods are approximate solutions which do not attempt to satisfy the boundary layer equations for every streamline. Instead, the equations are satisfied only on an average extended over the thickness of the boundary layer and are based on the momentum and energy equations of boundary layer theory. This classic method can be traced to two papers written in the 1920's, one due to Th. von Karman and the other to K. Pohlhausen. However, a good description is given by Schlicting, 1979.

What follows here is a brief description of the procedure used to apply the Karman and Pohlausen (K&P) method to the upper surface of the PIK-20E wing test section. Knowing both the airfoil shape from the wing splash and the pressure distribution from Profile, the K&P method was applied using microcomputer spreadsheets.

Profile outputs the surface pressure distribution in terms of pressure coefficient. From the pressure coefficient, the surface velocity distribution was found by using equation D.1.

$$\frac{u}{U} = \sqrt{1-Cp} \qquad (D.1)$$

Given the velocity distribution the boundary layer can be solved for in a five step process as follows:

1) Calculate the potential flow function ,U, and the derivative dU/ds in terms of arc length s.

2) Integration of equation D.2 determines the shape factor Z and equation D.3 determines the shape factor K. Momentum thickness δ_2 is found from equation D.4.

$$dZ/ds = \frac{F(K)}{U} \tag{D.2}$$

$$K = Z * (dU/ds) \tag{D.3}$$

$$\delta_2 = \sqrt{\frac{K\nu}{dU/ds}} \tag{D.4}$$

3) Given K, the shape factor Λ is implicitly defined by equation D.5. Since Λ cannot be isolated, the function was approximated using the three equations D.6, D.7, and D.8 which were found by graphing and curve fitting the function. The calculation begins with $\Lambda_0 = 7.052$ and $K_0 = 0.0770$.

$$K = \left(\frac{37}{315} - \frac{1}{945}\Lambda - \frac{1}{9072}\Lambda^2\right)^2 \Lambda \tag{D.5}$$

$$[-15 < \Lambda < 0] \quad \Lambda = -4.0569e\text{-}2 + 61.543\,K - 307{,}98\,K^2 - 3899.5\,K^3 - 1.6273e4\,K^4 \tag{D.6}$$

$$[0 < \Lambda < 7] \quad \Lambda = -6.3133e\text{-}5 + 73.397\,K - 29.632\,K^2 + 6601.9\,K^3 - 1.0300e5\,k^4 + 8.0441e5\,K^5 \tag{D.7}$$

$$[7 < \Lambda < 15] \quad \Lambda = -136.03 + 5400.2\,K - 6.9432e4\,K^2 + 3.0439e5\,K^3 \tag{D.8}$$

4) The shape factor, H_{12} and the displacement thickness, δ_1 are found from equations D.9 and D.10. The boundary layer thickness is found from equation D.11.

$$H_{12} = \frac{\delta_1}{\delta_2} = \frac{\frac{3}{10} - \frac{1}{120}\Lambda}{\frac{37}{315} - \frac{1}{945}\Lambda - \frac{1}{9072}\Lambda^2} \tag{D.9}$$

$$\delta_1 = H_{12}\,\delta_2 \tag{D.10}$$

$$\delta = \sqrt{\frac{\Lambda\nu}{dU/ds}} \tag{D.11}$$

5) The shape factor, H_{32} is found from equation D.12. This relationship is only valid up to the beginning of transition.

$$H_{32} = \frac{\delta_3}{\delta_2} = \frac{4H_{12}}{(3H_{12}-1)} \qquad (D.12)$$

In equation 12, δ_3 is the energy thickness. Table D.1 contains the equations used for the spreadsheet calculations and table D.2 contains an example spreadsheet for $\alpha = 2.0°$. Six spreadsheets were used to cover the alpha range from -4° to 6° in 2° increments.

The freestream velocity, U, was calculated using equations D.13 and D.14. Equation D.13 was derived from the Wing/Body analysis found in appendix A.

$$Cl = (0.098283 \text{ / degree}) \ (\alpha - \alpha_{l=0}) \qquad (D.13)$$

$$U = \sqrt{\frac{W}{\frac{1}{2}\rho S Cl}} = \frac{255.4}{\sqrt{\alpha - 5.28°}} \qquad (D.14)$$

$\alpha_{l=0} = -5.28°$

$S = 107.6 \text{ feet}^2$

$W = 820$ pounds

$\rho = 0.002377 \text{ slugs/feet}^3$

Table D.1. -Equations used for K&P spreadsheet analysis.

N = Station number

C = Airfoil Chord

X/C = Fraction of chord from leading edge

Y/C = Fraction of chord from chord line

$\Delta s = C\sqrt{X/C^2+Y/C^2}$ Increment along surface in inches

$s_i = s_{i-1} + ds$ Distance along surface in inches

Cp = Pressure coefficient from Profile

$u/U = \sqrt{1-Cp}$ Surface velocity as a fraction of freestream velocity

$du/ds = \frac{\Delta u}{\Delta s}$ First derivative of surface velocity

$Z_i = Z_{i-1} + (dZ/ds)\, ds$ Shape factor

$K = Z\,(dU/ds)$ Shape factor

Λ = Shape factor, implicitly defined from K

$$K = \left(\frac{37}{315} - \frac{1}{945}\Lambda - \frac{1}{9072}\Lambda^2\right)^2 \Lambda$$

$$F(K) = 2\left(\frac{37}{315} - \frac{1}{945}\Lambda - \frac{1}{9072}\Lambda^2\right)\left[2 - \frac{116}{315}\Lambda + \left(\frac{2}{945} + \frac{1}{120}\right)\Lambda^2 + \frac{2}{9072}\Lambda^3\right]$$

= Auxiliary function

$dZ/ds = \frac{F(K)}{U}$ First derivative of shape factor

$\delta_2 = \sqrt{\frac{K\nu}{dU/ds}}$ Momentum thickness in inches

$$H_{12} = \frac{\delta 1}{\delta 2} = \frac{\frac{3}{10} - \frac{1}{120}\Lambda}{\frac{37}{315} - \frac{1}{945}\Lambda - \frac{1}{9072}\Lambda^2}$$ Shape factor

$\delta_1 = H_{12}\,\delta_2$ Displacement thickness

$\delta = \sqrt{\frac{\Lambda\nu}{dU/ds}}$ Boundry layer thickness

$H_{32} = \frac{4H_{12}}{(3H_{12}-1)}$ Shape factor

Table D.2. -Results of K & P analysis, α=2°.

Chord= 26.2 Inch
U= 1122 inch/s
u"@0= -5953

N	X/C	Y/C	Δs (Inch)	s (Inch)	Cp	u/U	u (in/s)	du/ds
1	.00000	.00000	.371	0.00	1.000	0.00	0	2772.2
2	.00533	.01313	.231	0.37	0.159	0.92	1029	561.9
3	.01066	.02013	.277	0.60	-0.066	1.03	1159	415.0
4	.01807	.02767	.323	0.88	-0.288	1.13	1274	218.9
5	.02755	.03556	.368	1.20	-0.435	1.20	1344	127.5
6	.03905	.04364	.414	1.57	-0.537	1.24	1391	80.0
7	.05252	.05190	.460	1.98	-0.611	1.27	1424	70.3
8	.06792	.06036	.505	2.44	-0.685	1.30	1457	66.9
9	.08516	.06895	.547	2.95	-0.764	1.33	1491	61.2
10	.10417	.07754	.586	3.50	-0.844	1.36	1524	46.1
11	.12489	.08597	.622	4.08	-0.910	1.38	1551	40.8
12	.14720	.09413	.657	4.70	-0.973	1.40	1576	32.0
13	.17104	.10192	.688	5.36	-1.026	1.42	1597	29.6
14	.19627	.10923	.717	6.05	-1.078	1.44	1618	9.8
15	.22280	.11592	.743	6.77	-1.096	1.45	1625	17.1
16	.25049	.12209	.768	7.51	-1.129	1.46	1638	23.9
17	.27925	.12773	.791	8.28	-1.177	1.48	1656	32.4
18	.30902	.13272	.808	9.07	-1.245	1.50	1682	19.4
19	.33961	.13674	.822	9.88	-1.287	1.51	1697	10.4
20	.37086	.13965	.834	10.70	-1.310	1.52	1706	-0.4
21	.40266	.14139	.844	11.53	-1.309	1.52	1705	-0.4
22	.43488	.14200	.851	12.38	-1.308	1.52	1705	3.9
23	.46737	.14143	.857	13.23	-1.317	1.52	1708	-16.9
24	.50000	.13942	.860	14.09	-1.278	1.51	1694	-24.8
25	.53264	.13600	.860	14.95	-1.221	1.49	1673	-31.8
26	.56512	.13119	.860	15.81	-1.149	1.47	1645	-53.3
27	.59734	.12495	.855	16.67	-1.031	1.43	1599	-57.0
28	.62914	.11754	.847	17.52	-0.909	1.38	1551	-58.9

TABLE D.2: -Continued.

nu= 0.023 inch^2/S

N	Z	K in	K out	Λ fit	Λ real	F	dZ/ds
1	.00003	.0770	.0770	7.052	7.052	0.000	5.05E-05
2	.00005	.0261	.0261	1.978	1.978	0.302	2.93E-04
3	.00011	.0642	.0642	5.460	5.460	0.073	6.30E-05
4	.00013	.0546	.0546	4.472	4.472	0.129	1.01E-04
5	.00016	.0360	.0360	2.783	2.783	0.241	1.79E-04
6	.00023	.0294	.0294	2.238	2.238	0.282	2.03E-04
7	.00031	.0251	.0251	1.897	1.897	0.308	2.17E-04
8	.00041	.0291	.0291	2.215	2.215	0.284	1.95E-04
9	.00051	.0343	.0343	2.641	2.641	0.252	1.69E-04
10	.00060	.0370	.0370	2.869	2.869	0.235	1.54E-04
11	.00069	.0320	.0320	2.457	2.457	0.265	1.71E-04
12	.00080	.0327	.0327	2.508	2.508	0.261	1.66E-04
13	.00091	.0291	.0291	2.219	2.219	0.283	1.77E-04
14	.00103	.0306	.0305	2.335	2.335	0.275	1.70E-04
15	.00115	.0113	.0113	0.830	0.830	0.396	2.44E-04
16	.00134	.0229	.0229	1.720	1.720	0.323	1.97E-04
17	.00149	.0355	.0355	2.748	2.748	0.244	1.47E-04
18	.00160	.0520	.0520	4.219	4.219	0.144	8.57E-05
19	.00167	.0324	.0324	2.486	2.486	0.263	1.55E-04
20	.00180	.0186	.0186	1.389	1.389	0.349	2.05E-04
21	.00197	-.0009	-.0009	-0.064	-0.064	0.476	2.79E-04
22	.00221	-.0010	-.0010	-0.071	-0.071	0.476	2.79E-04
23	.00244	.0095	.0096	0.702	0.702	0.408	2.39E-04
24	.00265	-.0446	-.0447	-3.119	-3.119	0.776	4.58E-04
25	.00304	-.0755	-.0761	-5.290	-5.290	1.010	6.04E-04
26	.00356	-.1132	-.1126	-7.967	-7.967	1.304	7.93E-04
27	.00424	-.2261	-.1146	-27.141	-27.141	1.986	1.24E-03
28	.00531	-.3026	#####	-75.216	-75.216	4.262	2.75E-03

TABLE D.2. -Continued.

N	δ_2 (inch)	δ_2 (y/C)	H_{12}	δ_1 (inch)	δ (inch)	H_{32}
1	0.0008	0.00003	2.31	0.002	0.008	1.558
2	0.0010	0.00004	2.47	0.003	0.009	1.542
3	0.0016	0.00006	2.35	0.004	0.015	1.554
4	0.0017	0.00007	2.38	0.004	0.016	1.551
5	0.0019	0.00007	2.44	0.005	0.017	1.545
6	0.0023	0.00009	2.46	0.006	0.020	1.543
7	0.0027	0.00010	2.47	0.007	0.023	1.541
8	0.0031	0.00012	2.46	0.008	0.027	1.543
9	0.0034	0.00013	2.44	0.008	0.030	1.544
10	0.0037	0.00014	2.43	0.009	0.033	1.545
11	0.0040	0.00015	2.45	0.010	0.035	1.544
12	0.0043	0.00016	2.45	0.011	0.038	1.544
13	0.0046	0.00017	2.46	0.011	0.040	1.543
14	0.0049	0.00019	2.45	0.012	0.043	1.543
15	0.0052	0.00020	2.52	0.013	0.044	1.537
16	0.0055	0.00021	2.48	0.014	0.048	1.541
17	0.0059	0.00022	2.44	0.014	0.051	1.545
18	0.0061	0.00023	2.39	0.014	0.055	1.550
19	0.0062	0.00024	2.45	0.015	0.054	1.544
20	0.0064	0.00025	2.49	0.016	0.056	1.539
21	0.0067	0.00026	2.56	0.017	0.057	1.533
22	0.0071	0.00027	2.56	0.018	0.061	1.533
23	0.0075	0.00029	2.52	0.019	0.064	1.536
24	0.0078	0.00030	2.72	0.021	0.065	1.519
25	0.0084	0.00032	2.87	0.024	0.070	1.509
26	0.0091	0.00035	3.08	0.028	0.076	1.495
27	0.0099	0.00038	8.10	0.080	0.152	1.391
28	0.0111	0.00042	-2.17	-0.024	-0.026	1.156

APPENDIX E

Flight Data

This section contains the raw flight test data as recorded by the pilot and the quantities calculated in the data analysis section. Since there is a considerable amount of data, 15 flights and 150 data points, it is placed in tabular form and grouped by flight number.

The first table, table E.1, contains the raw flight recorded data and the quantities used to calculate true velocity (V_t). The true velocity from table E.1 and other quantities are used in table E.2 in order to calculate step height Reynolds number, Re_h.

Table E.1. -Calculation of true velocity.

Flight Card 1 Po= 30.04 In Hg

Point	V ind Knots	Ind Alt Feet	Temp °F	ΔVpc Knots	V cal Knots	Pa PSF	sigma	V true Knots	V true ft/s
1	50.0	7400	62.0	1.0	51.0	1614	0.758	58.6	98.9
2	60.0	7200	63.2	0.9	60.9	1626	0.762	69.8	117.8
3	70.0	6900	65.4	0.8	70.8	1645	0.767	80.8	136.5
4	80.0	6500	67.2	0.7	80.7	1670	0.776	91.6	154.6
5	90.5	6100	70.2	0.6	91.1	1696	0.784	102.9	173.7
6	100.0	5550	72.5	0.5	100.5	1731	0.797	112.6	190.1
7	109.5	5000	74.9	0.4	109.9	1767	0.810	122.1	206.2
8	50.0	5080	72.5	1.0	51.0	1762	0.811	56.6	95.6
9	60.0	4950	73.2	0.9	60.9	1770	0.814	67.5	114.0
10	70.0	4800	74.1	0.8	70.8	1780	0.817	78.3	132.3

Flight Card 2 Po= 30.03 In Hg

Point	V ind Knots	Ind Alt Feet	Temp °F	ΔVpc Knots	V cal Knots	Pa PSF	sigma	V true Knots	V true ft/s
1	51.0	9550	52.3	1.0	52.0	1486	0.711	61.7	104.1
2	60.0	9300	53.6	0.9	60.9	1500	0.716	72.0	121.5
3	69.5	9050	54.9	0.8	70.3	1515	0.721	82.8	139.8
4	81.0	8850	56.2	0.7	81.7	1526	0.725	95.9	162.0
5	90.0	8400	58.2	0.6	90.6	1553	0.735	105.7	178.5
6	100.0	7900	60.6	0.5	100.5	1583	0.745	116.4	196.5
7	109.5	7300	63.8	0.4	109.9	1620	0.758	126.2	213.1
8	90.0	7050	64.5	0.6	90.6	1635	0.764	103.6	175.0
9	100.0	6600	66.4	0.5	100.5	1663	0.774	114.2	192.8
10	110.0	6150	68.8	0.4	110.4	1692	0.784	124.6	210.5

Flight Card 3 Po= 30.03 in Hg

Point	V ind Knots	Ind Alt Feet	Temp °F	ΔVpc Knots	V cal Knots	Pa PSF	sigma	V true Knots	V true ft/s
1	50.0	8160	68.1	1.0	51.0	1567	0.727	59.8	101.0
2	60.0	7940	69.6	0.9	60.9	1581	0.732	71.2	120.2
3	70.0	7650	70.9	0.8	70.8	1598	0.738	82.4	139.2
4	80.0	7420	72.4	0.7	80.7	1612	0.742	93.6	158.2
5	89.0	7000	73.3	0.6	89.6	1638	0.753	103.2	174.4
6	100.0	6500	75.8	0.5	100.5	1670	0.764	115.0	194.2
7	110.0	6000	75.9	0.4	110.4	1701	0.778	125.1	211.3
8	51.0	6050	74.1	1.0	52.0	1698	0.779	58.9	99.4
9	60.0	5950	74.0	0.9	60.9	1705	0.782	68.8	116.3
10	71.0	5750	75.2	0.8	71.8	1718	0.787	80.9	136.7

Table E.1. -Continued.

Flight Card 4 Po= 30.03 in Hg

Point	V ind Knots	Ind Alt Feet	Temp °F	ΔVpc Knots	V cal Knots	Pa PSF	sigma	V true Knots	V true ft/s
1	50.0	7850	61.5	1.0	51.0	1586	0.745	59.1	99.7
2									
3	70.5	7500	63.3	0.8	71.3	1607	0.753	82.1	138.7
4	80.0	7250	64.6	0.7	80.7	1623	0.758	92.7	156.5
5	91.0	6950	66.3	0.6	91.6	1641	0.764	104.7	176.9
6	100.0	6550	67.8	0.5	100.5	1666	0.774	114.2	192.9
7	110.0	6150	70.4	0.4	110.4	1692	0.782	124.8	210.8
8	81.0	5850	71.5	0.7	81.7	1711	0.789	91.9	155.3
9	111.0	5200	75.4	0.4	111.4	1753	0.803	124.3	209.9
10	60.0	5250	73.6	0.9	60.9	1750	0.804	67.9	114.7

Flight Card 5 Po= 30.03 in Hg

Point	V ind Knots	Ind Alt Feet	Temp °F	ΔVpc Knots	V cal Knots	Pa PSF	sigma	V true Knots	V true ft/s
1	50.0	8410	66.8	1.0	51.0	1552	0.722	60.0	101.3
2	60.0	8200	68.0	0.9	60.9	1565	0.726	71.4	120.6
3	70.0	8020	68.9	0.8	70.8	1576	0.730	82.8	139.9
4	80.0	7800	69.9	0.7	80.7	1589	0.735	94.1	158.9
5	90.0	7450	71.4	0.6	90.6	1610	0.743	105.1	177.5
6	99.5	6880	74.0	0.5	100.0	1646	0.755	115.0	194.3
7	110.0	6300	76.5	0.4	110.4	1682	0.769	125.9	212.6
8	90.0	6200	76.9	0.6	90.6	1689	0.771	103.2	174.2
9	100.0	5750	78.0	0.5	100.5	1718	0.782	113.6	191.8
10	110.0	5200	79.6	0.4	110.4	1753	0.796	123.7	208.9

Flight Card 6 Po= 30.03 in Hg

Point	V ind Knots	Ind Alt Feet	Temp °F	ΔVpc Knots	V cal Knots	Pa PSF	sigma	V true Knots	V true ft/s
1	50.0	8410	66.8	1.0	51.0	1552	0.722	60.0	101.3
2	60.0	8200	68.0	0.9	60.9	1565	0.726	71.4	120.6
3	70.0	8020	68.9	0.8	70.8	1576	0.730	82.8	139.9
4	80.0	7800	69.9	0.7	80.7	1589	0.735	94.1	158.9
5	90.0	7450	71.4	0.6	90.6	1610	0.743	105.1	177.5
6	99.5	6880	74.0	0.5	100.0	1646	0.755	115.0	194.3
7	110.0	6300	76.5	0.4	110.4	1682	0.769	125.9	212.6
8	90.0	6200	76.9	0.6	90.6	1689	0.771	103.2	174.2
9	100.0	5750	78.0	0.5	100.5	1718	0.782	113.6	191.8
10	110.0	5200	79.6	0.4	110.4	1753	0.796	123.7	208.9

Table E.1. -Continued.

Flight Card 7 Po= 29.97 in Hg

Point	V ind Knots	Ind Alt Feet	Temp °F	ΔVpc Knots	V cal Knots	Pa PSF	sigma	V true Knots	V true ft/s
1	50.0	9440	57.4	1.0	51.0	1489	0.705	60.7	102.5
2	60.0	9140	59.2	0.9	60.9	1506	0.711	72.2	121.9
3	70.5	8920	60.9	0.8	71.3	1519	0.715	84.3	142.4
4	80.0	8600	62.4	0.7	80.7	1538	0.722	95.0	160.4
5	91.0	8100	64.2	0.6	91.6	1568	0.733	106.9	180.6
6	102.0	7400	66.4	0.4	102.4	1610	0.750	118.3	199.8
7	108.0	7800	70.1	0.4	108.4	1586	0.733	126.6	213.8
8	61.0	6960	67.7	0.9	61.9	1637	0.761	71.0	119.8
9	90.5	6850	69.3	0.6	91.1	1644	0.761	104.4	176.3
10	109.0	6750	73.5	0.4	109.4	1651	0.758	125.6	212.1

Flight Card 8 Po= 29.92 in Hg

Point	V ind Knots	Ind Alt Feet	Temp °F	ΔVpc Knots	V cal Knots	Pa PSF	sigma	V true Knots	V true ft/s
1	50.0	9440	57.4	1.0	51.0	1487	0.704	60.8	102.6
2	60.0	9140	59.2	0.9	60.9	1504	0.710	72.3	122.0
3	70.5	8920	60.9	0.8	71.3	1517	0.714	84.4	142.5
4	80.0	8600	62.4	0.7	80.7	1536	0.720	95.0	160.5
5	91.0	8100	64.2	0.6	91.6	1565	0.732	107.0	180.8
6	102.0	7400	66.4	0.4	102.4	1608	0.749	118.4	200.0
7	108.0	7800	70.1	0.4	108.4	1583	0.732	126.7	213.9
8	61.0	6960	67.7	0.9	61.9	1635	0.759	71.0	119.9
9	90.5	6850	69.3	0.6	91.1	1642	0.760	104.4	176.4
10	109.0	6750	73.5	0.4	109.4	1648	0.757	125.7	212.3

Flight Card 9 Po= 30.14 in Hg

Point	V ind Knots	Ind Alt Feet	Temp °F	ΔVpc Knots	V cal Knots	Pa PSF	sigma	V true Knots	V true ft/s
1	70.0	9600	50.8	0.8	70.8	1488	0.714	83.8	141.5
2	70.0	9350	51.6	0.8	70.8	1503	0.720	83.4	140.9
3	70.0	9240	52.2	0.8	70.8	1509	0.722	83.3	140.7
4	69.5	9050	52.8	0.8	70.3	1520	0.727	82.5	139.3
5	70.5	8840	53.8	0.8	71.3	1533	0.731	83.4	140.8
6	70.0	8500	54.9	0.8	70.8	1553	0.739	82.3	139.0
7	70.0	8300	56.0	0.8	70.8	1565	0.743	82.1	138.7
8	70.5	8150	56.6	0.8	71.3	1574	0.747	82.5	139.3
9	70.0	8000	57.4	0.8	70.8	1583	0.750	81.7	138.1
10	70.5	7800	58.4	0.8	71.3	1595	0.754	82.1	138.6

Table E.1 -Continued.

Flight Card 10 Po= 29.98 in Hg

Point	V ind Knots	Ind Alt Feet	Temp °F	ΔVpc Knots	V cal Knots	Pa PSF	sigma	V true Knots	V true ft/s
1	50.0	8850	51.4	1.0	51.0	1524	0.730	59.7	100.8
2	61.0	8600	52.5	0.9	61.9	1539	0.736	72.1	121.8
3	70.5	8400	53.2	0.8	71.3	1550	0.741	82.8	139.9
4	80.0	8100	54.4	0.7	80.7	1568	0.747	93.3	157.6
5	89.5	7700	56.0	0.6	90.1	1593	0.756	103.6	174.9
6	100.0	7300	57.5	0.5	100.5	1617	0.766	114.8	193.9
7	110.0	6700	58.4	0.4	110.4	1654	0.782	124.8	210.8
8	60.0	6800	58.6	0.9	60.9	1648	0.779	69.0	116.5
9	80.0	6420	58.7	0.7	80.7	1672	0.790	90.8	153.3
10	100.0	5700	61.3	0.5	100.5	1718	0.808	111.8	188.8

Flight Card 11 Po= 29.98 in Hg

Point	V ind Knots	Ind Alt Feet	Temp °F	ΔVpc Knots	V cal Knots	Pa PSF	sigma	V true Knots	V true ft/s
1	50.0	9250	50.0	1.0	51.0	1501	0.721	60.0	101.4
2	60.0	9000	50.8	0.9	60.9	1515	0.727	71.4	120.6
3	70.0	8800	52.2	0.8	70.8	1527	0.731	82.8	139.9
4	80.0	8450	54.3	0.7	80.7	1548	0.738	93.9	158.7
5	90.0	8050	56.6	0.6	90.6	1571	0.746	104.9	177.2
6	99.0	7500	59.1	0.5	99.5	1605	0.758	114.3	193.0
7	110.0	6900	61.5	0.4	110.4	1642	0.772	125.6	212.2
8	50.0	7200	59.1	1.0	51.0	1623	0.766	58.2	98.4
9	69.0	7000	59.3	0.8	69.8	1636	0.772	79.4	134.2
10	91.5	6500	62.6	0.6	92.1	1667	0.782	104.1	175.8

Flight Card 12 Po= 29.98 in Hg

Point	V ind Knots	Ind Alt Feet	Temp °F	ΔVpc Knots	V cal Knots	Pa PSF	sigma	V true Knots	V true ft/s
1	50	9700	44.9	1.0	51.0	1475	0.716	60.3	101.8
2	60	9460	46.1	0.9	60.9	1488	0.721	71.7	121.1
3	70	9220	45.9	0.8	70.8	1502	0.728	83.0	140.1
4	80	8920	43.6	0.7	80.7	1520	0.740	93.8	158.4
5	89.5	8500	44	0.6	90.1	1545	0.751	103.9	175.5
6	100	8000	45.3	0.5	100.5	1574	0.764	115.0	194.2
7	113	7350	47.9	0.3	113.3	1614	0.779	128.4	216.9
8	62	7600	46	0.9	62.9	1599	0.774	71.4	120.7
9	82.5	7300	47.9	0.7	83.2	1617	0.780	94.1	159.0
10	102	6850	49.7	0.4	102.4	1645	0.791	115.2	194.5

Table E.1. -Continued.

Flight Card 13 Po= 29.98 in Hg

Point	V ind Knots	Ind Alt Feet	Temp °F	ΔVpc Knots	V cal Knots	Pa PSF	sigma	V true Knots	V true ft/s
1	50.5	9360	45.3	1.0	51.5	1494	0.725	60.5	102.1
2	60	9200	43.9	0.9	60.9	1503	0.731	71.2	120.2
3	70	8920	42.9	0.8	70.8	1520	0.741	82.2	138.9
4	80.5	8580	43.2	0.7	81.2	1540	0.750	93.7	158.3
5	89.5	8200	44.3	0.6	90.1	1562	0.759	103.4	174.6
6	100	7800	46.1	0.5	100.5	1586	0.768	114.6	193.6
7	110	7260	48.8	0.4	110.4	1619	0.780	124.9	211.0
8	50	7460	46.2	1.0	51.0	1607	0.778	57.8	97.6
9	70	7200	47.7	0.8	70.8	1623	0.784	80.0	135.0
10	90	6720	49.9	0.6	90.6	1653	0.795	101.6	171.6

Flight Card 14 Po= 30.01 in Hg

Point	V ind Knots	Ind Alt Feet	Temp °F	ΔVpc Knots	V cal Knots	Pa PSF	sigma	V true Knots	V true ft/s
1	50.5	9440	42.8	1.0	51.5	1491	0.727	60.4	102.0
2	60	9240	43.9	0.9	60.9	1503	0.731	71.2	120.3
3	70	9000	45.0	0.8	70.8	1517	0.736	82.5	139.3
4	80	8620	46.8	0.7	80.7	1539	0.744	93.5	157.9
5	90	8200	48.3	0.6	90.6	1564	0.754	104.3	176.1
6	100	7700	50.6	0.5	100.5	1594	0.765	114.8	194.0
7	110	7150	53.9	0.4	110.4	1628	0.776	125.2	211.5
8	70	7100	53.0	0.8	70.8	1631	0.779	80.2	135.4
9	90.5	6600	55.2	0.6	91.1	1662	0.791	102.4	173.0
10	110	6100	57.3	0.4	110.4	1694	0.803	123.2	208.1

Flight Card 15 Po= 30.03 in Hg

Point	V ind Knots	Ind Alt Feet	Temp °F	ΔVpc Knots	V cal Knots	Pa PSF	sigma	V true Knots	V true ft/s
1	50	10050	41.3	1.0	51.0	1457	0.713	60.4	102.0
2	60	9880	42.3	0.9	60.9	1467	0.716	72.0	121.5
3	70	9650	43.3	0.8	70.8	1480	0.721	83.4	140.8
4	80	9360	45.6	0.7	80.7	1497	0.726	94.7	160.0
5	90	8880	48.2	0.6	90.6	1525	0.735	105.6	178.4
6	100	8240	51.2	0.5	100.5	1563	0.749	116.1	196.0
7	110	7700	53.6	0.4	110.4	1595	0.761	126.5	213.6
8	60.5	7780	52.8	0.9	61.4	1590	0.760	70.4	118.9
9	80	7470	55.2	0.7	80.7	1609	0.766	92.2	155.7
10	99	6850	58.7	0.5	99.5	1648	0.779	112.7	190.4

Table E.2. -Chord and step Reynolds numbers.

Flight Card 1 — Smooth wing

Point	V true Knots	nu ft^2/s	Chord Re	T.S. Alpha degrees
1	58.6	2.083E-4	1.08E+6	2.8
2	69.8	2.075E-4	1.30E+6	-0.1
3	80.8	2.067E-4	1.51E+6	-1.5
4	91.6	2.048E-4	1.72E+6	-2.4
5	102.9	2.038E-4	1.95E+6	-3.0
6	112.6	2.012E-4	2.16E+6	-3.3
7	122.1	1.986E-4	2.37E+6	-3.3
8	56.6	1.977E-4	1.10E+6	3.5
9	67.5	1.972E-4	1.32E+6	0.4
10	78.3	1.966E-4	1.54E+6	-1.3

Flight Card 2 — Smooth wing

Point	V true Knots	nu ft^2/s	Chord Re	T.S. Alpha degrees
1	61.7	2.188E-4	1.09E+6	1.8
2	72.0	2.177E-4	1.27E+6	-0.4
3	82.8	2.166E-4	1.47E+6	-1.7
4	95.9	2.159E-4	1.71E+6	-2.6
5	105.7	2.137E-4	1.91E+6	-3.1
6	116.4	2.113E-4	2.12E+6	-3.3
7	126.2	2.088E-4	2.33E+6	-3.3
8	103.6	2.073E-4	1.93E+6	-3.0
9	114.2	2.051E-4	2.15E+6	-3.3
10	124.6	2.033E-4	2.36E+6	-3.3

Flight Card 3 — Step height = 0.0313 — x/C = 24.40%

Point	V true Knots	nu ft^2/s	Chord Re	T.S. Alpha degrees	u/U	Step Re
1	59.8	2.189E-4	1.05E+6	2.4	1.47	1766
2	71.2	2.182E-4	1.26E+6	-0.3	1.37	1965
3	82.4	2.167E-4	1.47E+6	-1.7	1.32	2203
4	93.6	2.159E-4	1.67E+6	-2.5	1.29	2452
5	103.2	2.131E-4	1.87E+6	-3.0	1.27	2700
6	115.0	2.109E-4	2.10E+6	-3.3	1.26	3010
7	125.1	2.070E-4	2.33E+6	-3.3	1.26	3339
8	58.9	2.062E-4	1.10E+6	2.7	1.48	1861
9	68.8	2.053E-4	1.29E+6	0.1	1.39	2042
10	80.9	2.046E-4	1.53E+6	-1.5	1.32	2301

Table E.2. -Continued.

Flight Card 4 Step height = 0.0196 x/C = 24.40%

Point	V true Knots	nu ft^2/s	Chord Re	T.S. Alpha degrees	u/U	Step Re
1	59.1	2.116E-4	6.37E+5	2.6	1.48	1138
2						
3	82.1	2.101E-4	8.93E+5	-1.7	1.32	1420
4	92.7	2.090E-4	1.01E+6	-2.5	1.29	1573
5	104.7	2.078E-4	1.15E+6	-3.1	1.27	1756
6	114.2	2.057E-4	1.27E+6	-3.3	1.26	1920
7	124.8	2.044E-4	1.39E+6	-3.3	1.26	2112
8	91.9	2.029E-4	1.03E+6	-2.4	1.29	1610
9	124.3	2.005E-4	1.42E+6	-3.3	1.26	2144
10	67.9	1.997E-4	7.76E+5	0.3	1.39	1304

Flight Card 5 Step height = 0.0147 x/C = 24.40%

Point	V true Knots	nu ft^2/s	Chord Re	T.S. Alpha degrees	u/U	Step Re
1	60.0	2.201E-4	6.22E+5	2.3	1.47	829
2	71.4	2.192E-4	7.44E+5	-0.3	1.37	923
3	82.8	2.184E-4	8.66E+5	-1.7	1.32	1033
4	94.1	2.173E-4	9.89E+5	-2.5	1.28	1152
5	105.1	2.154E-4	1.11E+6	-3.1	1.26	1277
6	115.0	2.127E-4	1.23E+6	-3.3	1.26	1406
7	125.9	2.098E-4	1.37E+6	-3.3	1.26	1561
8	103.2	2.093E-4	1.13E+6	-3.0	1.27	1294
9	113.6	2.065E-4	1.26E+6	-3.3	1.26	1430
10	123.7	2.033E-4	1.39E+6	-3.3	1.26	1581

Flight Card 6 Step height = 0.0116 x/C = 42.60%

Point	V true Knots	nu ft^2/s	Chord Re	T.S. Alpha degrees	u/U	Step Re
1	60.0	2.201E-4	6.22E+5	2.3	1.52	680
2	71.4	2.192E-4	7.44E+5	-0.3	1.46	778
3	82.8	2.184E-4	8.66E+5	-1.7	1.42	884
4	94.1	2.173E-4	9.89E+5	-2.5	1.40	995
5	105.1	2.154E-4	1.11E+6	-3.1	1.39	1110
6	115.0	2.127E-4	1.23E+6	-3.3	1.38	1226
7	125.9	2.098E-4	1.37E+6	-3.3	1.39	1361
8	103.2	2.093E-4	1.13E+6	-3.0	1.39	1123
9	113.6	2.065E-4	1.26E+6	-3.3	1.38	1247
10	123.7	2.033E-4	1.39E+6	-3.3	1.38	1378

Table E.2. -Continued.

Flight Card 7 Step height = 0.0147 x/C = 42.60%

Point	V true Knots	nu ft^2/s	Chord Re	T.S. Alpha degrees	u/U	Step Re
1	60.7	2.222E-4	6.24E+5	2.1	1.52	859
2	72.2	2.210E-4	7.46E+5	-0.5	1.46	984
3	84.3	2.204E-4	8.73E+5	-1.8	1.42	1125
4	95.0	2.189E-4	9.91E+5	-2.6	1.40	1260
5	106.9	2.160E-4	1.13E+6	-3.1	1.39	1423
6	118.3	2.119E-4	1.27E+6	-3.3	1.38	1600
7	126.6	2.178E-4	1.33E+6	-3.3	1.39	1667
8	71.0	2.093E-4	7.74E+5	-0.3	1.46	1025
9	104.4	2.095E-4	1.14E+6	-3.0	1.39	1434
10	125.6	2.117E-4	1.35E+6	-3.3	1.39	1701

Flight Card 8 Step height = 0.0196 x/C = 42.60%

Point	V true Knots	nu ft^2/s	Chord Re	T.S. Alpha degrees	u/U	Step Re
1	60.8	2.226E-4	6.23E+5	2.1	1.52	1142
2	72.3	2.214E-4	7.45E+5	-0.5	1.46	1308
3	84.4	2.208E-4	8.72E+5	-1.9	1.42	1495
4	95.0	2.192E-4	9.90E+5	-2.6	1.40	1674
5	107.0	2.164E-4	1.13E+6	-3.1	1.39	1892
6	118.4	2.122E-4	1.27E+6	-3.3	1.38	2126
7	126.7	2.182E-4	1.33E+6	-3.3	1.39	2215
8	71.0	2.096E-4	7.73E+5	-0.3	1.46	1362
9	104.4	2.099E-4	1.14E+6	-3.0	1.39	1907
10	125.7	2.120E-4	1.35E+6	-3.3	1.39	2262

Flight Card 9 Smooth wing

Point	V true Knots	nu ft^2/s	Chord Re	T.S. Alpha degrees
1	83.8	2.173E-4	8.80E+5	-1.8
2	83.4	2.158E-4	8.83E+5	-1.8
3	83.3	2.154E-4	8.83E+5	-1.8
4	82.5	2.142E-4	8.79E+5	-1.7
5	83.4	2.132E-4	8.93E+5	-1.8
6	82.3	2.113E-4	8.90E+5	-1.7
7	82.1	2.105E-4	8.91E+5	-1.7
8	82.5	2.097E-4	8.98E+5	-1.7
9	81.7	2.091E-4	8.93E+5	-1.6
10	82.1	2.082E-4	9.00E+5	-1.6

Table E.2. -Continued.

Flight Card 10 Trip Strip Trip x/C = 42.60%

Point	V true Knots	nu ft^2/s	Chord Re	T.S. Alpha degrees	u/U
1	59.7	2.127E-4	6.41E+5	2.4	1.53
2	72.1	2.115E-4	7.79E+5	-0.5	1.46
3	82.8	2.104E-4	8.99E+5	-1.7	1.42
4	93.3	2.088E-4	1.02E+6	-2.5	1.40
5	103.6	2.068E-4	1.14E+6	-3.0	1.39
6	114.8	2.047E-4	1.28E+6	-3.3	1.38
7	124.8	2.007E-4	1.42E+6	-3.3	1.38
8	69.0	2.016E-4	7.81E+5	0.1	1.47
9	90.8	1.988E-4	1.04E+6	-2.3	1.41
10	111.8	1.952E-4	1.31E+6	-3.3	1.39

Flight Card 11 Step height = 0.0147 x/C = 10.50%

Point	V true Knots	nu ft^2/s	Chord Re	T.S. Alpha degrees	u/U	Step Re
1	60.0	2.149E-4	6.38E+5	2.3	1.37	794
2	71.4	2.135E-4	7.64E+5	-0.3	1.21	841
3	82.8	2.129E-4	8.88E+5	-1.7	1.13	911
4	93.9	2.116E-4	1.01E+6	-2.5	1.08	994
5	104.9	2.100E-4	1.14E+6	-3.1	1.05	1086
6	114.3	2.074E-4	1.26E+6	-3.3	1.04	1181
7	125.6	2.044E-4	1.40E+6	-3.3	1.04	1319
8	58.2	2.051E-4	6.49E+5	2.9	1.41	829
9	79.4	2.036E-4	8.91E+5	-1.4	1.15	930
10	104.1	2.021E-4	1.18E+6	-3.0	1.05	1122

Flight Card 12 Step height = 0.0116 x/C = 10.50%

Point	V true Knots	nu ft^2/s	Chord Re	T.S. Alpha degrees	u/U	Step Re
1	60.3	2.148E-4	6.41E+5	2.2	1.37	628
2	71.7	2.137E-4	7.66E+5	-0.4	1.21	665
3	83.0	2.116E-4	8.95E+5	-1.7	1.13	725
4	93.8	2.075E-4	1.03E+6	-2.5	1.08	801
5	103.9	2.045E-4	1.16E+6	-3.0	1.05	875
6	115.0	2.015E-4	1.30E+6	-3.3	1.03	966
7	128.4	1.984E-4	1.48E+6	-3.2	1.04	1102
8	71.4	1.989E-4	8.20E+5	-0.3	1.21	714
9	94.1	1.980E-4	1.09E+6	-2.5	1.08	841
10	115.2	1.959E-4	1.34E+6	-3.3	1.03	996

Table E.2. -Continued.

Flight Card 13 Step height = 0.0196 x/C = 10.50%

Point	V true Knots	nu ft^2/s	Chord Re	T.S. Alpha degrees	u/U	Step Re
1	60.5	2.123E-4	6.50E+5	2.1	1.36	1071
2	71.2	2.100E-4	7.74E+5	-0.3	1.22	1136
3	82.2	2.070E-4	9.07E+5	-1.7	1.13	1241
4	93.7	2.045E-4	1.05E+6	-2.5	1.08	1366
5	103.4	2.023E-4	1.17E+6	-3.0	1.05	1482
6	114.6	2.005E-4	1.31E+6	-3.3	1.03	1629
7	124.9	1.983E-4	1.44E+6	-3.3	1.04	1797
8	57.8	1.980E-4	6.67E+5	3.0	1.42	1141
9	80.0	1.971E-4	9.26E+5	-1.4	1.15	1282
10	101.6	1.950E-4	1.19E+6	-2.9	1.06	1518

Flight Card 14 Step height = 0.0116 x/C = 24.40%

Point	V true Knots	nu ft^2/s	Chord Re	T.S. Alpha degrees	u/U	Step Re
1	60.4	2.109E-4	6.54E+5	2.2	1.46	686
2	71.2	2.101E-4	7.74E+5	-0.3	1.37	760
3	82.5	2.090E-4	9.01E+5	-1.7	1.32	851
4	93.5	2.072E-4	1.03E+6	-2.5	1.29	950
5	104.3	2.050E-4	1.16E+6	-3.0	1.27	1054
6	114.8	2.027E-4	1.29E+6	-3.3	1.26	1164
7	125.2	2.008E-4	1.42E+6	-3.3	1.26	1283
8	80.2	1.998E-4	9.16E+5	-1.5	1.33	871
9	102.4	1.976E-4	1.18E+6	-3.0	1.27	1077
10	123.2	1.953E-4	1.44E+6	-3.3	1.26	1296

Flight Card 15 Step height = 0.0147 x/C = 24.40%

Point	V true Knots	nu ft^2/s	Chord Re	T.S. Alpha degrees	u/U	Step Re
1	60.4	2.146E-4	6.43E+5	2.2	1.46	852
2	72.0	2.140E-4	7.68E+5	-0.4	1.36	950
3	83.4	2.128E-4	8.94E+5	-1.8	1.31	1066
4	94.7	2.122E-4	1.02E+6	-2.6	1.28	1186
5	105.6	2.102E-4	1.15E+6	-3.1	1.26	1315
6	116.1	2.073E-4	1.28E+6	-3.3	1.26	1455
7	126.5	2.047E-4	1.41E+6	-3.3	1.26	1608
8	70.4	2.048E-4	7.85E+5	-0.2	1.37	978
9	92.2	2.041E-4	1.03E+6	-2.4	1.29	1206
10	112.7	2.017E-4	1.28E+6	-3.3	1.26	1454

APPENDIX F

Hot Film Data

Samples From Each Airspeed

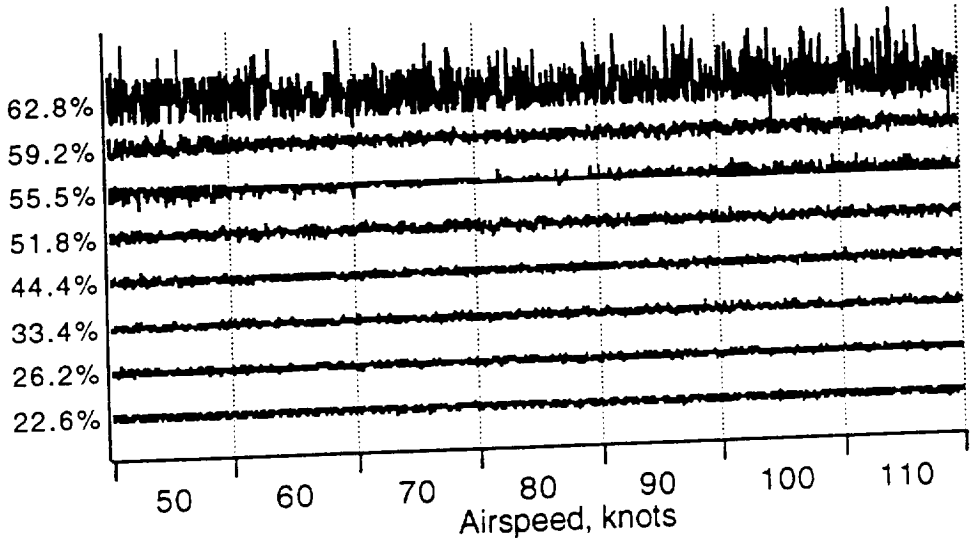

Figure F.1. -Flight, signal samples, 1 smooth wing.

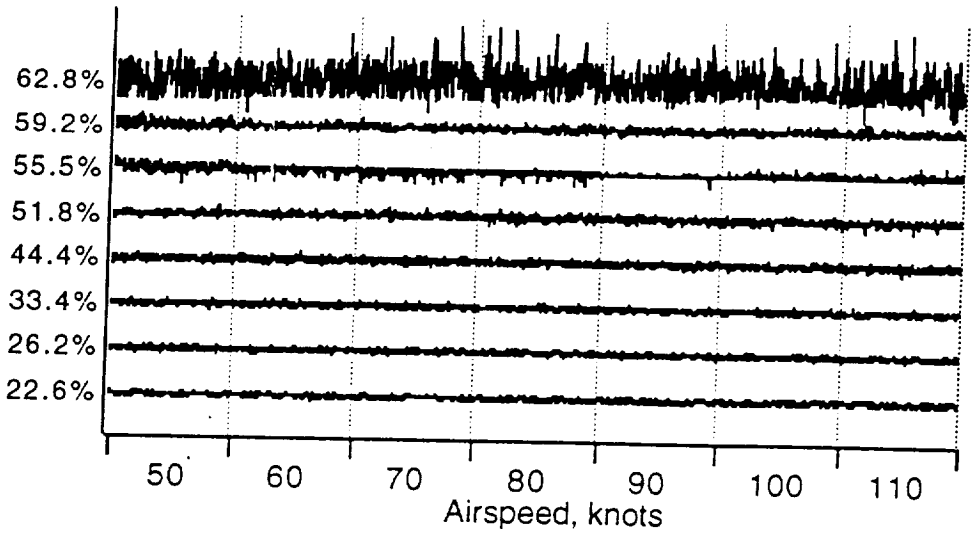

Figure F.2. -Flight 2, signal samples, smooth wing.

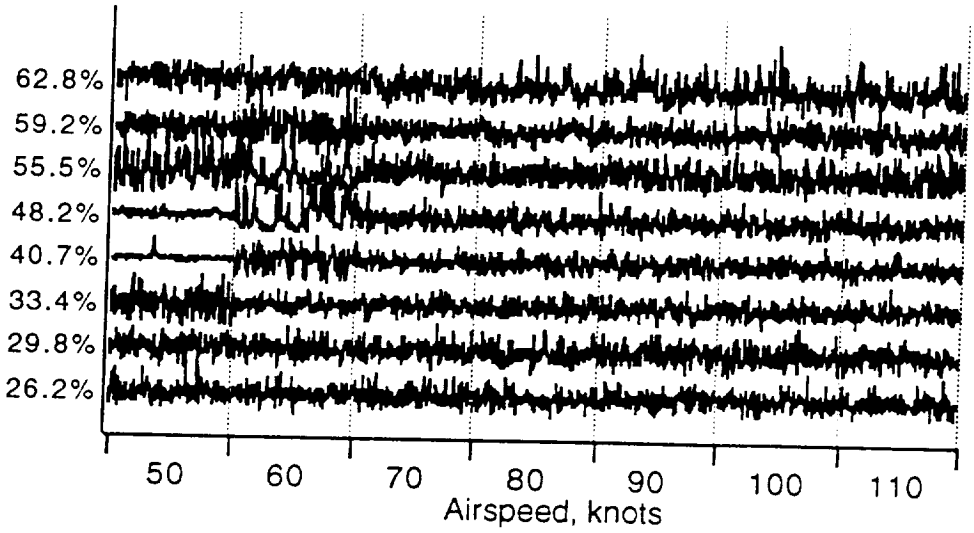

Figure F.3. -Flight 3, signal samples, 0.0313 aft step at 24.4%.

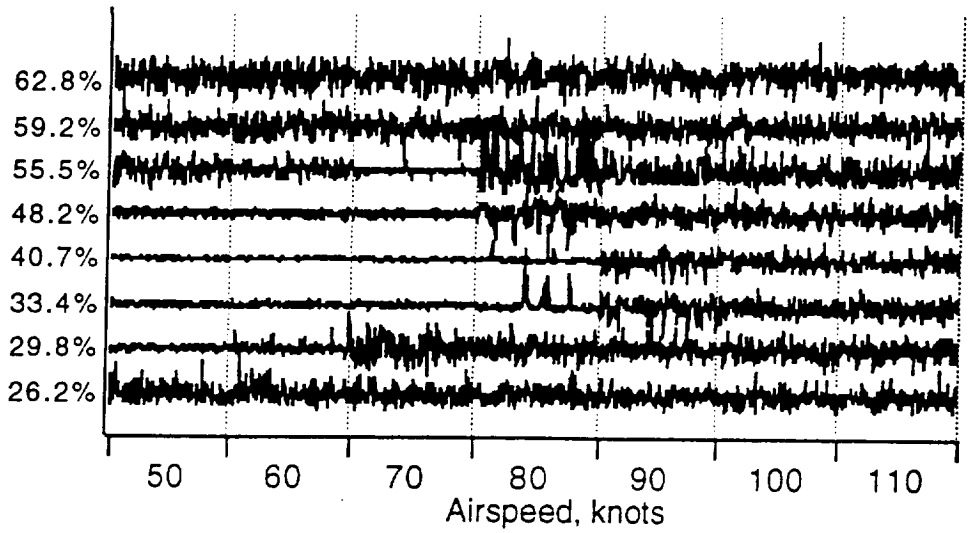

Figure F.4. -Flight 4, signal samples, 0.0196 aft step at 24.4%.

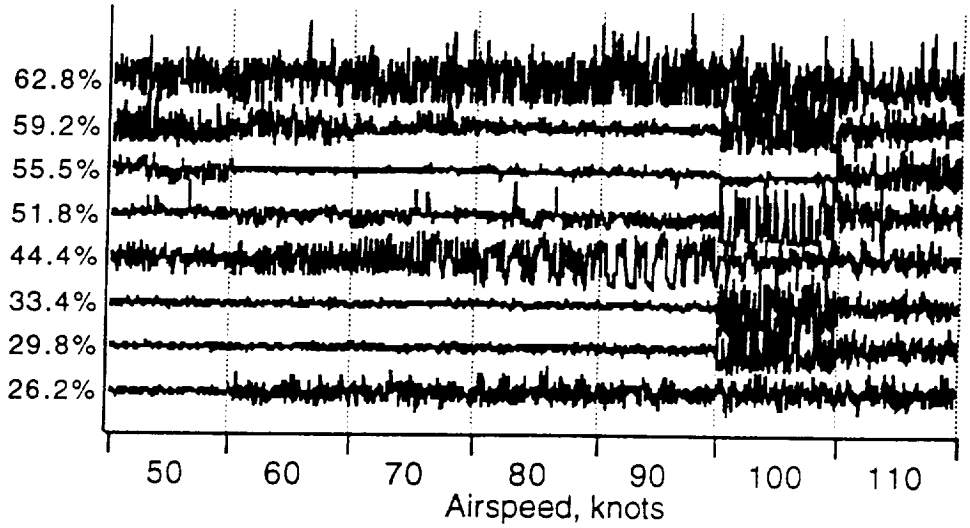

Figure F.5. -Flight 5, signal samples, 0.0147 aft step at 24.4%.

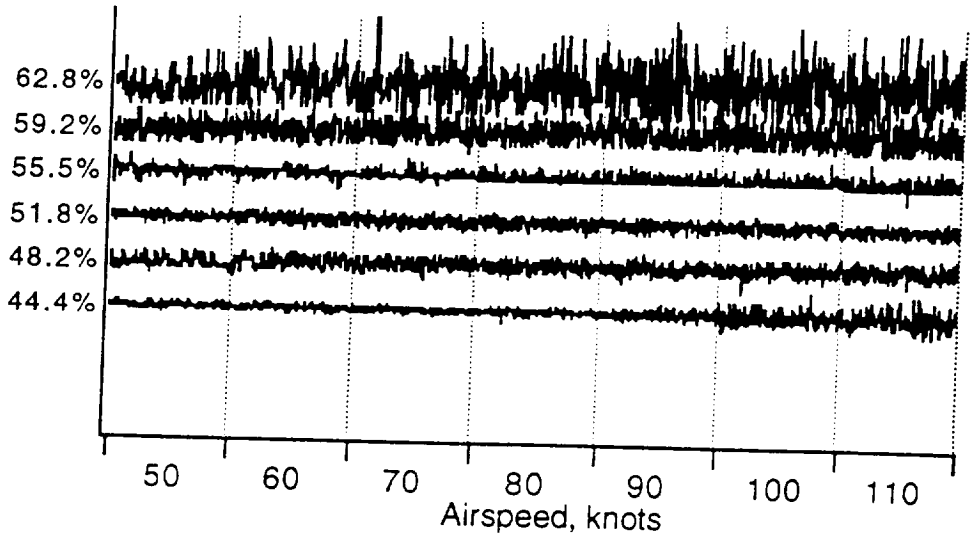

Figure F.6. -Flight 6, signal samples, 0.0116 aft step at 42.6%.

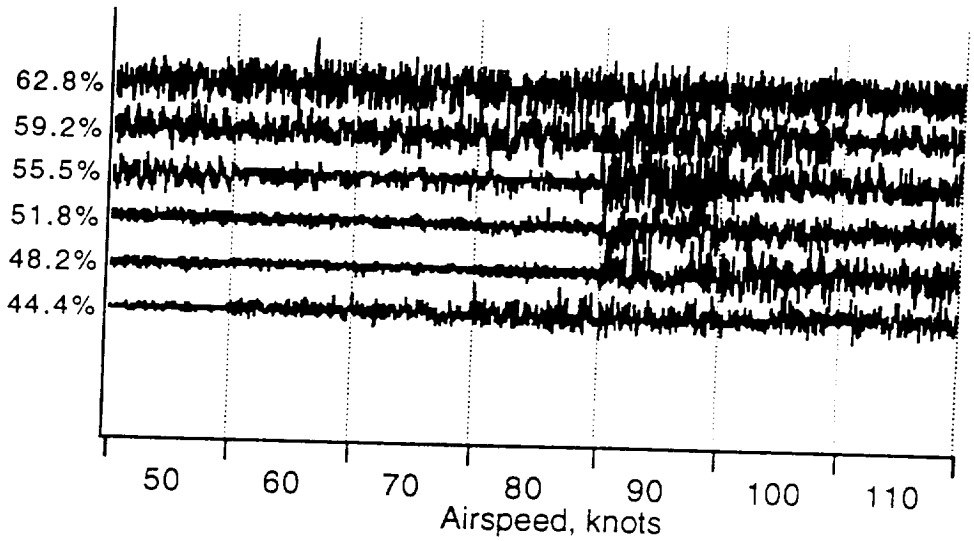

Figure F.7. -Flight 7, signal samples, 0.0147 aft step at 42.6%.

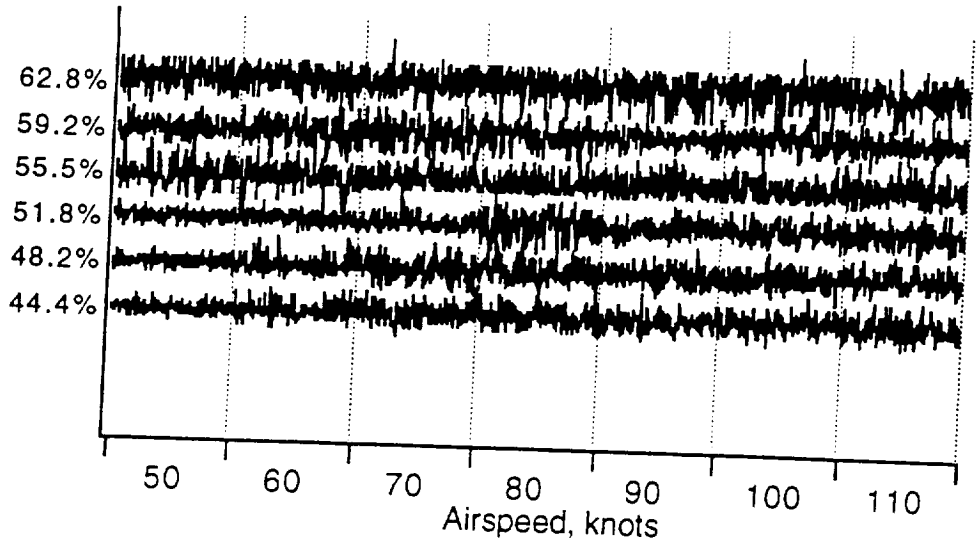

Figure F.8. -Flight 8, signal samples, 0.0196 aft step at 42.6%.

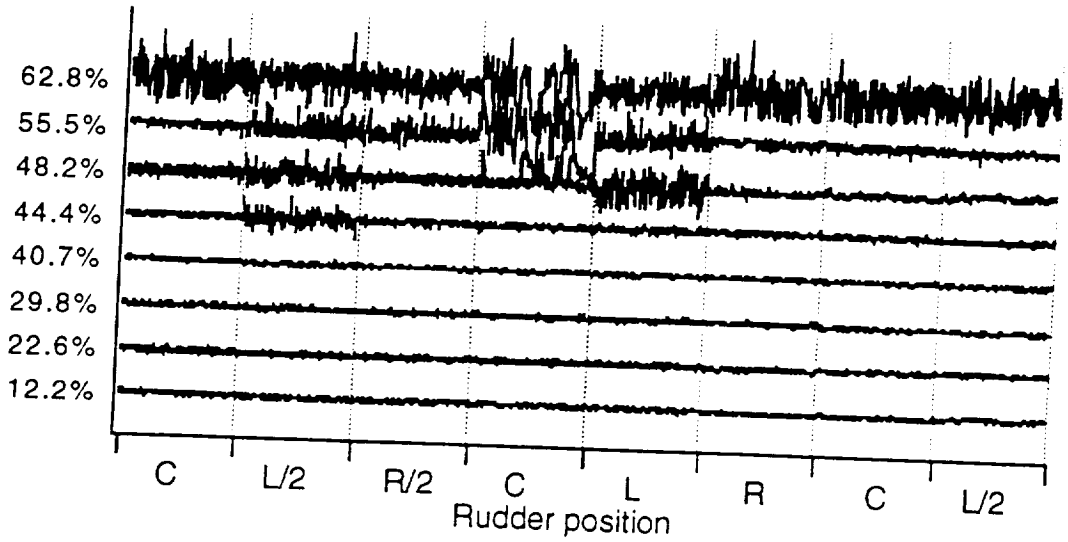

Figure F.9. -Flight 9, signal samples, side slip.

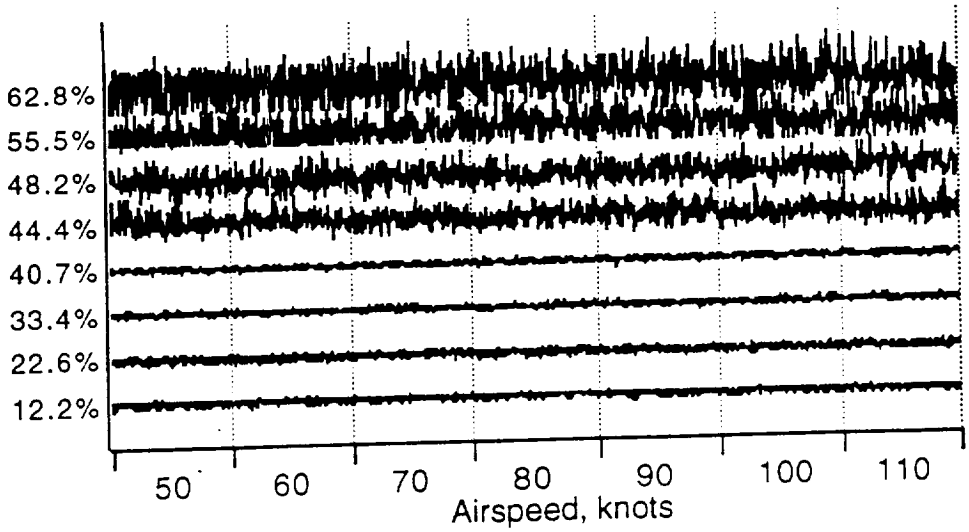

Figure F.10. -Flight 10, signal samples, grit strip at 42.6%.

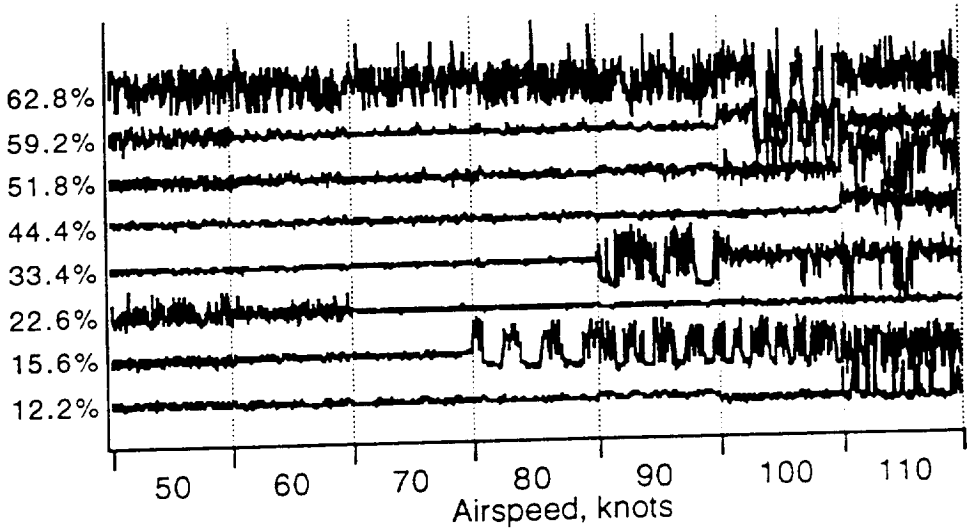

Figure F.11. -Flight 11, signal samples, 0.0147 aft step at 10.5%.

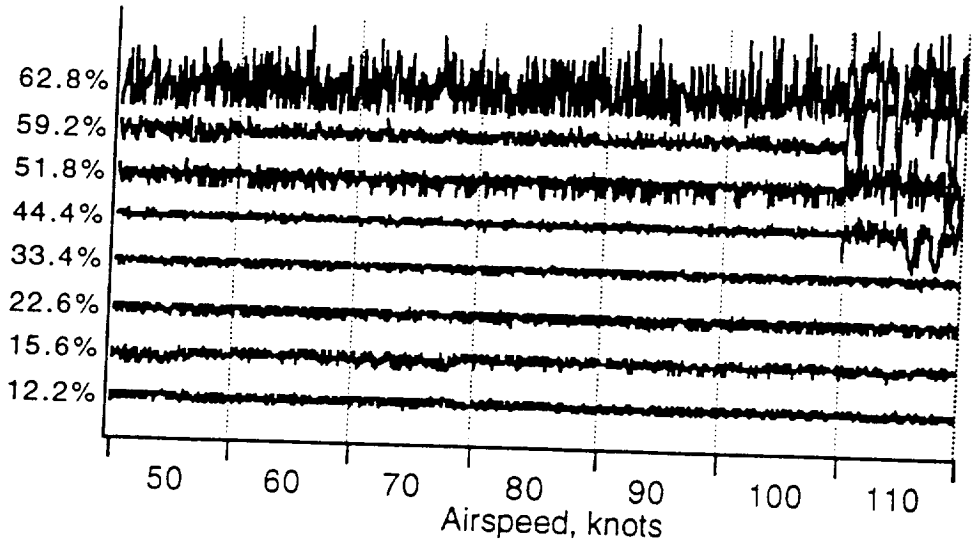

Figure F.12. -Flight 12, signal samples, 0.0116 aft step at 10.5%.

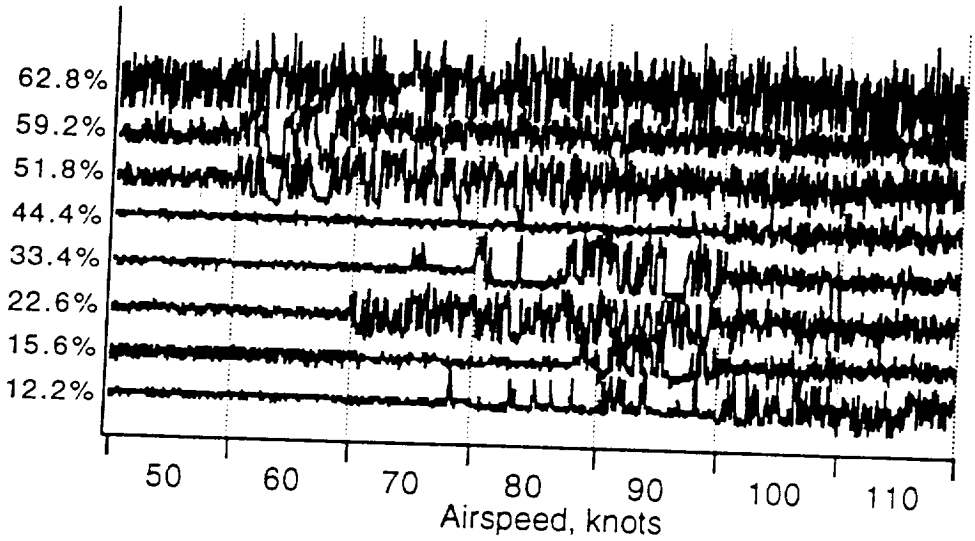

Figure F.13. -Flight 13, signal samples, 0.0196 aft step at 10.5%.

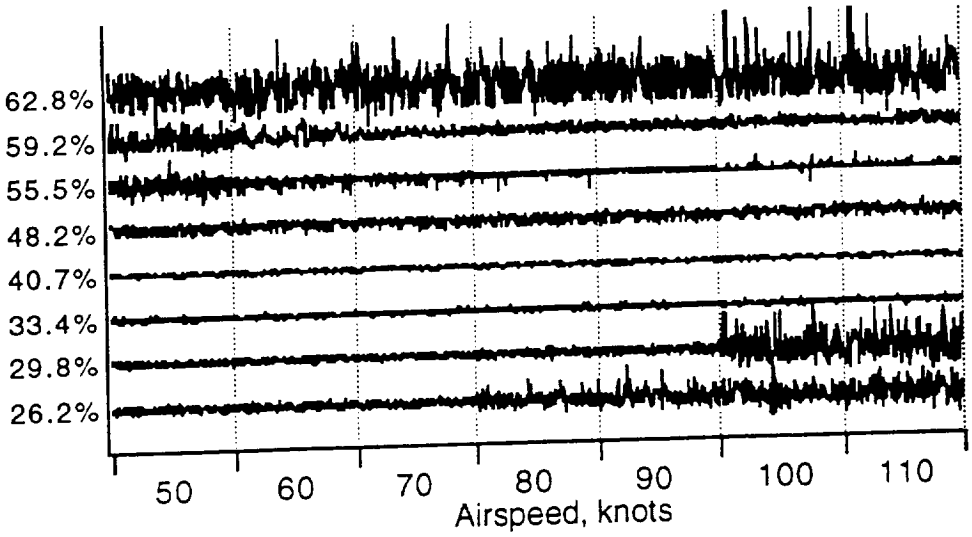

Figure F.14. -Flight 14, signal samples, 0.0116 aft step at 24.4%.

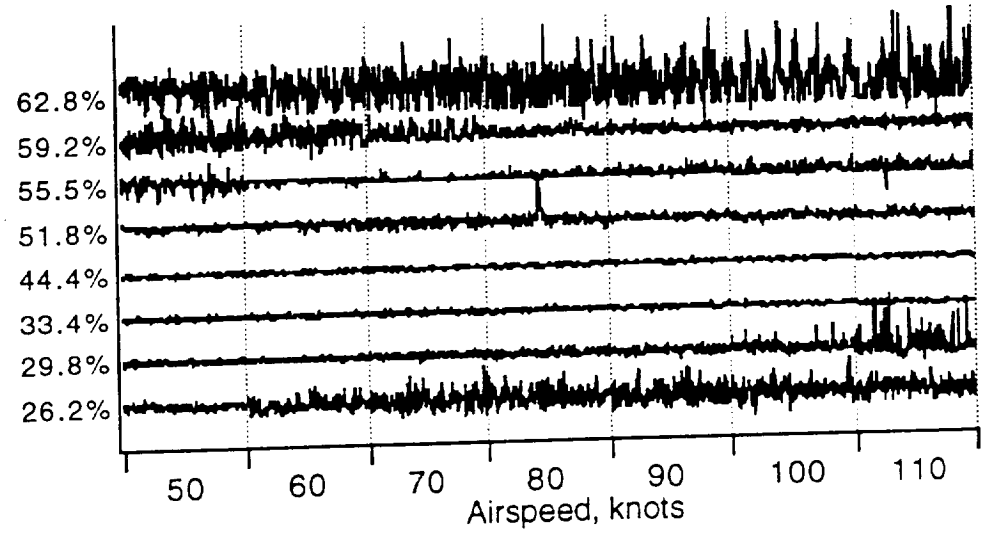

Figure F.15. -Flight 15, signal samples, 0.0147 aft step at 24.4%.

RMS Signal Intensity

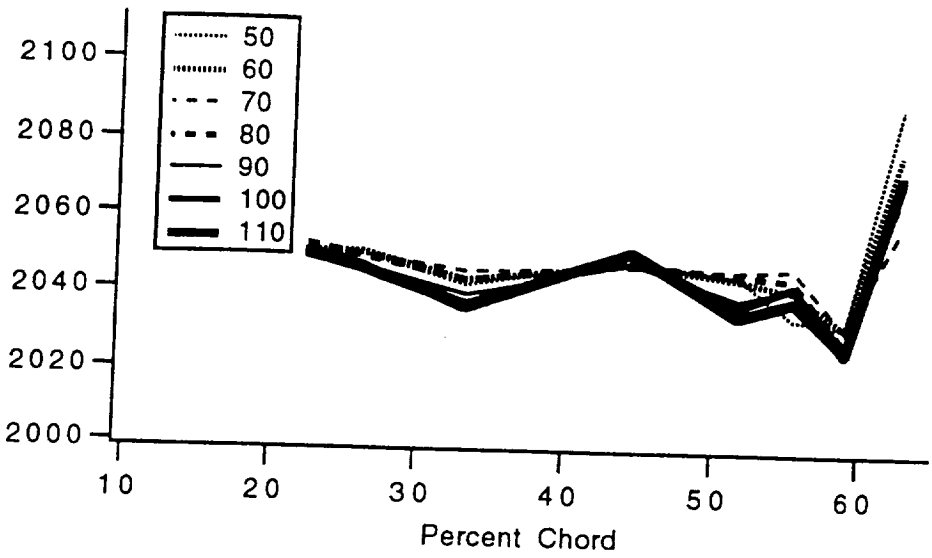

Figure F.16. -Flight 1, RMS Intensity, smooth wing.

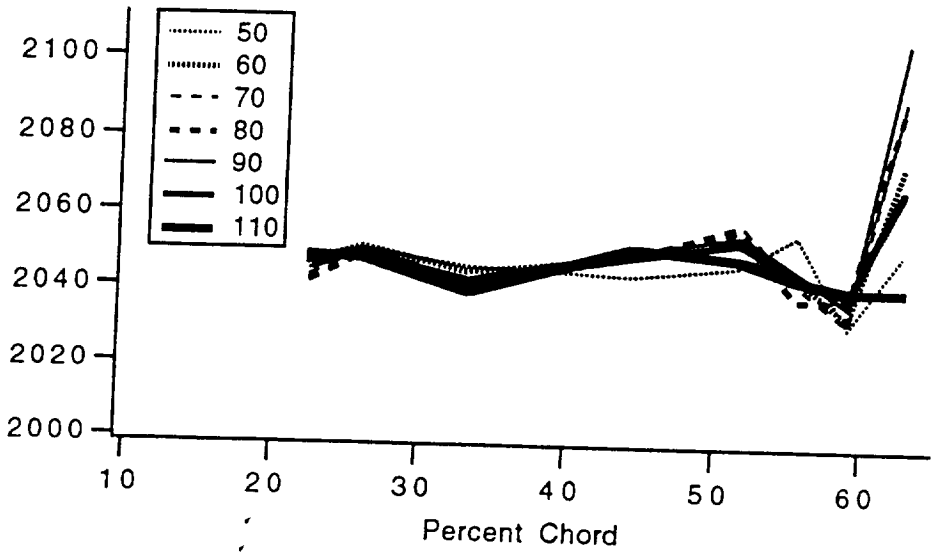

Figure F.17. -Flight 2, RMS Intensity, smooth wing.

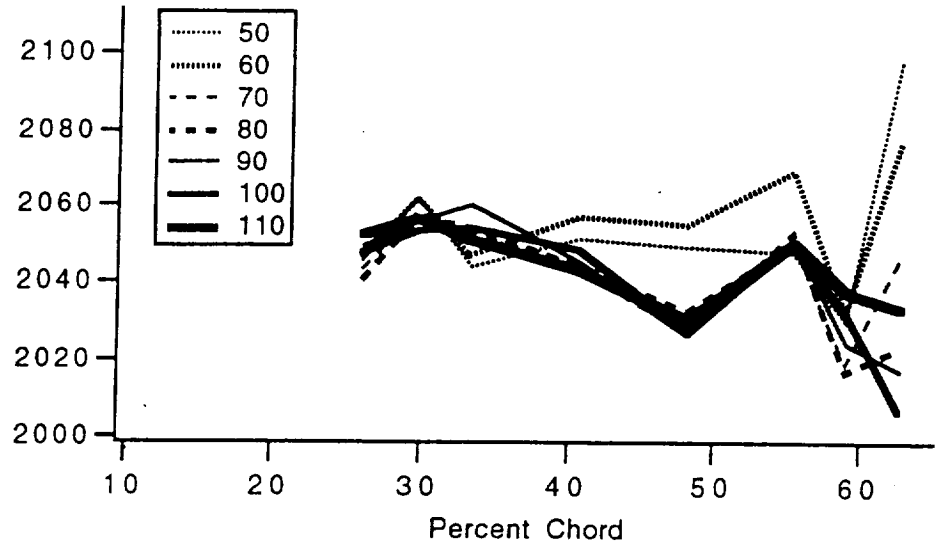

Figure F.18. -Flight 3, RMS Intensity, 0.0313 aft step at 24.4%.

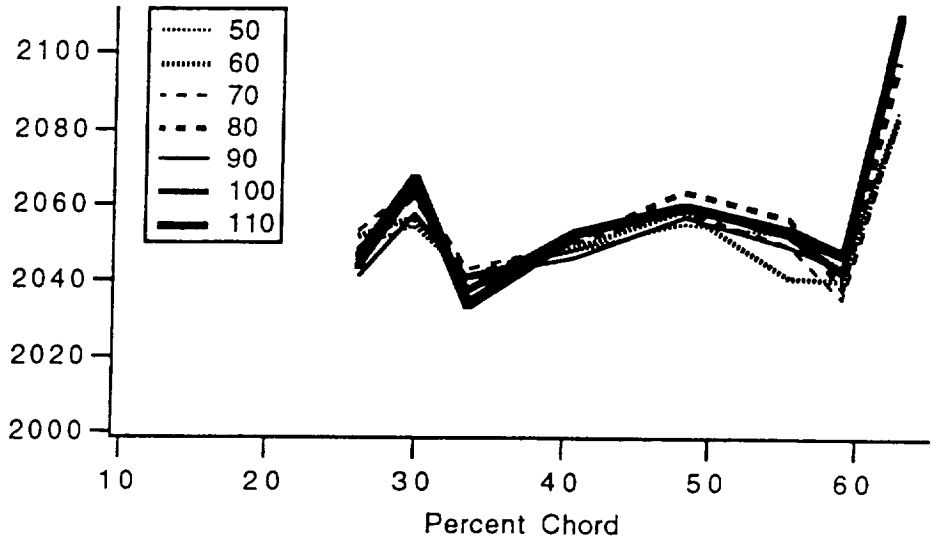

Figure F.19. -Flight 4, RMS Intensity, 0.0196 aft step at 24.4%.

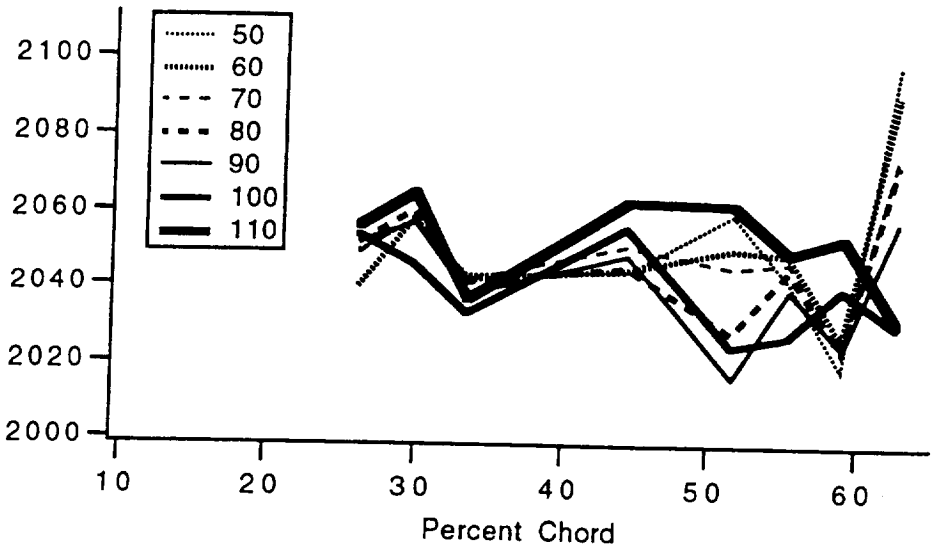

Figure F.20. -Flight 5, RMS Intensity, 0.0147 aft step at 24.4%.

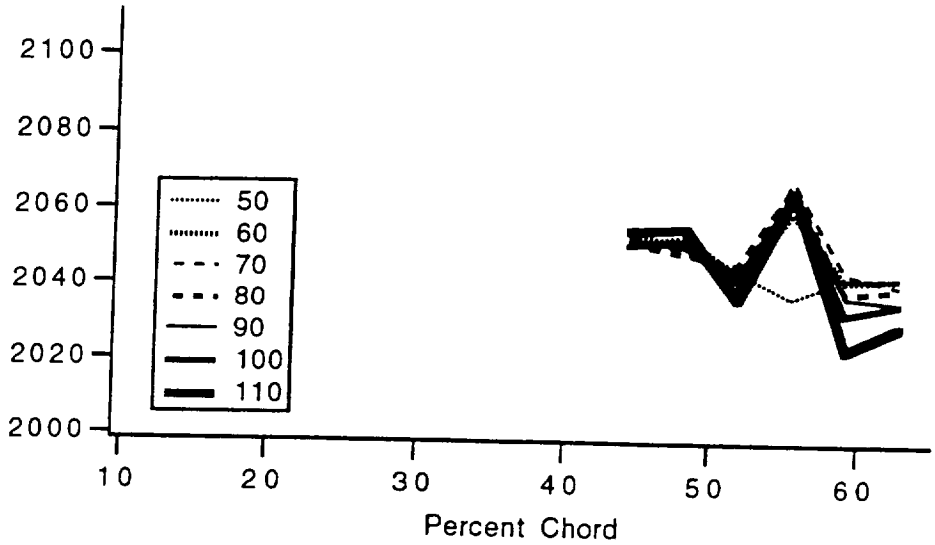

Figure F.21. -Flight 6, RMS Intensity, 0.0116 aft step at 42.6%.

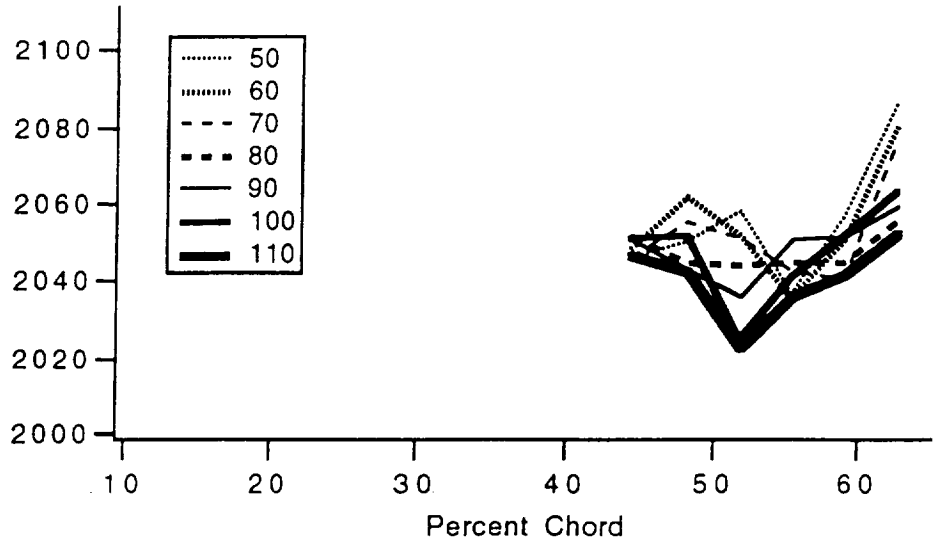

Figure F.22. -Flight 7, RMS Intensity, 0.0147 aft step at 42.6%.

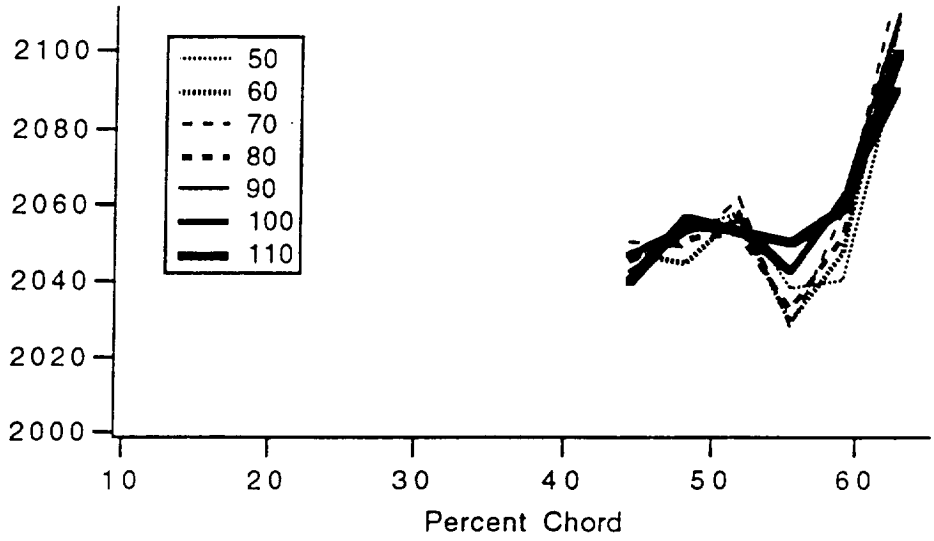

Figure F.23. -Flight 8, RMS Intensity, 0.0196 aft step at 42.6%.

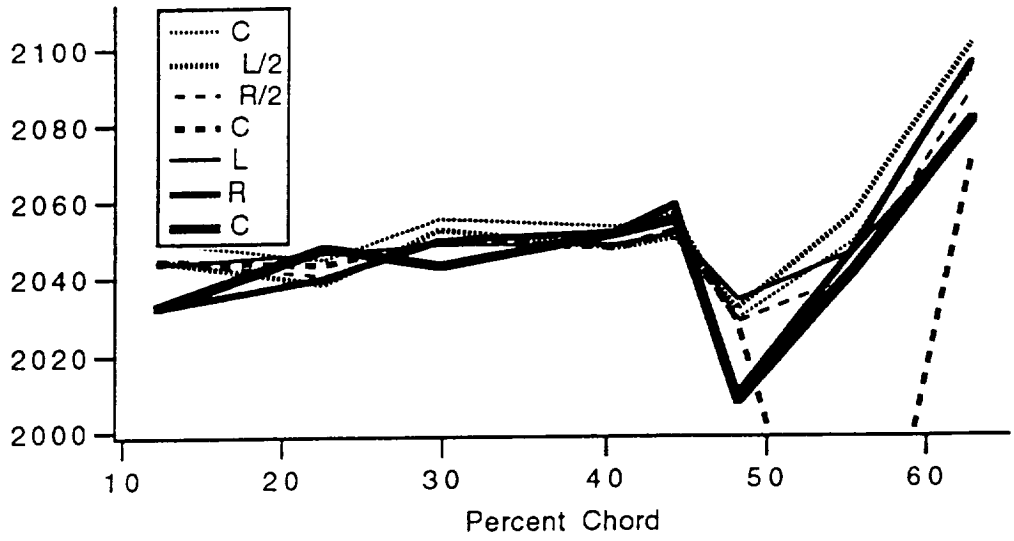

Figure F.24. -Flight 9, RMS Intensity, side slip.

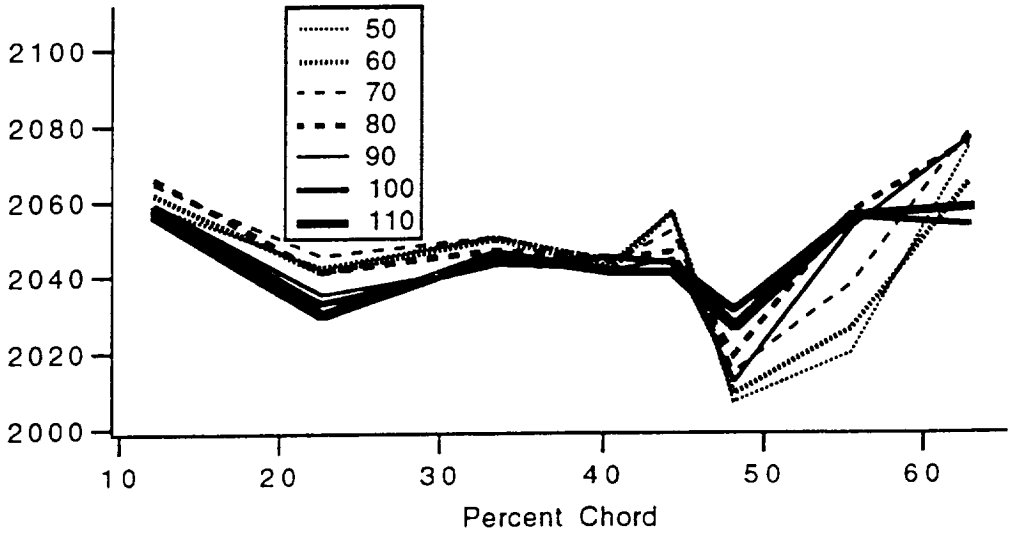

Figure F.25. -Flight 10, RMS Intensity, grit strip at 42.6%.

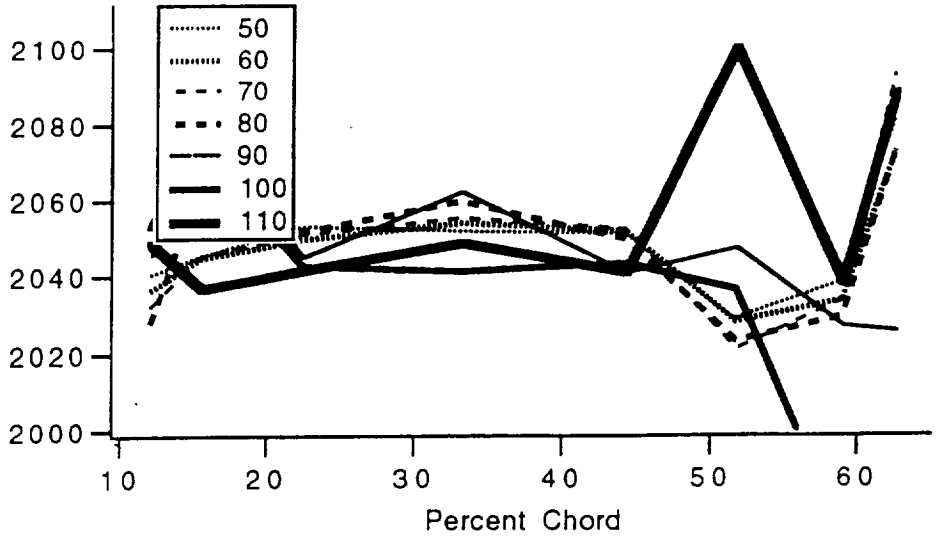

Figure F.26. -Flight 11, RMS Intensity, 0.0147 aft step at 10.5%.

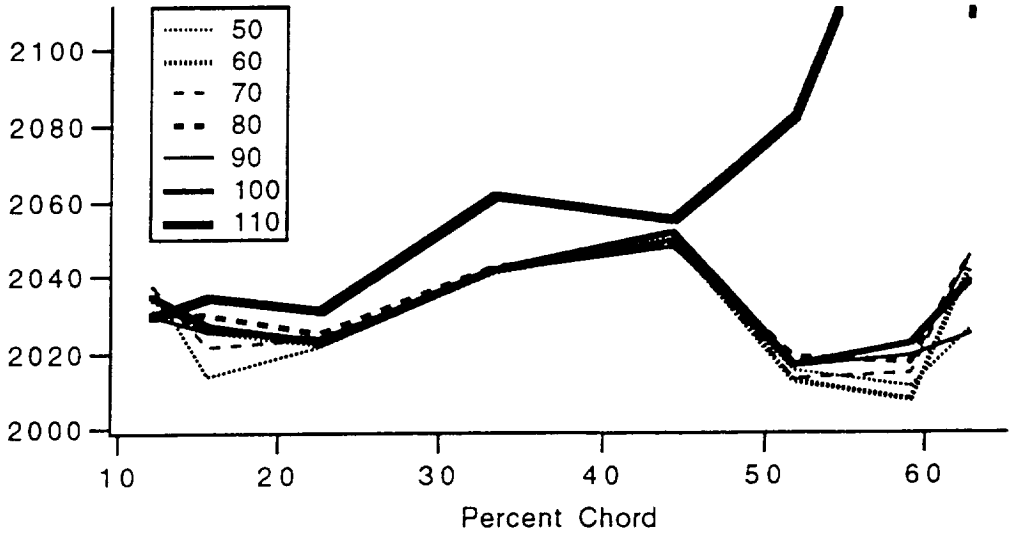

Figure F.27. -Flight 12, RMS Intensity, 0.0116 aft step at 10.5%.

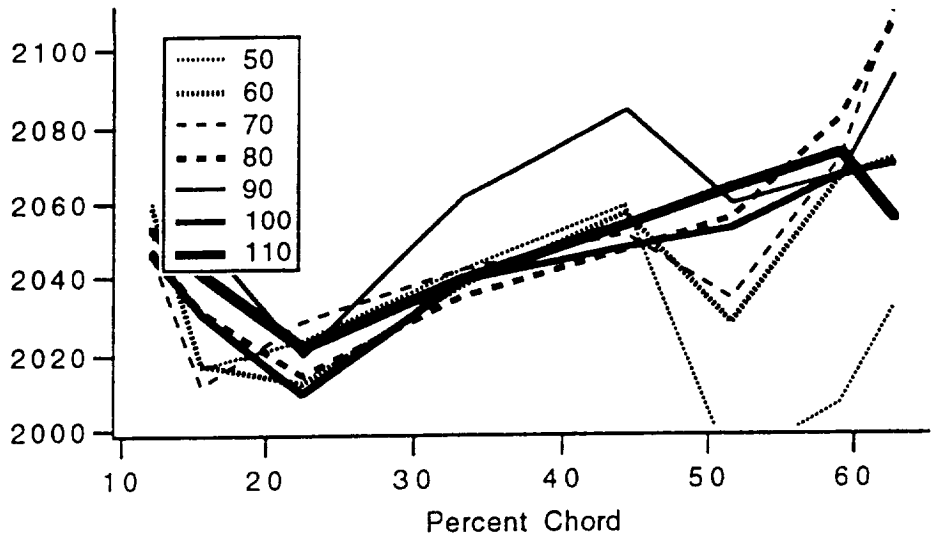

Figure F.28. -Flight 13, RMS Intensity, 0.0196 aft step at 10.5%.

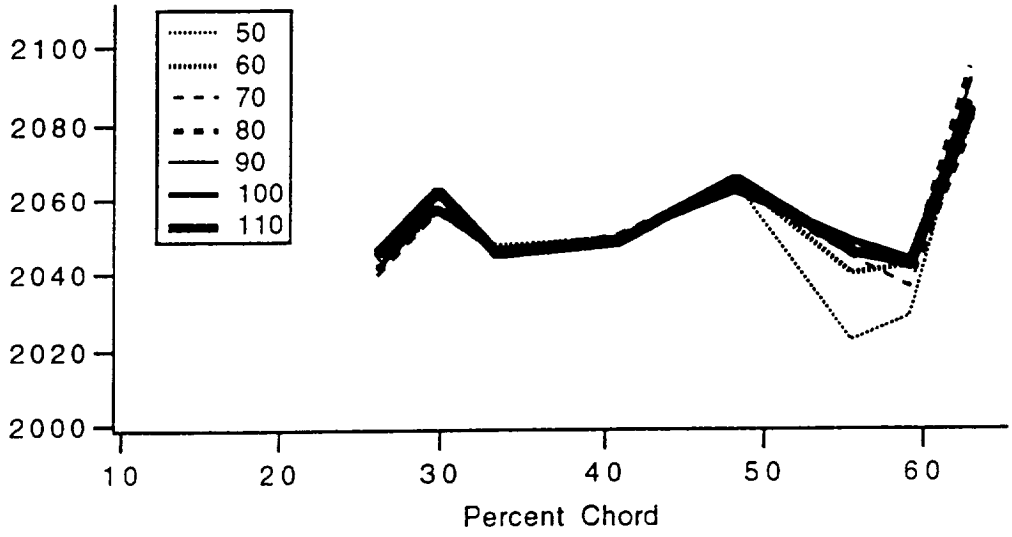

Figure F.29. -Flight 14, RMS Intensity, 0.0116 aft step at 24.4%.

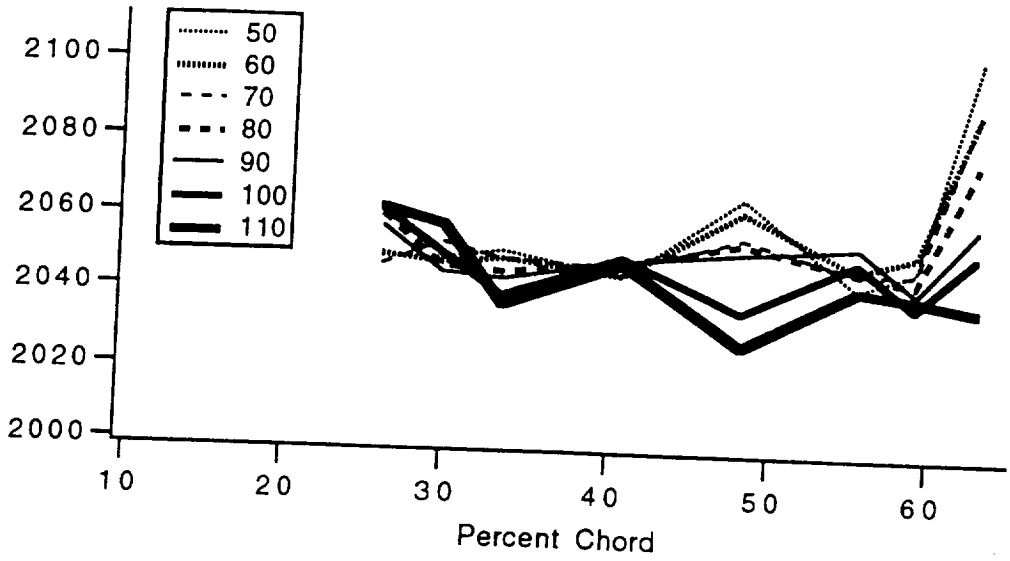

Figure F.30. -Flight 15, RMS Intensity, 0.0147 aft step at 24.4%.

Standard Deviation

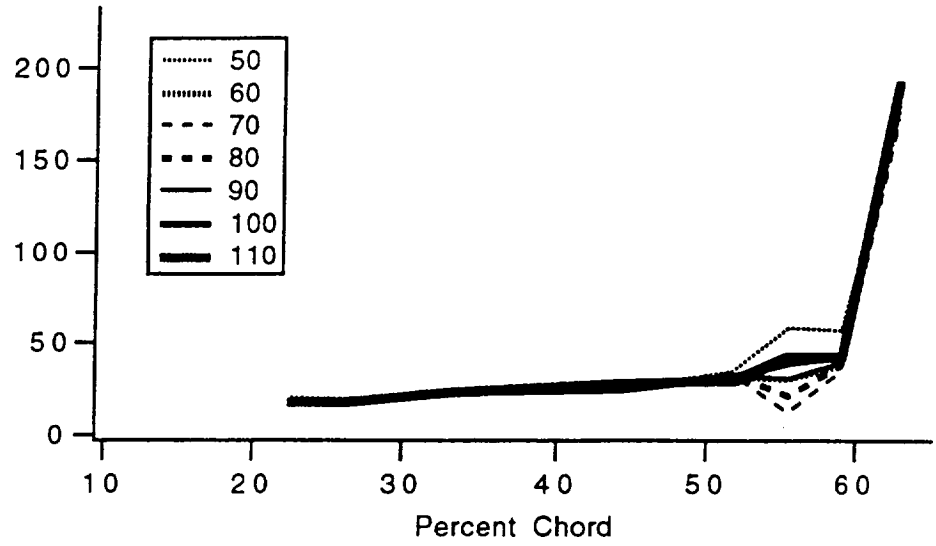

Figure F.31. -Flight 1, standard deviation, smooth wing.

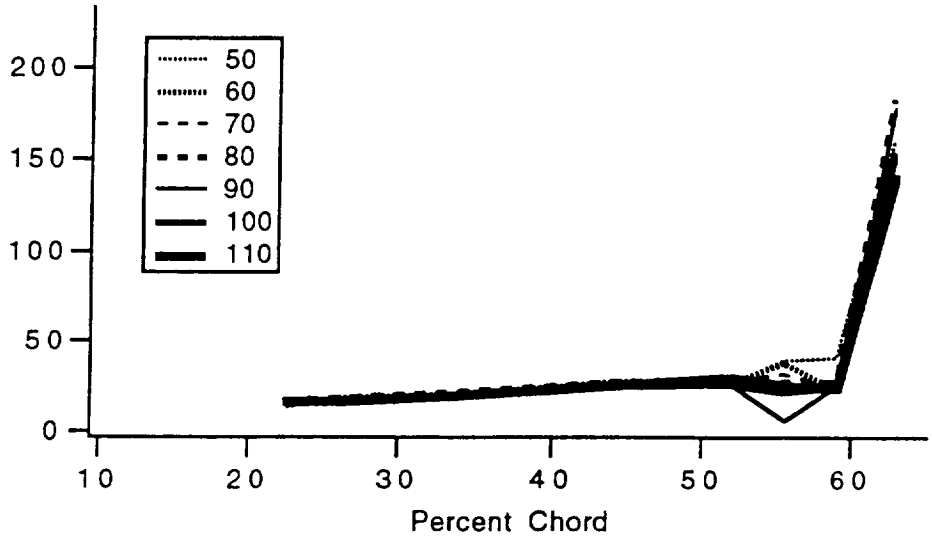

Figure F.32. -Flight 2, standard deviation, smooth wing.

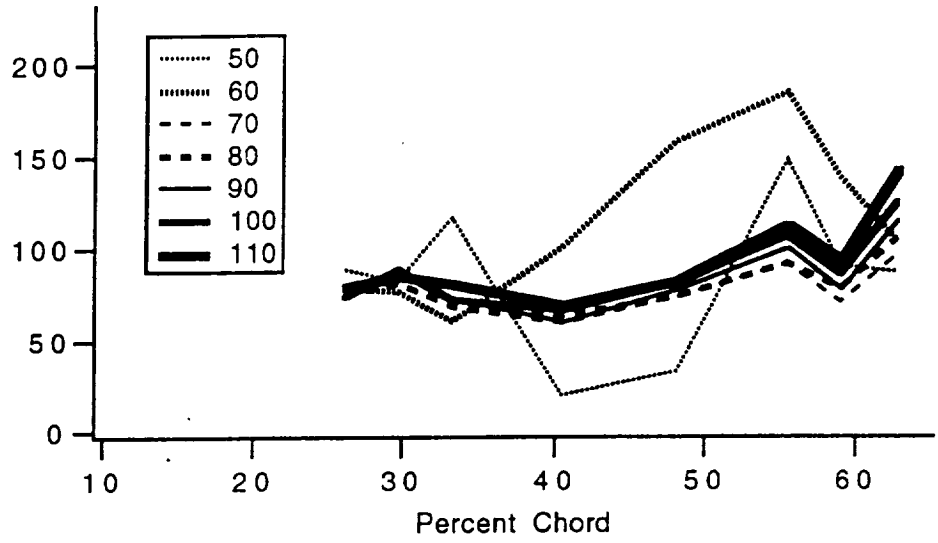

Figure F.33. -Flight 3, standard deviation, 0.0313 aft step at 24.4%.

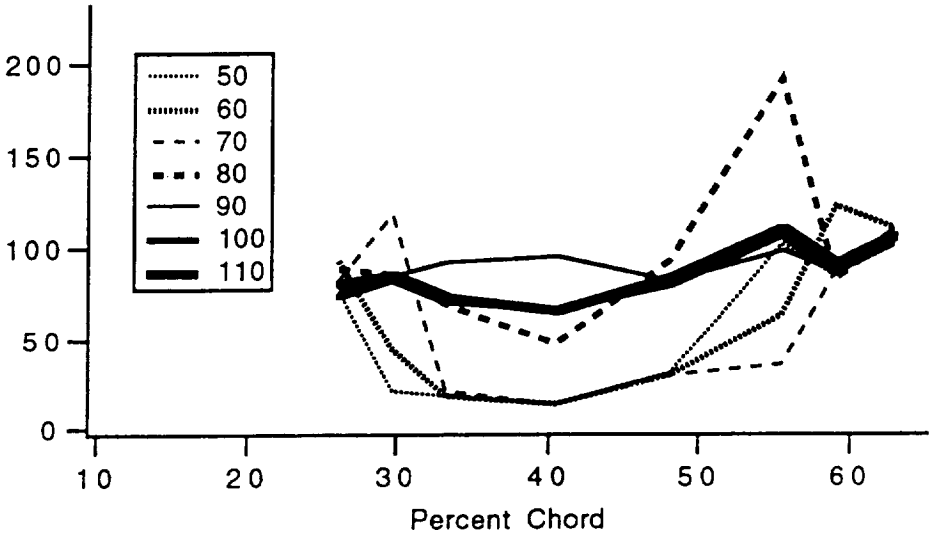

Figure F.34. -Flight 4, standard deviation, 0.0196 aft step at 24.4%.

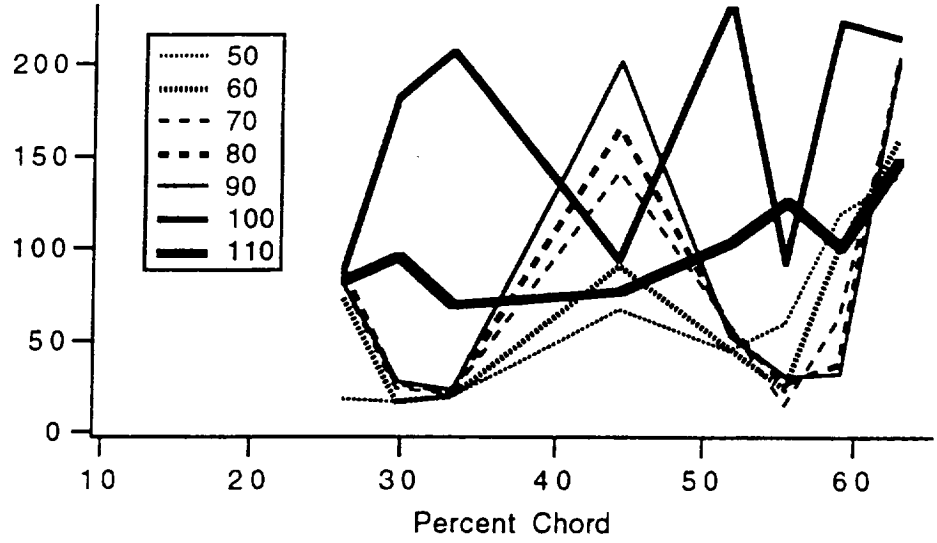

Figure F.35. -Flight 5, standard deviation, 0.0147 aft step at 24.4%.

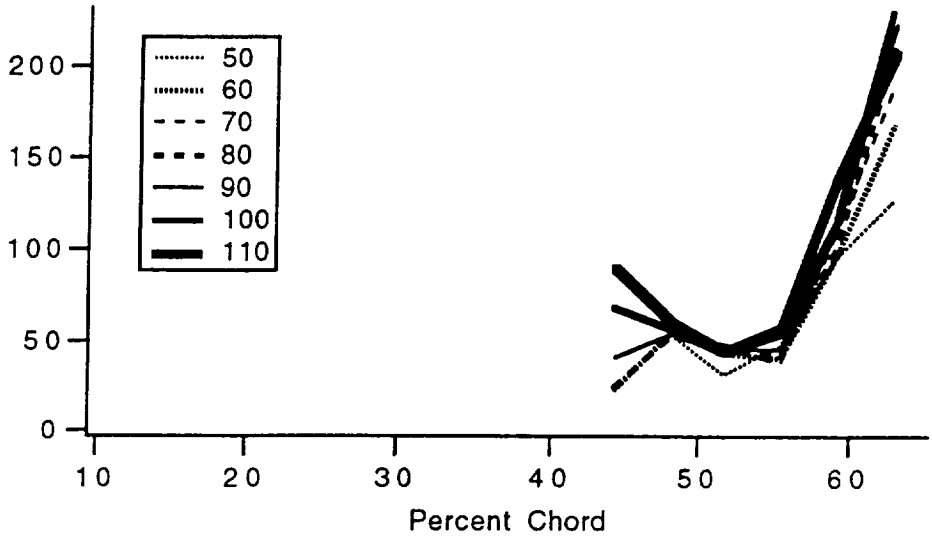

Figure F.36. -Flight 6, standard deviation, 0.0116 aft step at 42.6%.

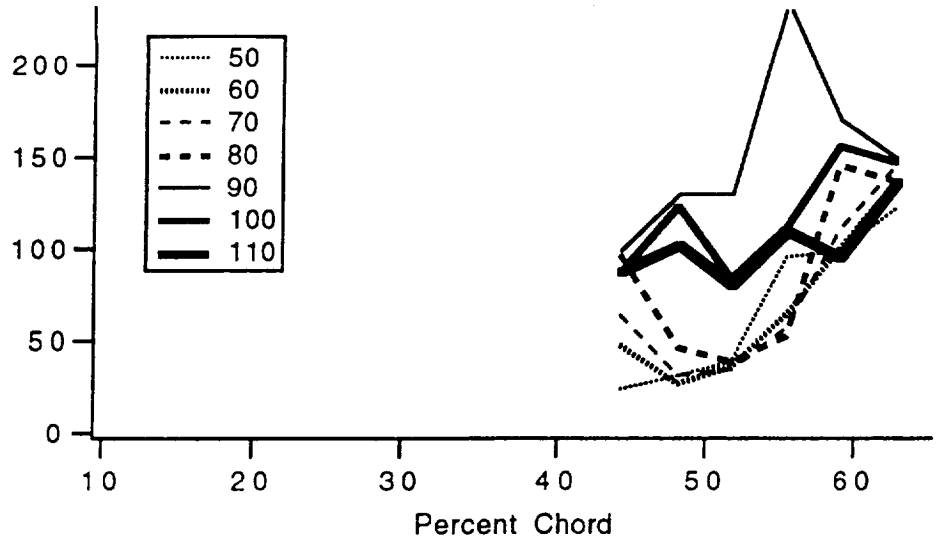

Figure F.37. -Flight 7, standard deviation, 0.0147 aft step at 42.6%.

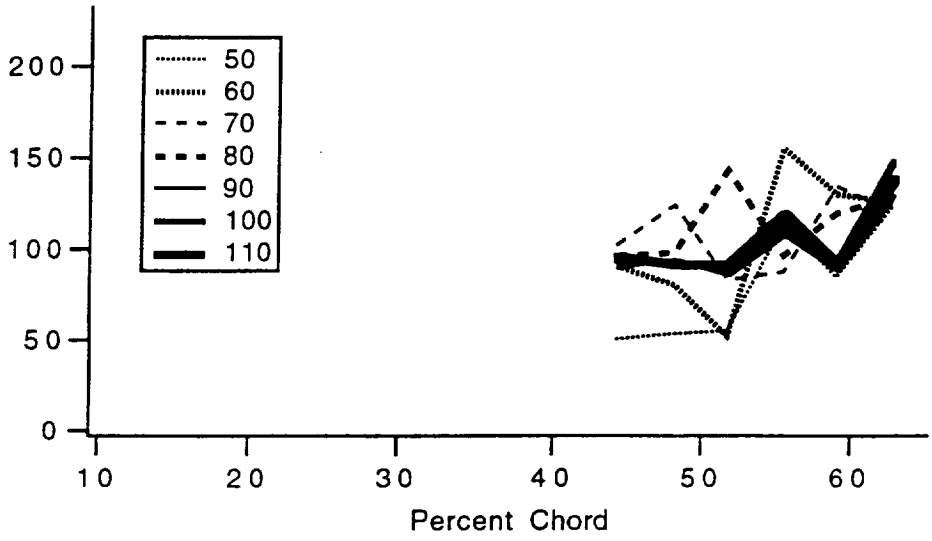

Figure F.38. -Flight 8, standard deviation, 0.0196 aft step at 42.6%.

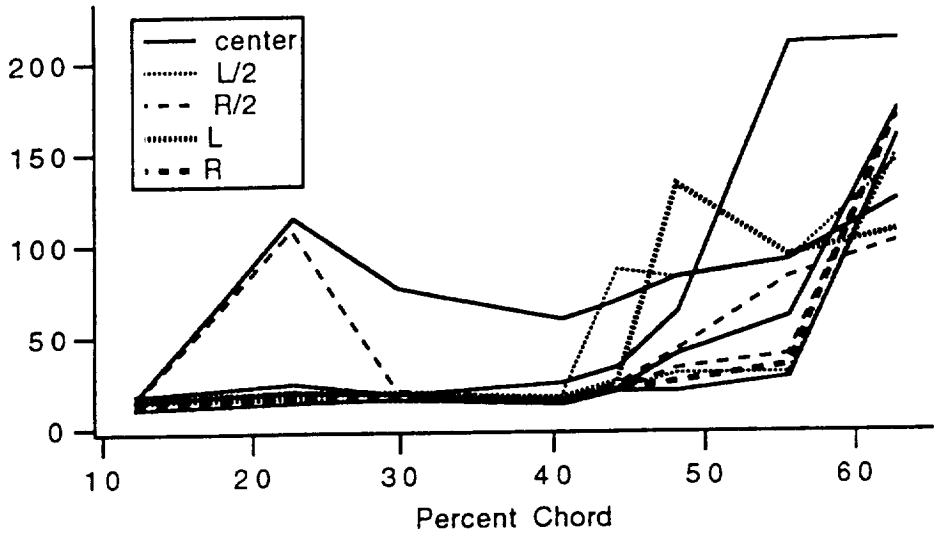

Figure F.39. -Flight 9, standard deviation, side slip.

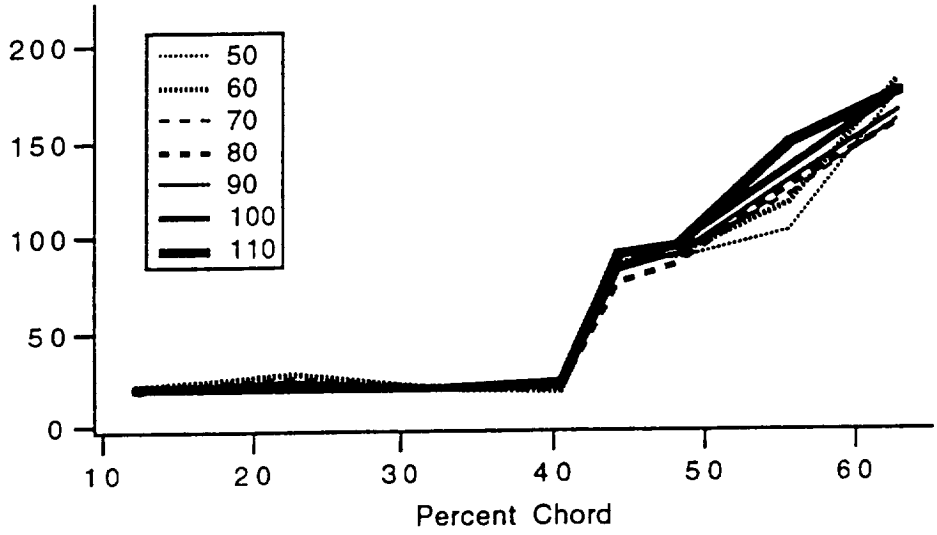

Figure F.40. -Flight 10, standard deviation, grit strip at 42.6%.

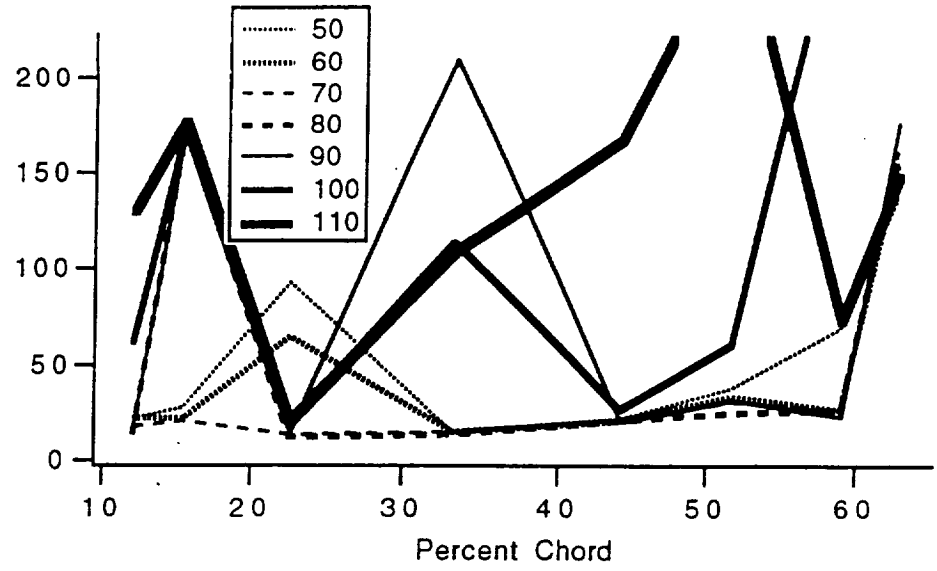

Figure F.41. -Flight 11, standard deviation, 0.0147 aft step at 10.5%.

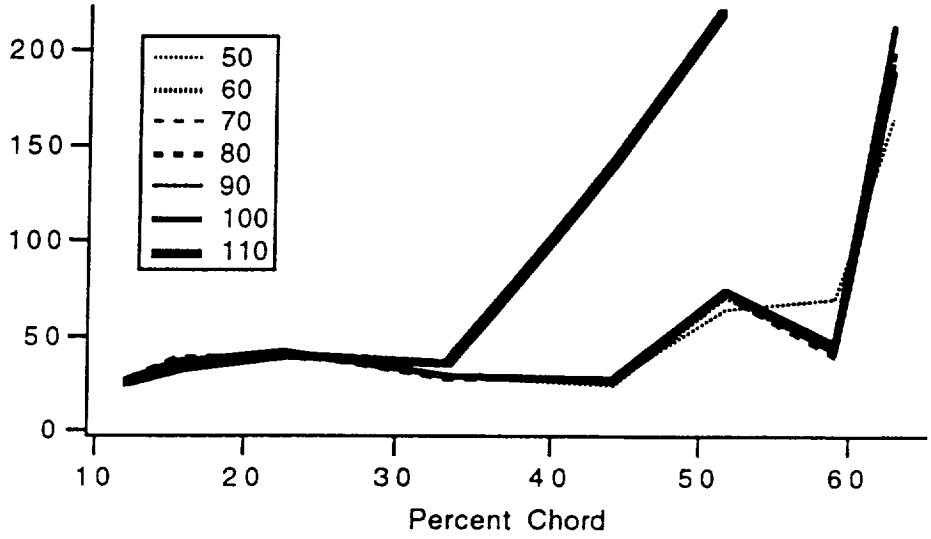

Figure F.42. -Flight 12, standard deviation, 0.0116 aft step at 10.5%.

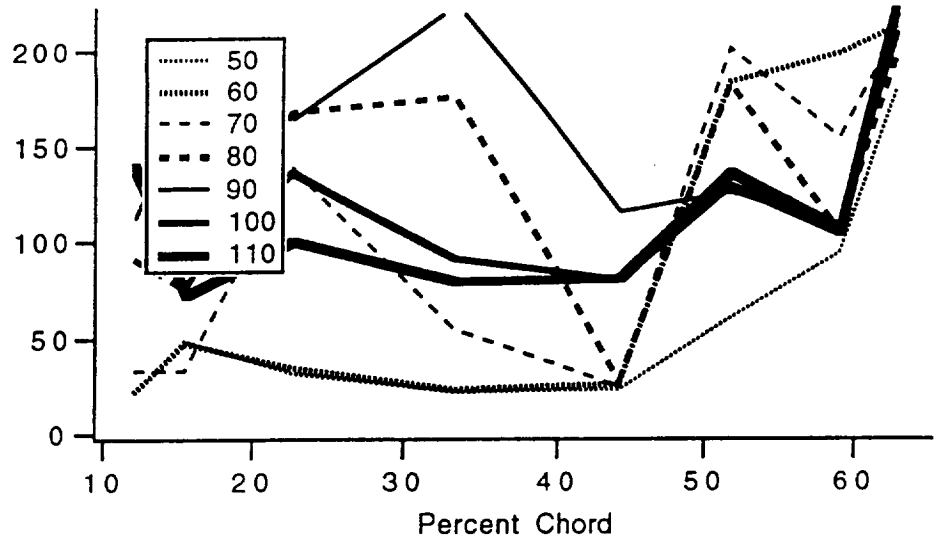

Figure F.43. -Flight 13, standard deviation, 0.0196 aft step at 10.5%.

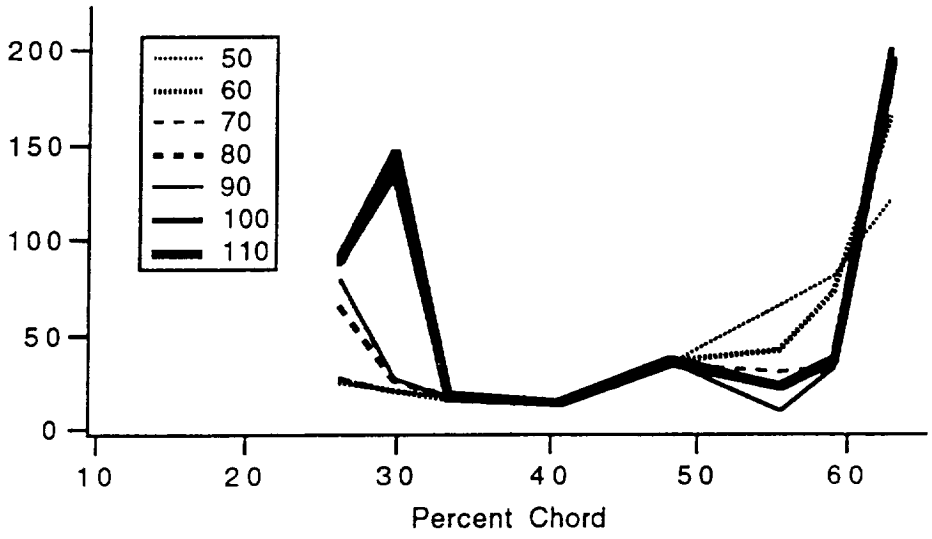

Figure F.44. -Flight 14, standard deviation, 0.0116 aft step at 24.4%.

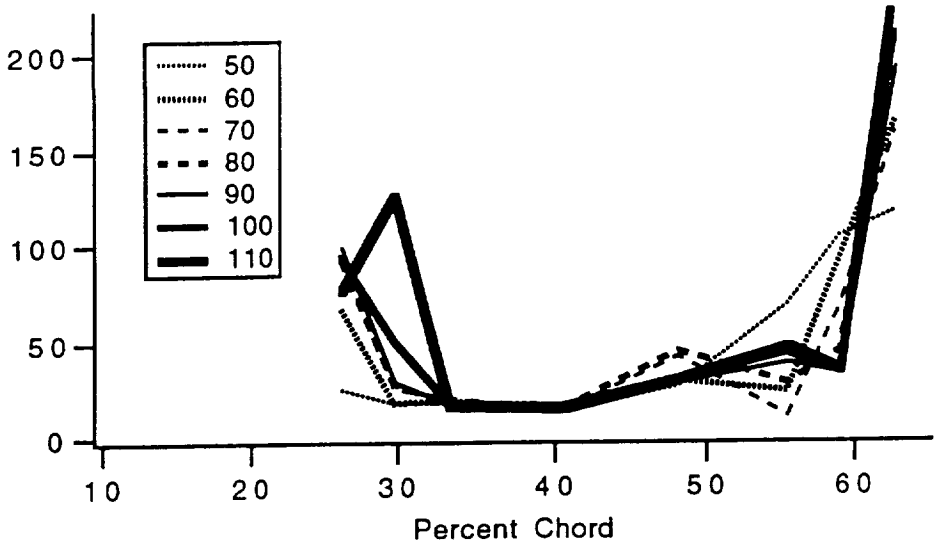

Figure F.45. -Flight 15, standard deviation, 0.0147 aft step at 24.4%.